

SHAPE MEMORY ALLOY ACTUATED SWITCH (SMAAS)

A Thesis

by

MOUSTAFA TAWFIK OMAR RASLAN

Submitted to the Office of Graduate and Professional Studies of
Texas A&M University
in partial fulfillment of the requirements for the degree of

MASTER OF SCIENCE

Chair of Committee,	Robert S. Balog
Co-Chair of Committee,	Bilal Mansoor
Committee Member,	Ibrahim Karaman
Head of Department,	Mark Weichold

December 2019

Major Subject: Interdisciplinary Engineering

Copyright 2019 Moustafa Tawfik Omar Raslan

ABSTRACT

In the light of recent research advancements in the field of shape memory alloy (SMA) actuators and devices, an idea of employing shape memory alloys in an electric switching device emerged. In this SMA actuated switch, SMA members are used as resistively heated actuators to separate or engage electric contacts for load circuit(s). Advantages of using SMA actuators in electric switching include; no holding power requirement (unlike some electromagnetic and solid-state relays), low power losses at the contacts (using metallic contacts as opposed to semiconductor junctions) and ease of miniaturization. One potential application for this device is the smart photovoltaic non-planar skin made of individual PV cells arranged together into pixels that can adapt to environmental conditions. One smart method of adaptation is to use miniature switches embedded onto the PV skin to group homogenous cells (according to exposure, solar intensity and other environmental conditions) to yield maximum energy harvest. Therefore, this research work investigates the feasibility of bi-stable shape memory alloy actuated switches and develops a framework for designing, optimizing and manufacturing them with respect to the intended application.

In this thesis, 15 conceptual designs for the SMAAS (inspired by the literature and novel concepts) are presented, 5 of which were down-selected as having the most potential in terms of robustness, manufacturability and scalability. The governing equations for the SMAAS concepts are formulated in the form of analytical and empirical models. In addition, two functional proof of concept prototypes for the switch are presented in this document as well as case studies for the optimization and

manufacturing of some of the down selected SMAAS concepts in the micro level. The outcome of this work is a proof of the feasibility of the SMAAS and its potential for miniaturization as well as the detailed design and manufacturing framework for SMA-based devices. An extension of this research work would be to develop and manufacture an energy-optimal micro SMAAS that satisfies the PV skin application's constraints and objectives.

ACKNOWLEDGEMENTS

I would like to thank my committee chair, Dr. Robert S. Balog, my committee co-chair, Dr. Bilal Mansoor, and my committee member, Dr. Ibrahim Karaman, for their guidance and support throughout the course of this research.

Thanks also go to my friends and colleagues for making my time at Texas A&M University a great experience.

Finally, special thanks to my family for their encouragement and support throughout.

CONTRIBUTORS AND FUNDING SOURCES

Contributors

This work was supervised by a thesis committee consisting of Dr. Robert Balog [Advisor - Associate Professor of the Department of Electrical and Computer Engineering], Dr. Bilal Mansoor [co-advisor – Assistant Professor of the Department of Mechanical Engineering and Material Science and Engineering] and Dr. Ibrahim Karaman [Committee Member – Professor and Head of the Department of Material Science and Engineering].

The cyclic testing data analyzed in Chapter IV was provided by colleague Lei Xue [PhD student of the Department of Material Science and Engineering] and is not yet published.

All other work conducted for this thesis was completed by the student independently.

Funding Sources

This research was made possible by NPRP grant #7-299-2-124 from the Qatar National Research Fund (a member of Qatar Foundation). The statements made herein are solely the responsibility of the author.

NOMENCLATURE

SMA	Shape Memory Alloy
SMAAS	Shape Memory Alloy Actuated Switch
SME	Shape Memory Effect
OWSME	One-way Shape Memory Effect
TWSME	Two-way Shape Memory Effect
PV	Photovoltaic
Nitinol	Nickel-titanium alloy
NiTi	Nickel-titanium alloy
EPSE	Energy per Switch Event

TABLE OF CONTENTS

	Page
ABSTRACT	ii
ACKNOWLEDGEMENTS	iv
CONTRIBUTORS AND FUNDING SOURCES.....	v
NOMENCLATURE.....	vi
TABLE OF CONTENTS	vii
LIST OF FIGURES.....	x
LIST OF TABLES	xiv
CHAPTER I INTRODUCTION	1
Shape Memory Alloys (SMAs).....	2
Shape Memory Alloy Actuated Switch (SMAAS)	3
Intended and Potential Application(s).....	4
Research Objectives and Approach.....	6
Thesis Organization.....	6
CHAPTER II LITERATURE REVIEW.....	9
SMA Fundamentals.....	9
One-Way Shape Memory Effect (SME)	9
Two-way Shape Memory Effect	11
Pseudoelasticity	11
SMA Materials & Shapes.....	12
SMA Actuators.....	16
Configurations.....	16
Applications.....	18
Challenges	19
CHAPTER III CANDIDATE DESIGNS	30
Design Framework	30
Objectives & Constraints.....	30

Locking Mechanisms	32
Conceptual Designs	32
Qualitative Assessment	47
Criteria	47
Assessment	48
Prototyping	50
Candidate Design I	51
Candidate Design II	56
Learning from Prototyping	57
 CHAPTER IV MODELLING AND ANALYSIS	 59
SMA Models	59
SMA Wire Models	59
SMA Spring Models	65
Mechanical Structure & Motion	69
Free-Body Diagrams	69
Locking Mechanisms	74
Relaxation Model	76
Energy Model	81
Transient-State Model	81
Simplified Design Model	82
SMA Springs Energy Model	83
Manufacturing Analysis	84
Joining Techniques	84
Micro-Fabrication & Assembly Techniques	86
Fatigue	91
 CHAPTER V CASE STUDIES	 94
Case Study I: Micro Fabrication of SMAAS Design	94
Substrate	96
Conductive Plunger	97
SMA Members	98
Leaf Springs	99
Assembly	100
Case Study II: Numerical Optimization of SMAAS Design	101
Problem Formulation	102
Optimization	110
 CHAPTER VI CONCLUSIONS	 117
Thesis Conclusion	117
Future Work	119

REFERENCES	120
APPENDIX A FIRST-ORDER DESIGN EQUATIONS FOR SMA WIRES*	125
APPENDIX B MATLAB OPTIMIZATION CODE	126

LIST OF FIGURES

	Page
Figure 1: Energy Density of Active Materials (Reprinted from [1])	2
Figure 2: Antagonistic Formation of SMAs.....	4
Figure 3: Sample PV Skin on Which the SMAAS is to Be Embedded [3].....	5
Figure 4: Stress-Strain-Temperature Curve of NiTi Illustrating SME (Reprinted from [1])	10
Figure 5: Hysteresis Curve of SMAs (Reprinted from [4])	11
Figure 6: Pseudoelastic Behavior of SMAAS (Reprinted from [1]).....	12
Figure 7: Effect of Composition on Transformation Temperatures (Reprinted from [7])	14
Figure 8: Stress-Strain Curve of SMAs Showing the Transformation Region (Reprinted from [13])	19
Figure 9: Schematic of SMA Antagonist Motion Showing Inactive Regions (Reprinted from [15])	21
Figure 10: Cyclic Testing of Antagonistic SMAs Showing Relaxation (Reprinted from [48]).....	22
Figure 11: SMA Cryogenic Thermal Switch (Reprinted from [10])	23
Figure 12: SMA Damper-Controlled Switch (Reprinted from [19])	24
Figure 13: SMA Bistable Electric Switch Concept (Reprinted from [20]).....	25
Figure 14: SMA Planar Micro Electric Switch Concept (Reprinted from [21]).....	26
Figure 15: SMA Diaphragm Based Switch Concept (Reprinted from [22]).....	26
Figure 16: Bistable SMA Leaf Spring Switch Concept (Reprinted from [23])	27
Figure 17: SMA Flexible-Member Switch Concept (Reprinted from [24])	28
Figure 18: SMA Bistable Lever-based Switch Concept (Reprinted from [25])	29

Figure 19: Locking mechanisms for actuators (Reprinted from [27]). 1- Mechanical mechanisms 2- Friction-based mechanism 3- Singularity mechanisms	32
Figure 20: Terminology for Electrical Connections in the Design Concepts	33
Figure 21: Top-View Schematic of the SMAAS Conceptual Design #1	34
Figure 22: Top-View Schematic of the SMAAS Conceptual Design #2.....	35
Figure 23: Top-View Schematic of the SMAAS Conceptual Design #3.....	36
Figure 24: Top-View Schematic of the SMAAS Conceptual Design #4.....	37
Figure 25: Top-View Schematic of the SMAAS Conceptual Design #5.....	38
Figure 26: Top-View Schematic of the SMAAS Conceptual Design #6.....	38
Figure 27: Top-View Schematic of the SMAAS Conceptual Design #7.....	39
Figure 28: Top-View Schematic of the SMAAS Conceptual Design #8.....	40
Figure 29: Top-View Schematic of the SMAAS Conceptual Design #9.....	41
Figure 30: Top-View Schematic of the SMAAS Conceptual Design #10.....	42
Figure 31: Top-View Schematic of the SMAAS Conceptual Design #11	43
Figure 32: Top-View Schematic of the SMAAS Conceptual Design #12.....	43
Figure 33: Top-View Schematic of the SMAAS Conceptual Design #13.....	44
Figure 34: A Micro-Machined Microgripper (Reprinted from [26])	45
Figure 35: Top-View Schematic of the SMAAS Conceptual Design #14.....	46
Figure 36: Top-View Schematic of the SMAAS Conceptual Design #15.....	46
Figure 37: Testing Setup for the Proof-of-Concept Prototypes	51
Figure 38: Top-View Schematic of the First Prototype Concept.....	52
Figure 39: Side-View Schematic of the First Prototype	52
Figure 40: Actuation Structure for Prototype I (a) Individual Components (b) Assembled Structure	53
Figure 41: Actuation Mechanism of Prototype I with SMA Actuators Installed.....	54

Figure 42: Exploded-View Schematic of the Switch Prototype	55
Figure 43: Fully Functional Bistable SMAAS Prototype I.....	56
Figure 44: Top-View Schematic of Prototype II Concept	56
Figure 45: Fully Functional Bi-stable SMAAS Prototype II	57
Figure 46: Stress-Temperature Curve of SMAs Showing Linear Stress Coefficients (Reprinted from [1])	62
Figure 47: Curve-Fitted SMA Wire Properties Produced from Manufacturer Datasheet ([8])	64
Figure 48: Calculated and Measured SMA Spring Force vs. Temperature (Reprinted from [47]).....	68
Figure 49: Schematic of the First Design Concept to be Analyzed	70
Figure 50: Schematic of the Second Design Concept to be Analyzed.....	72
Figure 51: Inactive Strain Vs. Pre-Strain Curve (Left) and Stress-Strain Curve (Right) of a SMA Ribbon (Reprinted from [15]).....	77
Figure 52: Sample Thermal Cycling Test for SMA Wire Segments (Reprinted from [48])	78
Figure 53: Smallest Ring Terminal for Crimping Resistively-heated SMAs (Reprinted from [8]).....	85
Figure 54: Micro-Snake NiTi Actuator Machined Using Laser from a 120 μ m NiTi Sheet (Reprinted from [41]).....	86
Figure 55: Micro “Box”-Type SMA Spring Actuator Laser-Machined (Reprinted from [44]).....	87
Figure 56: A Micro-Gripper Laser Machined out of SMA Sheet (Reprinted from [46])	87
Figure 57: Wire Bonding of Micro SMA Wire (Reprinted from [45]).....	88
Figure 58: Galvanic Riveting of Micro SMA Springs (Reprinted from [44])	89
Figure 59: SMA Wires Submergence Example (Reprinted from [39])	90
Figure 60: Schematic S-N Fatigue and Deterioration Curves for SMAs (Reprinted from [7]).....	91

Figure 61: Cyclic Training of SMAs (Reprinted from [1]).....	93
Figure 62: SMAAS Design Schematic: Top View (Left) and Side View (Right).....	94
Figure 63: Schematic of the Micro SMAAS Substrate	97
Figure 64: Schematic of the Micro SMAAS Plunger	98
Figure 65: Schematic of the Micro SMAAS Plunger and Micrometer Pre-Straining Process (Reprinted from [39])	99
Figure 66: Schematic of the Micro SMAAS Electrical Contacts Structure	99
Figure 67: Schematic of the Assembly Process of the Micro SMAAS	101
Figure 68: A Schematic of the Conceptual Design of the SMAAS to be Optimized	102
Figure 69: Design Variables Illustration for the Optimal SMAAS Concept	103
Figure 70: Block Diagram of Multi-Disciplinary Modules Interactions.....	109
Figure 71: Normalized Sensitivities of the Design Variables.	112
Figure 72: Pareto Front for the Design Objective Functions.	113
Figure 73: Trade-off Analysis from Optimizing Design Objectives Separately.....	114
Figure 74: Selected Trade-off Point from Optimizing Design Objectives Separately...	115

LIST OF TABLES

	Page
Table 1: Detailed List of SMA Materials and their Characteristics (Reprinted from [6])	13
Table 2: SMA Shapes and Parameters in the Market (Adapted from [8] & [17])	15
Table 3: Comparison Between NiTi Wires and Springs (Reprinted from [12])	16
Table 4: Efficiency of SMA Actuators under Different Loading Cases (Reprinted from [14]).....	16
Table 5: Configurations of SMA Actuators (Adapted from [8][12][18])	17
Table 6: Potential Applications for SMAs (Reprinted from [12])	18
Table 7: Design Objectives and Constraints for the SMAAS	31
Table 8: Pugh Matrix for Qualitative Down Selection of SMAAS Concepts	48
Table 9: Down-Selected Design Concepts After a Qualitative Assessment	49
Table 10: Force-Deflection Equations of Locking Components (Adapted from [31] [32])	75
Table 11: Recommended Maximum Strain and Stress for SMA Cycle Life (Reprinted from [42]).....	92
Table 12: Component-Specific Requirements and Material Selection for Fabricating the SMAAS Concept	95
Table 13: Material Properties and User-specified Parameters [8]	104
Table 14: Governing Equations for the Optimization of the SMAAS	108

CHAPTER I

INTRODUCTION

Electrically-operated electrical switches are either mechanical (e.g. electromagnetic relays - EMRs) or electronic (e.g. solid state Relays - SSRs) or hybrid (e.g. Hybrid Solid State Relay - HSSRs). Electromagnetic relays rely on current passing through a coil to create a magnetic field which generates a force to open or close metallic contacts. Electronic switches are referred to as solid-state relays because they typically use semiconductor components (e.g. Transistors, Thyristor, Triac..etc) instead of moving parts to turn on or turn off the flow of current in the output circuit. The hybrid relays employ a parallel combination of SSRs and EMRs [2].

A major drawback associated with some electromagnetic relays and some semiconductor switches is that they require a holding power to maintain the switch state. Semiconductor switches also have the additional drawback of more power losses across the junctions when compared to metallic contactors – contact resistance of semiconductor junctions is an order of magnitude higher than that of metal contactors [2]. In the light of these drawbacks, a need arises for an electrically-operated electric switch that has no holding power requirement and minor losses during switching. One candidate solution to satisfy such need is a shape memory alloy (SMA) actuated electric switch.

Shape Memory Alloys (SMAs)

Shape Memory Alloys are smart materials that can be set to a specific shape and remember this shape even after undergoing a plastic deformation at a low temperature [1]. Heating shape memory alloys above a certain temperature called, the austenitic transformation temperature, forces the material to return to its original set shape. Meanwhile, a significant force is generated by the material while reverting shape. SMAs are a part of a family of materials called active materials that change properties as a response to external stimulation. They are considered multi-functional since they can be used as actuators, temperature sensors or structural members [4]. However, actuation functions are emphasized for SMAs since they have the highest energy density among active materials as shown in diagonal lines of Figure 1 [1]. Their work density is estimated to be 25 times greater than that of electric motors [5].

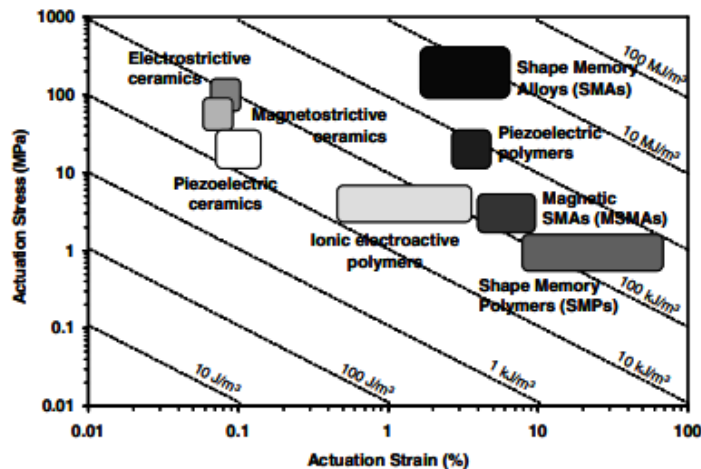


Figure 1: Energy Density of Active Materials (Reprinted from [1])

SMA as actuators have some advantages and disadvantages. The main advantages are; high force-to-weight and force-to-volume ratios, high compactness/simplicity, easy to miniaturize and silent operation. On the other hand, they do have the disadvantages of; nonlinearity, slow operation, inaccurate positioning and high fatigue rate [4]. This thesis investigates the feasibility of using SMA to actuate an electric switch (SMAAS) taking into consideration the aforementioned advantages and challenges.

Shape Memory Alloy Actuated Switch (SMAAS)

Activating SMA can be through heating by an external heat source or internally by ohmic heating (passing current through the materials and using its internal resistance to generate heat). Once SMA reverse shape, the heat source can be disconnected and the material would hold its shape (state) [1]. Recoverable deformation of SMA can be in the form of axial extension/straining, bending or torsion. For instance, if two SMA pieces were joined in an antagonistic formation shown in figure 2 where each piece is connected separately to an electric power supply and one of the pieces was pre-strained (axially stretched), a bi-directional motion can be achieved.

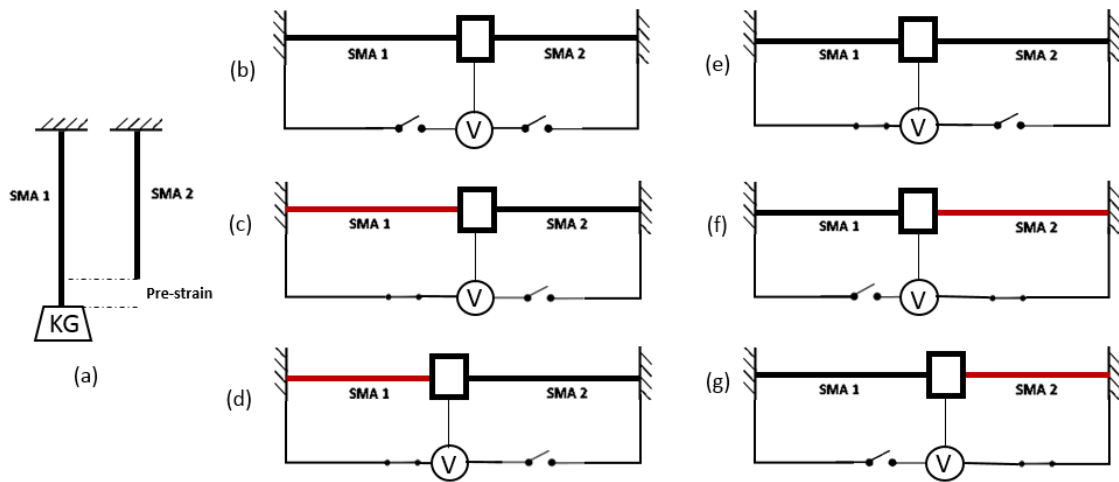


Figure 2: Antagonistic Formation of SMAs

Ohmic heating of the stretched SMA piece (e.g. SMA 1) would force the SMA to recover the axial deformation and contract, thus, extends the opposite SMA piece (SMA 2). Subsequently heating SMA 2 would force it to contract and stretch SMA 1. This way a bi-directional axial motion is generated. If pairs of metal contacts for electric circuits are placed on both sides along the SMA assembly axial movement direction and a conductive metal piece is placed at the junction of the two SMA pieces then a multi-state electric switch can be created. This constitutes the basis upon which the SMAAS will be investigated while considering various configurations and deformations modes of SMAs.

Intended and Potential Application(s)

One key application for such technology is photovoltaic energy systems. Current research efforts in the field of photovoltaics (particularly in the affiliated lab – Renewable Energy and Power Electronics Lab at Texas A&M University) are directed towards developing non-planar flexible photovoltaic skin made out of individual PV

cells (shown in the figure below). These cells are arranged together into smart pixels that can adapt to environmental conditions. One method of adaptation is to group homogenous cells (according to exposure, solar intensity and other environmental conditions) together to yield maximum energy harvest. In order to achieve that, a grid of micro switches is to be embedded to the photovoltaic skin to (de)group PV cells [3].

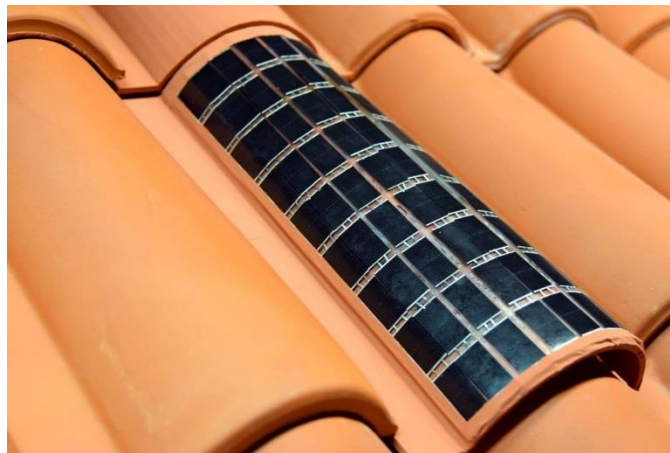


Figure 3: Sample PV Skin on Which the SMAAS is to Be Embedded [3]

Since these smart PV pixels are intended to maximize energy production, a miniature electric switch with low switching energy and low electrical power losses is required. An SMA-based switch satisfies those energy requirements. The SMA high energy density, compactness and ease of miniaturization also supports its use in micro switches for PV pixels. In addition, since environmental conditions that change the operation of the photovoltaic cells do not change very rapidly and frequently, high switching speed and frequency are not required for such application. Therefore, this thesis will be investigating SMA actuated switches (SMAAS) in the light of smart PV

cells application, however, such technology can be potentially used in any other applications where there is a need for an electrically-controlled electric switch with no holding power requirement and low operation frequency/response time.

Research Objectives and Approach

The research objectives for this thesis can be summarized as follows:

- 1. Identify candidate design concepts for a shape memory alloy actuated switch (SMAAS).*
- 2. Investigate the feasibility of SMAs as actuators driving the switch contacts.*
- 3. Analyze & model SMAAS analytically, numerically or empirically for design purposes.*
- 4. Develop an optimization model for the SMAAS.*
- 5. Investigate manufacturability of the SMAAS in the micro scale.*

The main approach taken to achieve the mentioned objectives is to investigate with sufficient depth all areas of the SMAAS, consider a comprehensive set of designs possibilities and provide recommendations for designing such a device rather than focusing on fully designing a single-concept SMAAS. In addition, this thesis work is not meant to research shape memory alloys but rather the use SMAs as a tool for the design of the SMAAS.

Thesis Organization

This thesis is organized into 6 chapters as listed in the contents table. Chapter I begins with the motivation behind developing a SMAAS and gives a brief introduction

to SMAs including their advantages and drawbacks. It then describes the working principle of a multi-state switch that employs SMA and the potential application for such a device. Lastly, it lists the research objectives of this thesis and the approach taken to meet those objectives.

Chapter II is a literature review that presents in sufficient details the fundamentals of SMAs in terms of the working principle and different behaviors as well as the available SMA materials and their characteristics. It also gives an overview of the different shapes of SMAs in the market as well as different configurations for arranging SMAs and their respective advantages/disadvantages. This chapter ends with a survey of the state of the art of SMA actuators in general and SMA-actuated switches in specific.

Chapter III presents the feasible candidate designs for a SMA-actuated switch. It starts with a description of the framework upon which the conceptual designs for the SMAAS were generated. The conceptual designs are then explained both graphically and in text before performing a qualitative assessment of those design concepts and down-selecting the key potential concepts. This chapter ends with a description of the prototyping process of two of the potential design concepts and the outcomes of this process.

Chapter IV provides the main skeleton of modeling and analyzing a SMAAS. It provides the thermal, electrical and mechanical models of different shapes of SMAs as well as an analysis of the mechanical structure and motion of the SMAAS. It also describes the energy analysis for activating and deactivating the switch and the locking mechanisms for the switch motion. Lastly, it provides an overview of the electrical

design considerations in the SMAAS and potential micro fabrication and assembly techniques for such miniature device.

Chapter V provides detailed case studies for the micro fabrication of one of the potential design concepts and a numerical optimization of another concept. Lastly, Chapter VI summarizes what was learned through the course of this thesis work and provides recommendations for the development of a SMAAS and for future work.

CHAPTER II

LITERATURE REVIEW

SMA Fundamentals

One-Way Shape Memory Effect (SME)

The SMA material exhibit shape memory effect while changing phase from martensite (low temperature phase) to austenite (high temperature phase). An unloaded (unstrained) SMA material in its martensite state is said to have a twinned crystalline formation. Loading (deforming) the SMA while at low temperature causes detwinning which is represented by the reorientation of the crystalline formation to cause an inelastic strain. When the SMA is unloaded, it maintains its detwinned martensitic state. Heating the material above its austenitic transformation (start) temperature and in the absence of stress, will cause the material to re-orient its structure and recover any inelastic (transformation) strain in the process. When the material cools down, it transforms back to martensite and its twinned structure with no shape change [1]. This shape memory effect is illustrated in the figure below.

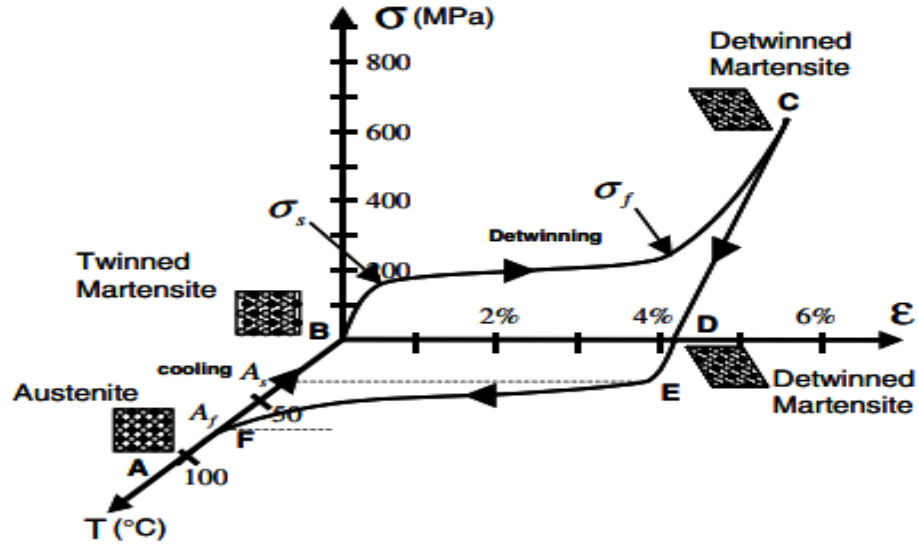


Figure 4: Stress-Strain-Temperature Curve of NiTi Illustrating SME (Reprinted from [1])

This is called a one-way shape memory effect since the strain recovery occurs in one direction only when the material is heated. Phase transformations from/to austenitic and martensitic states are transformations in the lattice that involves shearing deformations and synchronized atomic movements. The difference in free energy between the two phases is the main cause of transformation. While the SMA undergoes this transformation process, it follows different forward and reverse paths, thus, exhibits a thermal hysteresis. The hysteresis curve is shown in the figure below. The typical definition of hysteresis is the difference between the temperature at which 50% of austenite is transformed while heating and 50% of martensite is formed while cooling. This hysteresis, along with nonlinearity of SMAs, causes a lot of issues for position control of SMA actuators, thus, is an active modelling area of research [10].

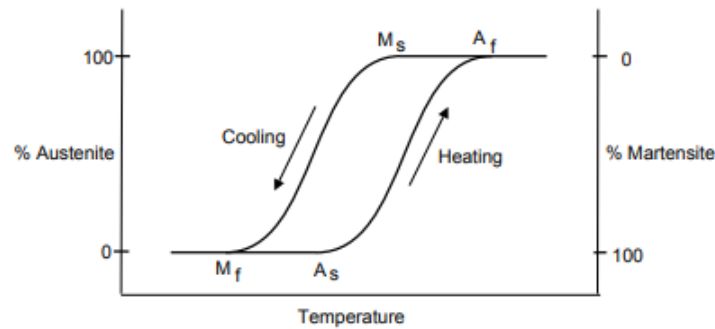


Figure 5: Hysteresis Curve of SMAs (Reprinted from [4])

Two-way Shape Memory Effect

SMA also exhibit a two-way shape memory effect (TWSME) when subjected to thermal cyclic loading under constant stress. This manifests itself as a two-way shape change (e.g. extension-contraction) between a memorized austenitic shape and another memorized shape in the martensitic phase without the need for mechanical loading. It occurs after a material has been thermo-mechanically loaded for large number of cycles along the same path. A process that is referred to as “training” of SMAs [1].

Pseudoelasticity

Another unique feature of SMA is pseudoelasticity or sometimes referred to as “superelasticity”. This describes SMA when they undergo a stress-induced phase transformation at high temperature (above austenite finish temperature). It is referred to as superelasticity because the material can be strained for up to 12% and recover it all once unloaded. Unlike SMEs which are temperature-induced, superelasticity occurs when materials in the austenite phase are stressed at constant temperature and martensite starts forming which can exhibit large recoverable strain with no plastic deformation

[11]. An illustration of the superelasticity feature of SMAs can be shown in the stress-strain curve in Figure 6. It shows the stress-induced phase change from austenite to martensite (while loading) then back to austenite after unloading with no permanent strain.

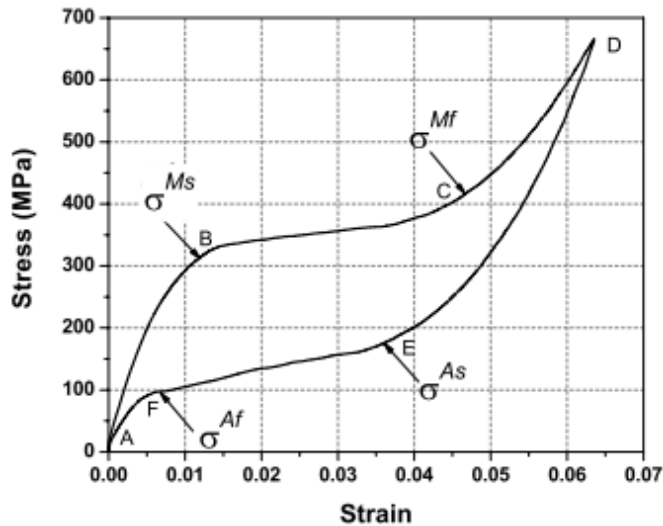


Figure 6: Pseudoelastic Behavior of SMAAS (Reprinted from [1])

SMA Materials & Shapes

Different SMA materials currently exist, however, nickel titanium (referred to as nitinol) is the most widely used and most well documented material by literature and manufacturers. NiTi based alloys (e.g. NiTiFe, NiTiCu, NiTi-Nb..etc) are also widely used and commercially available [16]. A detailed list of SMA materials and their characteristics is shown in the table below.

Table 1: Detailed List of SMA Materials and their Characteristics (Reprinted from [6])

Alloy	Composition	Range of transformation temperatures (A_s) °C	Transformation hysteresis, °C
AgCd	44 ~49 at %Cd	-190 ~50	~15
AuCd	46.5~50 at %Cd	30~100	~15
CuAlNi	14~14.5 wt %Al 3~4.5 wt % Ni	-140~100	~35
CuSn	~15 at % X	-120~30	
CuZn	38.5~41.5 wt % Zn	-180~-10	~10
CuZn X (X=Si,Sn,Al)	small wt % X	-180~200	~10
InTl	18~23 at %Tl	60~100	~4
NiAl	36~38 at % Al	-180~100	~10
TiNi	46.2~51 at % Ti	-50~110	~30
TiNi X (X=Pd,Pt)	50 at % Ni+X 5~ 50 at % X	-200~700	~100
TiNiCu	~15 at % Cu	-150~100	~50
TiNiNb	~15 at % Nb	-200~50	~125
TiNiAu	50 at % Ni+Au	20~610	
TiPd X (X=Cr,Fe)	50 at % Pd+X ~15 at % X	0~600	~50
MnCu	5~35 at % Cu	-250~180	~25
FeMnSi	32 wt% Mn, 6wt%Si	-200~150	~100
FePt	~25 at % Pt	~-130	~4
FePd	~30 at % Pd	~50	
FeNi X (X=C,Co,Cr)	small wt% X		

A material that is not in the list above is NiTiFe which started becoming more accessible in the market and is typically used for low temperature applications. NiTiCu has the advantages of improved functional fatigue when compared to NiTi while NiTi-Pd/Pt/Zr and Hf are widely used for high temperature applications [16].

The composition of SMA materials also significantly affects not only its mechanical properties but also its transformation/activation temperatures. The figure below shows the effect of Ni and Ti content concentration on the martensitic and austenitic start temperature. It also shows the effect of Aging on stabilizing the transformation temperatures. An aged 50-51 atomic percentage of Nickel and 50 atomic

percentage of Ti compound is recommended for a stable transformation temperature [7].

The 50%-50% NiTi is the most common in the market [16].

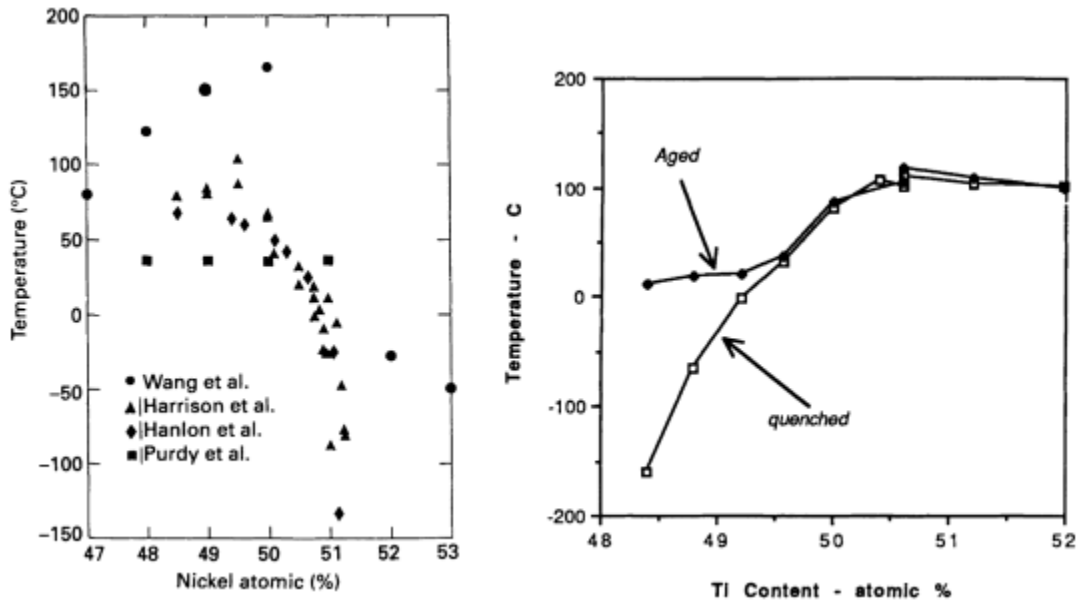





Figure 7: Effect of Composition on Transformation Temperatures (Reprinted from [7])

As for the shapes of SMAs, aside from custom production, SMAs are standardly available as wires, rods, sheets, plates, ribbons and springs [17]. However, since the intended application for this research is a planar miniature device and since the literature studied intensively SMA wires and springs only, emphasis is put on those shapes.

The available SMA springs and wires in the market for miniature devices and their geometric ranges are shown in Table 2.

Table 2: SMA Shapes and Parameters in the Market (Adapted from [8] & [17])

	Wire	Micro Helical Spring	Micro Flat Spring
Shape			
Selection Parameters	Length (L), Diameter (D) & Transformation Temperature (T)	Wire Diameter (d), Mandrel Size (D), Pitch (P), Transition Temperature (T), Length (L)	Wire Diameter (d), Transition Temperature (T), Length (L) Spring Amplitude(A), Spring Wavelength (WL)
Available Ranges	L (unlimited) D (0.025 – 0.75 mm) T (70 / 90 C)	L (unlimited) d (0.025 – 0.75 mm) T (-15 / 20 / 35 / 45 / 70 / 80 / 90 C) D (0.5 – 3.2 mm) P (0.5-4 times d)	L (unlimited) d (0.025 – 0.75 mm) T (-15 / 20 / 35 / 45 / 70 / 80 / 90 C) A – Per Request WL – Per Request

The main difference between SMA wires and springs is in the maximum actuation stroke and force. This difference is inherited from the type of motion that each shape exhibit. For example, tensile/compression springs exhibit a rigid-body motion when loaded which is governed by shear stresses at the coils while stretching or contracting. On the other hand, wires (or circular rods in general) undergo straining when elongated or compressed which is governed by tensile or compressive stresses. Therefore, SMA wires generally exhibit less actuation stroke than SMA springs. On the other hand, SMA wires exerts larger actuation force to recover the strain once loaded and heated [12]. A summary of the functional difference between SMA wires and springs in terms of stroke length, force and fatigue is listed in the table below.

Table 3: Comparison Between NiTi Wires and Springs (Reprinted from [12])

Actuator form	Properties	Remarks
Wire	<ul style="list-style-type: none"> ▪ Actuation stroke up to ca. 5% strain. ▪ Actuation force up to 200 MPa (full stroke) or 350 MPa (reduced stroke) for trained NiTi actuators. ▪ Very moderate dynamic requirements (less than 1 Hz). ▪ On-Off actuation. ▪ Translational movement or rotation angles less than 90. ▪ Fatigue cycles up to 10^6. 	<ul style="list-style-type: none"> ▪ Optimal usage of material where minimal use of material for amount of work generated. ▪ Tension loading: produces highest efficiency compared to other load types.
Spring	<ul style="list-style-type: none"> ▪ Recommended to apply external heat source for heating. ▪ Any kind of stroke, but typically less than 30mm. ▪ No dynamic requirements. ▪ Actuation force up to 200 MPa (full stroke) or 350 MPa (reduced stroke) for trained NiTi actuators. ▪ Translational movement. ▪ Fatigue cycles up to 0.5×10^6 	<ul style="list-style-type: none"> ▪ Large macroscopic displacement out of a relatively small microscopic strain, but the stress distribution over the cross-section of the spring is not constant. ▪ Need greater material volume to generate the same force (low efficiency than wire). ▪ Poor dynamic response (low bandwidth) due to the larger material (low surface area-to-volume ratio). ▪ Only the outer surface actually contracts, but the inner surface acts as both heat dissipater and opposing force to the desired direction.

SMA Actuators

Configurations

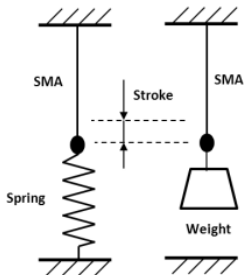
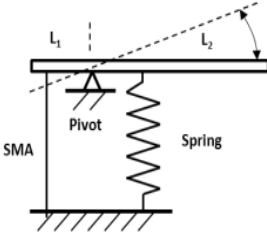
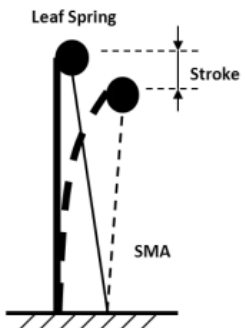
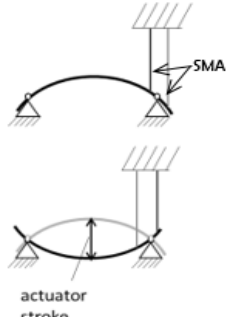
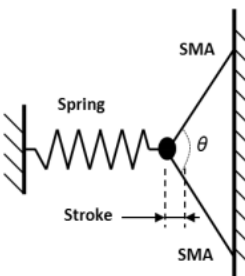
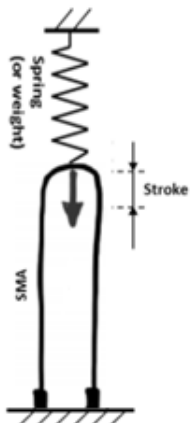
Although the SMA effect is often demonstrated using a piece of bent wire, SMAs are more efficient as actuators when loaded in tension/compression. In terms of work density and energy efficiency, tension/compression is more than 5 times better than torsion and 100 times better than bending [14]. An evaluation of the work density and energy efficiency of those different loading cases is summarized in the following table.

Table 4: Efficiency of SMA Actuators under Different Loading Cases (Reprinted from [14])

Load case	Work density ($\frac{J}{kg}$)	Energy efficiency (%)
Tension/Compression	466	1.3
Torsion	82	0.23
Bending	4.6	0.013

Therefore, for a SMA-actuated device, it is recommended to use SMAs under tension/compression. Accordingly, a research of different configurations of SMA actuators under tension/compression and their resultant stroke length and force was conducted and summarized in the table below.

Table 5: Configurations of SMA Actuators (Adapted from [8][12][18])

Configuration	Notes	Configuration	Notes
	<p>Max Stroke = $4\%.L_{SMA}$ Max Force = $100\%.F_{SMA}$</p>		<p>Max Stroke = 120° Max Force = $(L_1/L_2).F_{SMA}$</p>
	<p>Max Stroke = $7\%.L_{SMA}$ Max Force = $100\%.F_{SMA}$</p>		<p>Stroke $\gg 4\%.L_{SMA}$ Force $\gg 100\%.F_{SMA}$</p>
	<p>Max Stroke = $14\%.L_{SMA}$ Max Force = $25\%.F_{SMA}$</p> <p>Formulation: $\Delta x = L_{SMA} \cos \alpha - \sqrt{((L_{SMA} - \Delta L_{SMA})^2 - (L_{SMA} \cdot \sin \alpha)^2)}$ where $\alpha = \theta/2$</p>		<p>Max Stroke = $4\%.L_{SMA}$ Max Force = $100\%.F_{SMA}$</p>

Those configurations are helpful when designing SMA actuated devices to select the SMA geometry/shape that will yield the required the stroke length and force under the selected configurations. These configurations are application-specific. For example, the above-listed configurations are for translational, rotary and deformational motions. Using a lever rotational configuration would result in a mechanical force and actuation stroke gain. This can be helpful if either force or actuation stroke need to be amplified. Similarly, the levered beam from two ends which undergoes a snap-like deformational motion can be used for a higher stroke and force. The rest of the configurations are for marginally higher strokes 4%-14% under the same actuation forces.

Applications

SMA actuators are applicable to a wide range of industries including aerospace, automotive, robotics and infrastructure. Some potential applications in those industries are listed in the table below.

Table 6: Potential Applications for SMAs (Reprinted from [12])

<i>Configuration</i>	<i>Potential Applications</i>
SMA tendons, wires and cylinders	Adaptive control and actuation of aircraft flight surfaces
Embedded SMA wires	Shape-adaptive composite materials
SMA actuators	Transmission line sag control and ice removal from overhead power lines
SMA energy absorbers and tendons	Earthquake-resistant building and bridges, bridge and structural repairs
SMA dampers	Engine mountings, structural supports
SMA wires, wings, legs, actuators, etc.	Mobile micro-robots, robot arms and grippers
SMA wires, composites, etc.	Prosthetics, artificial muscles

Challenges

In the face of many incentives to use SMAs as actuators (e.g. work density, ease of miniaturization..etc), there are some challenges associated their use. Aside from the non-linearity and slow operation which was deemed unnecessary for the intended application in Chapter I, main challenge of SMA actuators is the small recoverable strain. Typically, a NiTi SMA has a maximum of 8% recoverable strain after undergoing transformation. This 8% max recoverable strain is found experimentally from a stress strain curve of loading in martensite similar to the one shown below where ϵ_L represents the maximum recoverable strain [13].

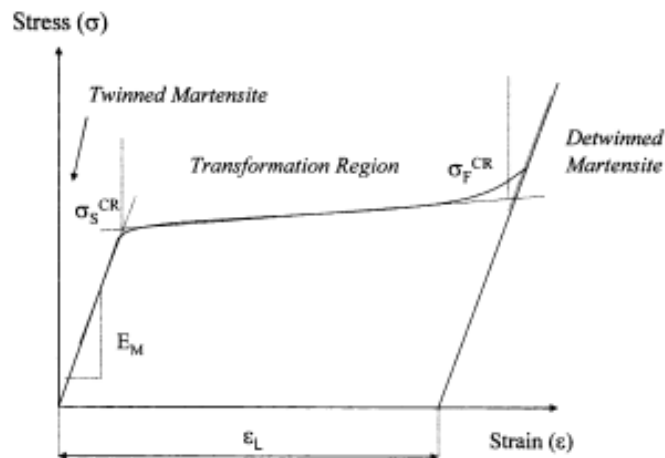


Figure 8: Stress-Strain Curve of SMAs Showing the Transformation Region (Reprinted from [13])

When an SMA is loaded while in martensitic state, it first undergoes elastic strain up until it reaches a start critical stress above which the martensite starts detwinning

results in inelastic strain. The change in the martensitic crystal structure occurs until a critical stress limit is reached after which plastic deformation occurs. The strain value corresponding to the final critical stress is what's called the max recoverable strain for SMAs during transformation. This is found to be around 8% for NiTi wires [13].

However, the 8% max recoverable strain is not suitable for cyclic loading as it fatigues at a high rate. Therefore, a rule of thumb for SMA wires is to account for 4% actuation strain only to achieve a multiple thousands lifecycle [1]. This rule-of-thumb is empirically based and a more detailed examination of the fatiguing of SMAs is discussed in Chapter IV.

Aside from the small actuation stroke range, two major issues arise with actuating SMAs particularly against a load or in a protagonist-antagonist formation. Those two challenges are; 1- unrecoverable strain within the actuation range even when heated 2- relaxation of the SMA wire after cooling [15]. Those two challenges are illustrated in the diagram below in the transition from figure f to figure g and figure g to figure h or figure I to figure j respectively.

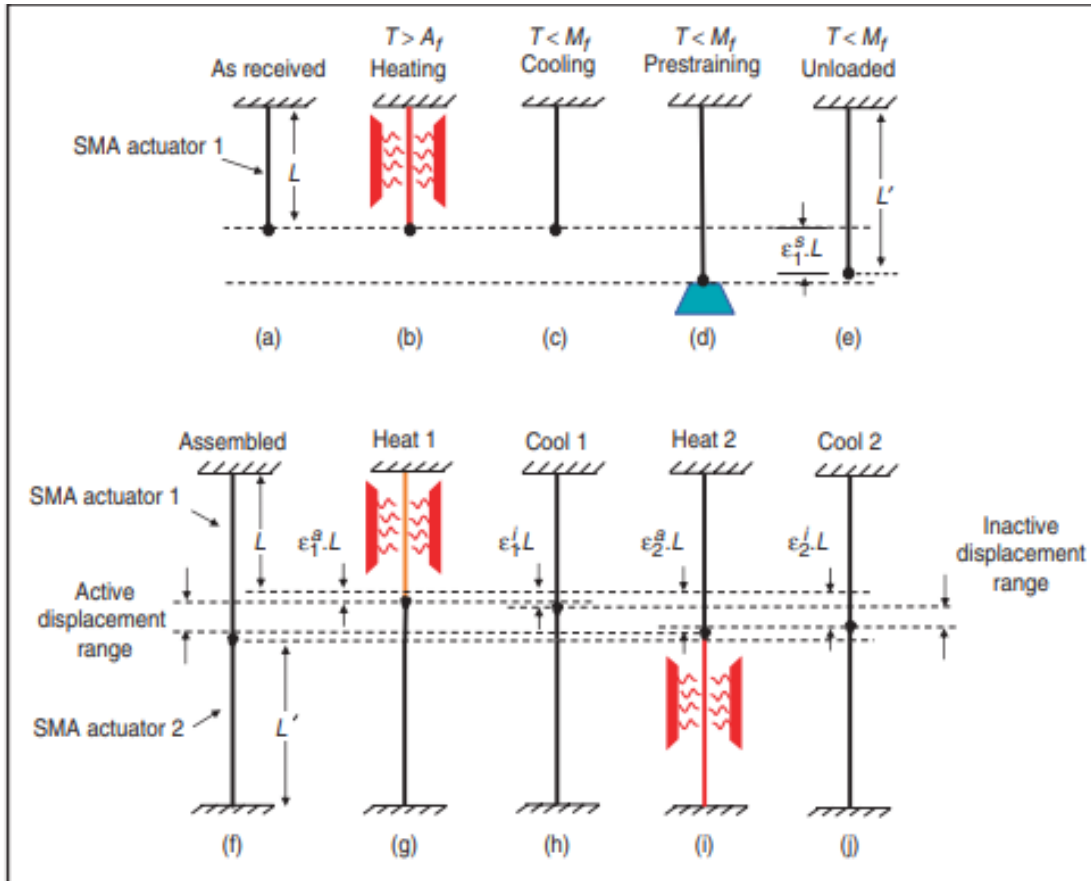


Figure 9: Schematic of SMA Antagonist Motion Showing Inactive Regions (Reprinted from [15])

The unrecoverable strain in the actuation range occurs when an SMA actuator contracts when heated while being resisted from the other antagonist SMA actuator. The resistance force from the un-heated competing SMA causes the formation of a stress-induced martensite (even when heated above the austenite finish temperature). This stress-induced martensite corresponds to the unrecovered strain since it was not fully transformed to austenite. The relaxation of the SMA occurs after the material cools down to twinned martensite state due to internal stresses and mostly stresses from the antagonist SMA which causes detwinning of the martensite in protagonist SMA causing

it to relax [15]. This relaxation was also observed in cyclic testing performed by a colleague on a segmented SMA wire of which each segment (of equal length) was selectively heated. Results from his cyclic testing can be seen in the figure below where red represents heating and blue color represents cooling [48].

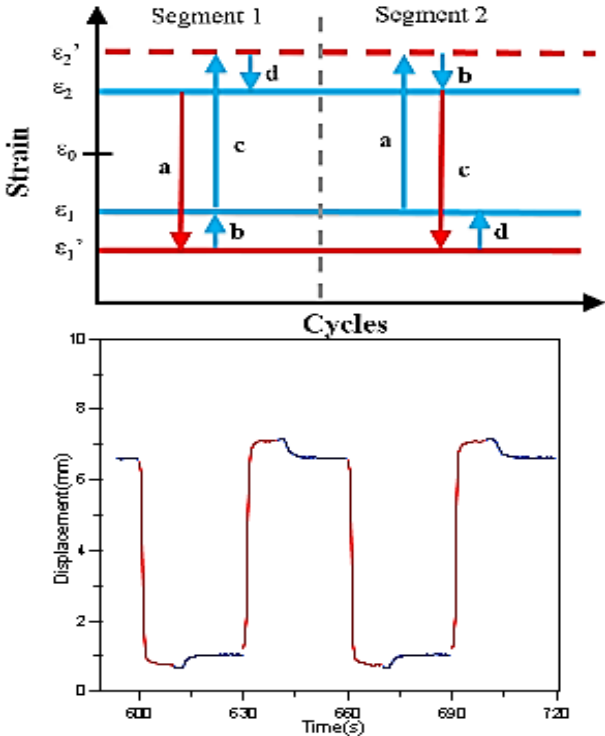


Figure 10: Cyclic Testing of Antagonistic SMAs Showing Relaxation (Reprinted from [48])

Those challenges would greatly affect the performance of a SMA-actuated switch since any unrecoverable strain or relaxation or disturbance in the motion of the actuator (which is driving the electric contacts) may lead to instable switching of electric load circuits. Therefore, in this thesis, emphasis will be put on designing for minimal

strain requirement ($\leq 4\%$) and accounting for unrecoverable strain and relaxation in the design of SMAAS.

SMA-Based Switches

Initial literature review showed no practical applications of SMAs for an electric switching device. However, multiple sources in the literature employed SMAs in actuators and thermal switches in a fashion that can inspire design concepts for an electric switch. In addition, some theoretical design concepts for SMA electric switches were found in the literature mostly in a patent format. Below is the list of these SMA-based switches as found in the literature.

1. SMA cryogenic thermal switch [10]

A master thesis project involved the design and fabrication of a thermal switch where an SMA spring is activated (through heat transferred from a hot liquid) in order to bring copper contacts together and start conducting heat through them. The advantage of such idea is the integration of sensing and actuation mechanisms in the form of SMAs and a potential application for it is heat sinks. A schematic of the proposed thermal switch is shown in the figure below.

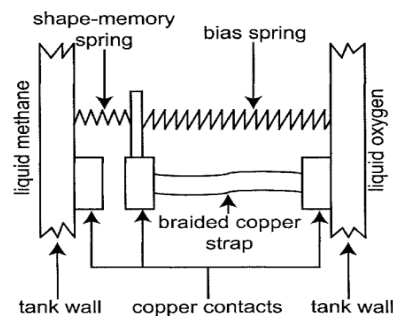


Figure 11: SMA Cryogenic Thermal Switch (Reprinted from [10])

2. SMA Damper-Controlled Switch [19]

This is a patented-concept of a device that controls the speed of actuation of an SMA wire through controlling the heating power supply to the SMA. As seen in the schematic below, a high-speed actuation of the SMA would force the moving contact away from the stationary contact breaking the heating electric circuit, thus, slows or stops the actuation of the SMA (i.e. damping its motion).

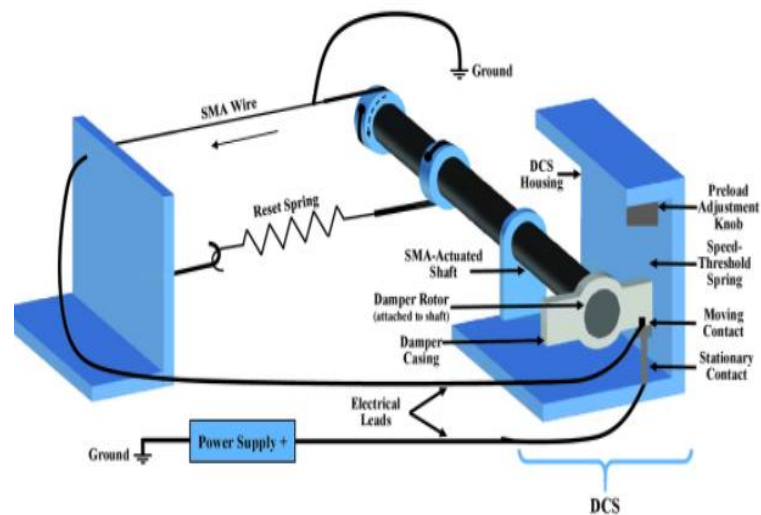


Figure 12: SMA Damper-Controlled Switch (Reprinted from [19])

3. SMA Bistable Electric Switch [20]

This patent describes a SMA-actuated bi-stable switch that consists of a flexural member (14) which is actuated by two antagonistic SMAs (16 & 18) as shown in the figure below. In one configuration (left), the flexural member is used to push a plunger (28) that pushes two electric contacts together (38/30 and 32). In another configuration

(right), the flexural member itself is used to conduct electricity between two stationary electric contacts (38 and 32).

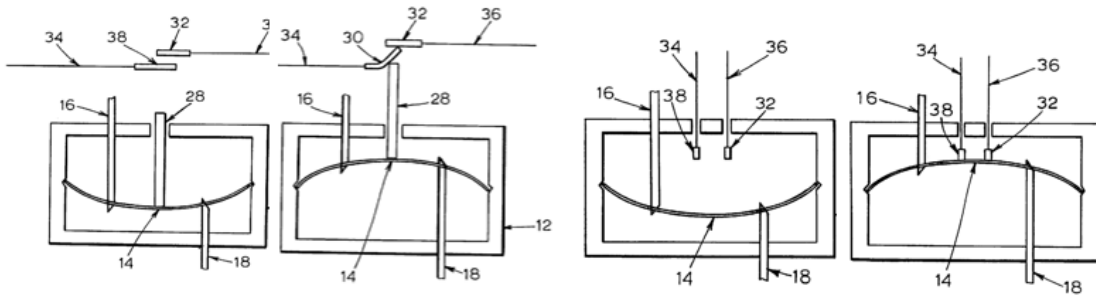


Figure 13: SMA Bistable Electric Switch Concept (Reprinted from [20])

4. SMA Planar Micro Electric Switch [21]

This patent describes a SMA switch consisting of a SMA wire crimped using flaps onto a metal stamped substrate and a profiled plunger. The SMA is actuated against a spring to push a pair of electric cantilever contacts together, thus, closing an electric circuit. A schematic of the patent and the labels for its components can be seen in the figure below.

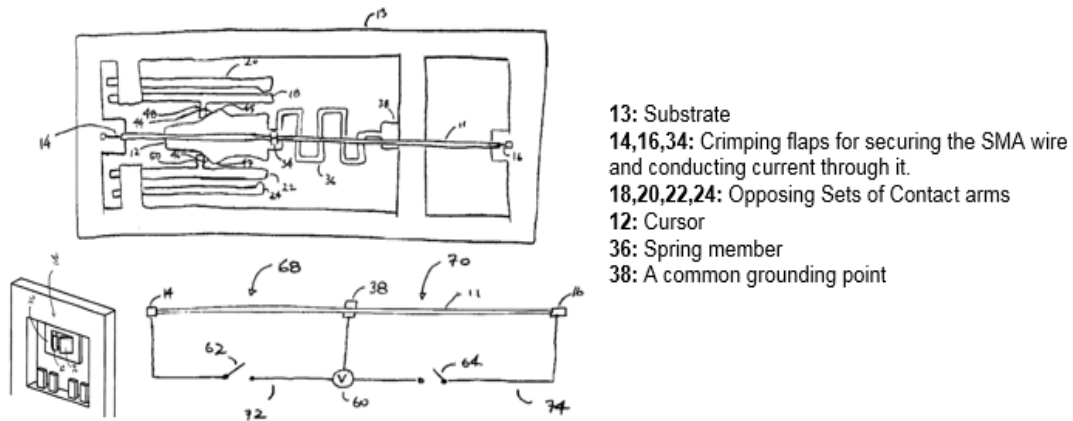


Figure 14: SMA Planar Micro Electric Switch Concept (Reprinted from [21])

5. SMA Diaphragm Based Switch [22]

This patent describes a circular switch that consists of a flapper pivoted on top of a SMA- wire-biasing-spring system. When the SMA is actuated, the flapper pivots around the actuation system onto the walls of the switch where electric contacts are embedded, thus, closing an electric circuit once it touches the walls. A schematic of the device and the labels for its components can be seen in the figure below.

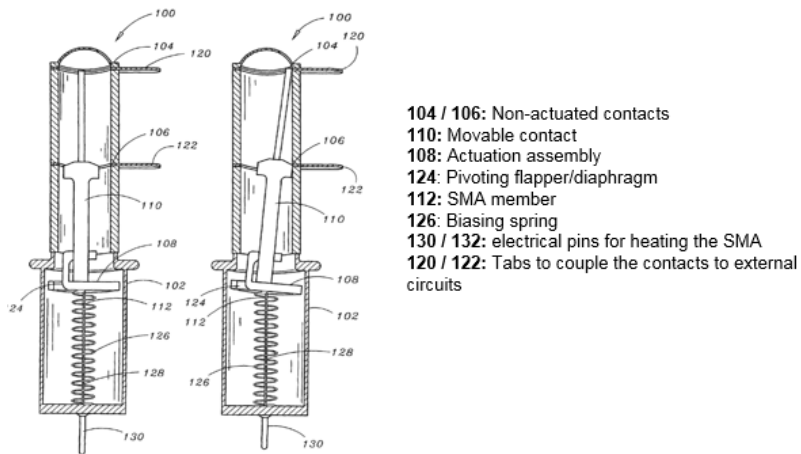


Figure 15: SMA Diaphragm Based Switch Concept (Reprinted from [22])

6. Bistable SMA Leaf-spring Switch [23]

This patent describes a SMA bi-stable switch that (similarly to patent #3 described above) is based on a flexural member/leaf spring. This leaf spring has a drive element embedded in its center which is being pushed by opposite SMA wires once activated. The drive element pushes the inactive SMA towards a stationery contact (i.e. completing an electric circuit). A schematic of this switch and its operation modes are shown in the figure below.

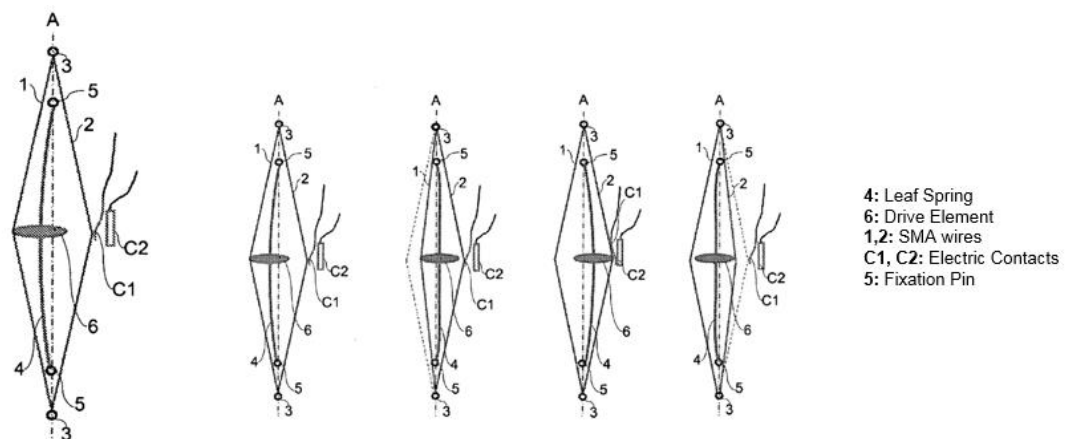


Figure 16: Bistable SMA Leaf Spring Switch Concept (Reprinted from [23])

7. SMA Flexible-member Switch [24]

This patent describes a switch that consists of a cantilevered flexural member (12a) that is anchored to a substrate at point 14 and has a SMA wire (60) routed through its tip and fixated too to the substrate at point 64. At the free end of the flexural member a conductive pad (22) is placed such that once the SMA is activated, the flexural member is deformed vertically and the conductive pad connects two stationery contact

(20 a & b). The schematic below shows the key components of the switch and its operation modes.

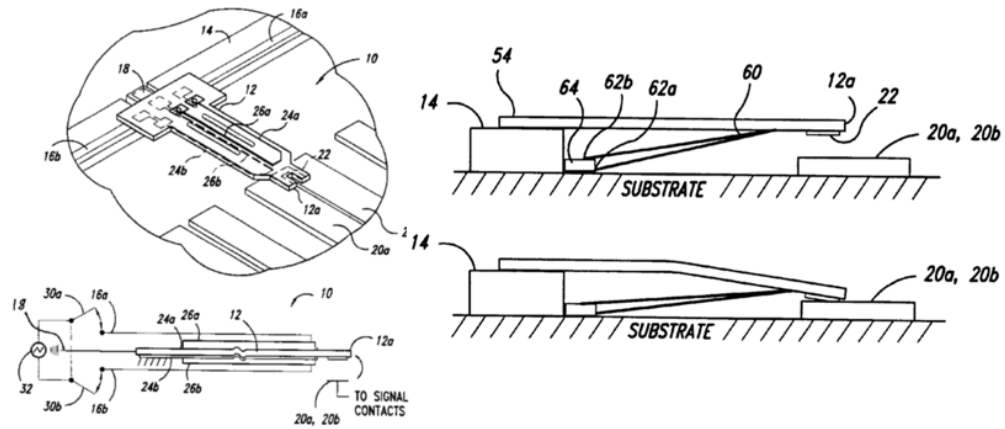


Figure 17: SMA Flexible-Member Switch Concept (Reprinted from [24])

8. SMA Bistable Lever-based Switch [25]

This patent describes a bi-stable switch concept that is based on antagonistic SMA members and a lever as shown in the schematic below. In the first configuration (left), SMAs (11 & 22) drives a lever member (18) to close/open an electric circuit through movable and stationary contacts (27 & 28). In the other configuration (right), the SMA members (11) are used to deform a flexural member (32) anchored at a lever point in the center (31). The deformation brings together or separates electric contacts pairs (28-27 & 34-35), thus, switching on/off electric circuits.

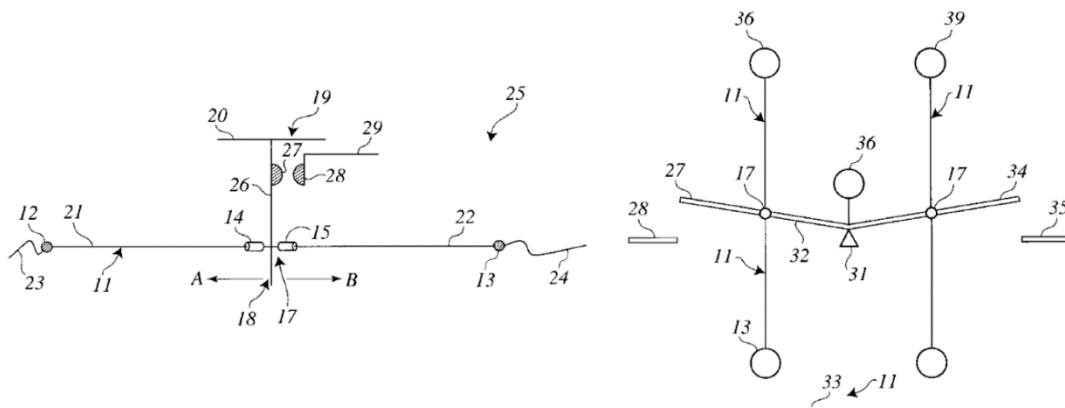


Figure 18: SMA Bistable Lever-based Switch Concept (Reprinted from [25])

These design concepts provide a good starting point for the design of a SMAAS. However, as discussed earlier, the SMAAS is required to have two stable switching states (i.e. 2 pairs of electric contacts in each side) and need to account for relaxation in the SMA. The switch concepts in the literature are based on one external circuit and a biasing mechanism (i.e. one stable state). In addition, most of these designs do not have a mechanism in place to overcome SMA relaxation. Therefore, accounting for these limitations, in the next chapter, a list of design concepts are generated for the SMAAS; some of which are inspired by the aforementioned switch concepts in the literature while the majority are novel concepts.

CHAPTER III
CANDIDATE DESIGNS

Design Framework

Objectives & Constraints

First step to investigate the feasibility of the SMAAS is to define a design framework that will guide the design process. This high-level framework can be represented in terms of the constraints imposed on, and the objectives that needs to be achieved by, the SMAAS to be a viable option for the intended application. As discussed in Chapter I, the intended application is to embed a grid of SMAASs onto Smart Photovoltaic Skin to switch between active and inactive PV cells on demand.

Therefore, the SMAAS need to be relatively small and planar with a low profile in order to fit on the back of the PV skin. Since PV skins are intended to maximize energy harvesting, the SMAAS need to be energy-efficient with low energy-per actuation event. In addition, PV cell electrical connections won't be reconfigured all that frequently except for when the environmental conditions change (e.g. solar irradiance angle change). Therefore, high switching frequency is not necessary and a high cycle lifetime is not required but preferable to the extent that this implies long-service life with high reliability. In order to put a scale to these constraints, the table below shows the objectives and a quantification of the imposed constraints on the SMAAS design.

Table 7: Design Objectives and Constraints for the SMAAS

Design Objectives	Design Constraints
<ul style="list-style-type: none">• Minimize EPSE (Energy per switch event)• Minimize out-of-plane (z-height) switch thickness	<ul style="list-style-type: none">• Cycle lifetime: 10,000 cycles min.• Switch cycle rate: once per solar hour• Blocking voltage (Ex: 100V min)• Conducting current (Ex: 0.5A min)• Max Footprint (20mm*20mm)• Max spot temperature imposed on PV skin (ex: 100C for EVA)

The switch actuation energy and planarity are objectives that need to be minimized. No quantification or a scale is required for the initial design. The maximum footprint and spot temperature value come from the current size and material of PV skin. The switch cycle rate, cycle lifetime, blocking voltage and conducting current are reasonable values for the application. It is worth noting that these constraints' values are exemplary and are intended to guide the design process but not limit it. In addition to the above mentioned constraints, the following considerations are to be considered during the design process of the SMAAS:

- The design need to account for the relaxation in the SMA and account for any instability or vibrations that may jeopardize the stability of the electrical connections.
- The design is to have a bi-stable mode. i.e. two separate stable electrical connections (for external load circuit).
- The design is to utilize one-way shape memory effect only.
- The design is to have a high potential for miniaturization.

The aforementioned constraints and considerations will guide the generation of design concepts process which is discussed later in this chapter.

Locking Mechanisms

One way to account for relaxation of the SMA and to have robustness against vibration is to install a locking mechanism on the actuator. A survey of locking mechanisms for actuators is shown in the figure below by [27]. Those locking mechanisms will inspire the design concepts for the SMAAS.

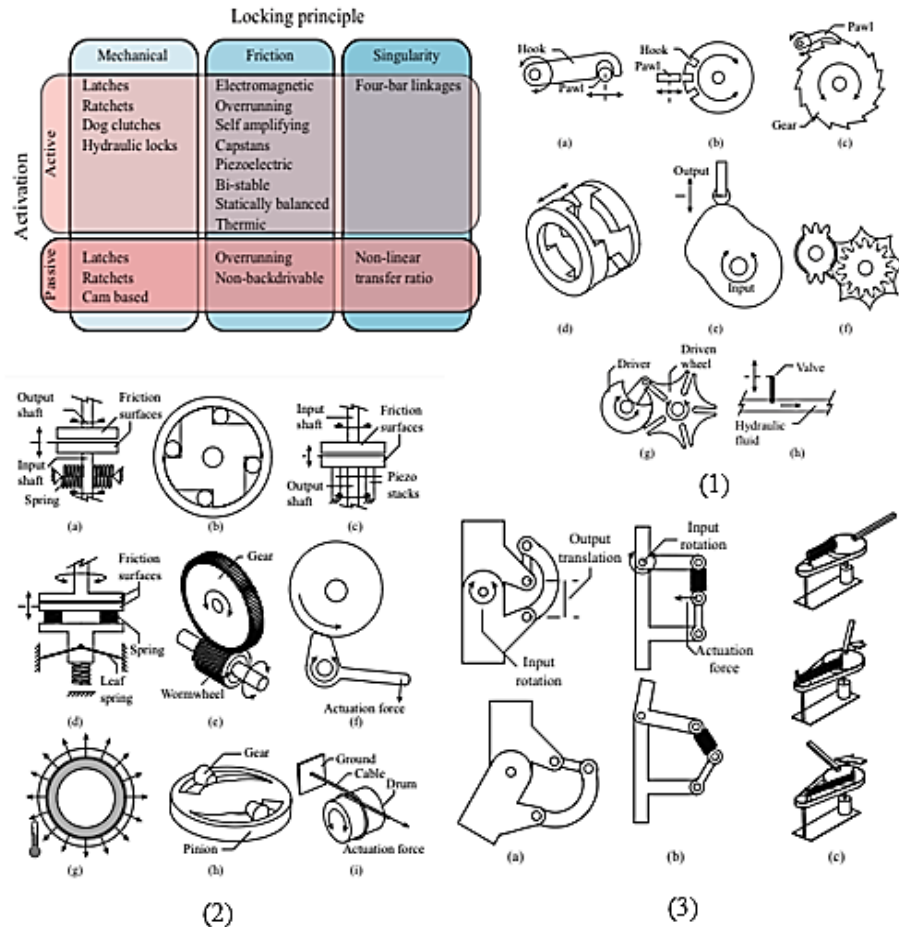


Figure 19: Locking mechanisms for actuators (Reprinted from [27]). 1- Mechanical mechanisms 2- Friction-based mechanism 3- Singularity mechanisms Conceptual Designs

Based on the designs in the literature, the intended application and the design framework aforementioned, 15 conceptual designs are generated covering the entire spectrum of SMAAS configurations, concepts and technologies used. No elimination of concepts is done at this stage. However, the conceptual designs need to clearly illustrate the mechanical moving parts, electrical connections (see figure below) and SMA configurations. The use of SMA springs or wires in these design concepts is interchangeable. A list of generated design concepts is as follows:

P	: Positive Power Signal Terminal
N	: Negative Power Signal Terminal
C+	: Positive Control Signal Terminal
C-	: Negative Control Signal Terminal

Figure 20: Terminology for Electrical Connections in the Design Concepts

1. Tri-state Spring-biased Lever Concept

This lever concept provides a tri-state operation mode where the lever arm is controlled by a torsional spring and two SMA actuators from both sides that when activated, they toggle the lever arm towards one of the two stationary electrical contacts. A schematic of this design concept is shown in the figure below.

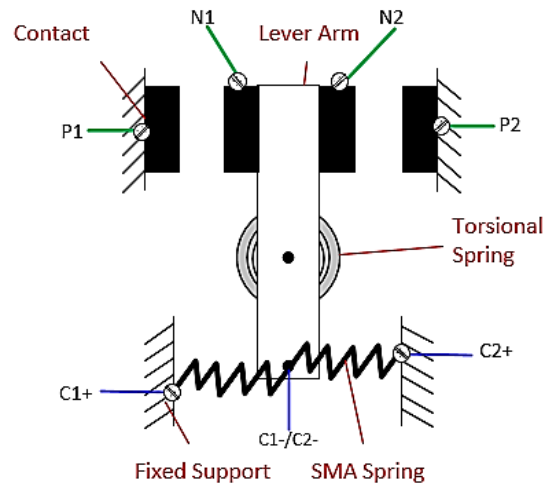


Figure 21: Top-View Schematic of the SMAAS Conceptual Design #1

Advantages of this design concept include; planarity and tri-state operation with center-off configuration. However, this concept does not provide a stable electrical connection at the switching states without holding power except for the neutral state. In addition, manufacturability of such concept in the micro scale could be challenging because of the presence of moving joints and a torsional spring.

2. Spring-Loaded Lever Concept

This design concept is inspired by the toggle switch mechanism where a spring-loaded lever arm slides horizontally along another lever arm (movable contact) which comes in contact with stationary contacts located below the two ends of the second lever arm. The spring-loaded lever is attached to two antagonistic SMA actuators from the top end. A schematic of this concept showing the neutral position versus the state position is shown below.

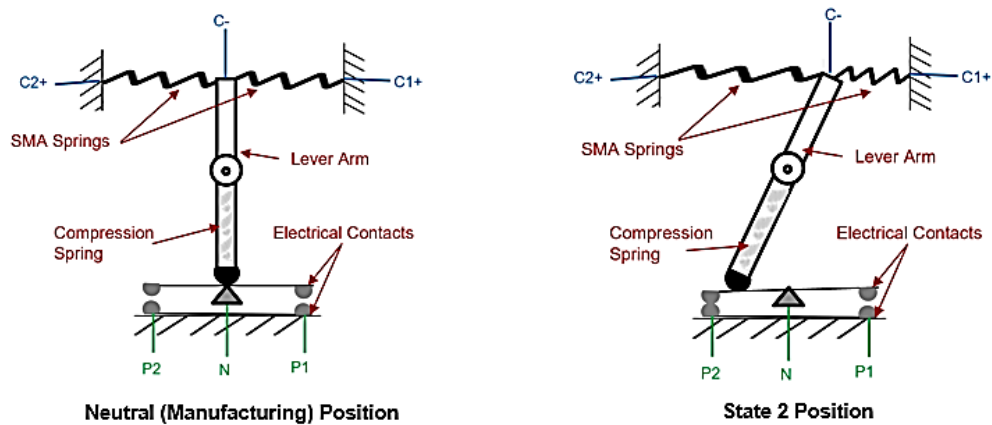


Figure 22: Top-View Schematic of the SMAAS Conceptual Design #2

This concept has the advantages of mechanical gain, robustness against vibrations and SMA relaxation as well as bi-stable operation mode. However, it does not have a center-off tri-state mode and manufacturability in the micro scale is potentially challenging for this concept due to the complexity of small moving parts and need for a pivot point.

3. Deformable Lever Concept

This concept adds on to the same lever concept in the first concept but uses a deformable lever and without a torsional biasing spring. The idea behind having a deformable lever is that the restoring energy from the deformation of the lever after being brought to one end by the SMA would overcome the relaxation stress in the SMA, thus, provide stable electrical connection. Not using a torsional spring would allow for a bi-stable operation mode. A schematic of this design concept is shown in the figure below.

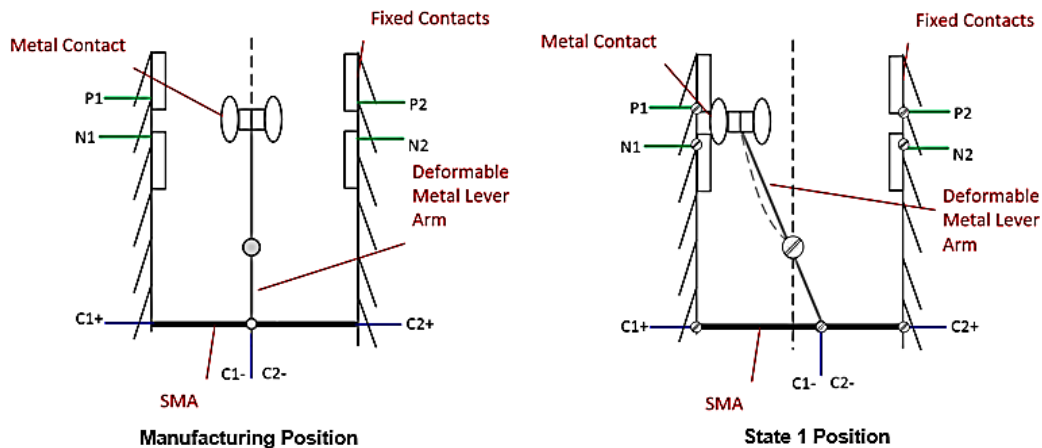


Figure 23: Top-View Schematic of the SMAAS Conceptual Design #3

Advantages of such design concept include; mechanical stroke gain, robustness against relaxation and bi-stability. However, a deformable lever is susceptible to vibrations and the deformation of the lever does not mechanically lock the movable and stationary contacts together, thus, could potentially not be enough to overcome relaxation.

4. Leaf-Spring loaded Contactor Concept

This concept moves from the rotary configuration to the linear translational configuration where a metal sphere “bullet” is actuated linearly by two antagonistic SMA actuators. The metal bullet is then brought to contact by the SMAs with stationary metal leaf spring contacts that are connected to the external load circuit. The idea behind the use of leaf spring contacts is that if designed such that the distance between them is less than the metal sphere width, they will deform elastically to accommodate the sphere. The restorative energy from this elastic deformation would produce pressure on the metal sphere, thus, locks it in place. A schematic of this design concept is shown below.

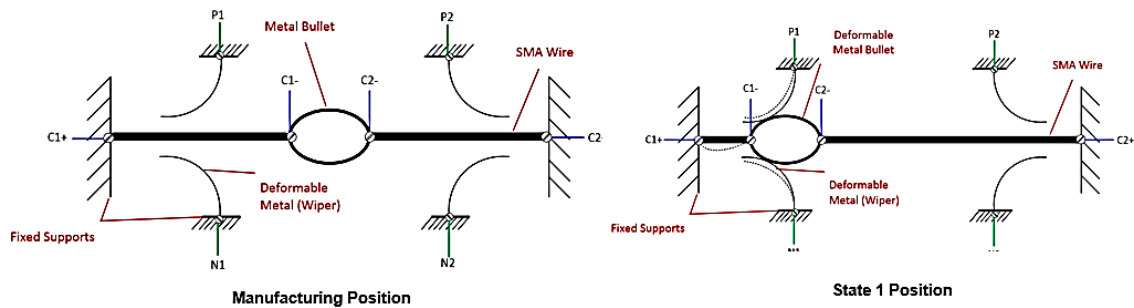


Figure 24: Top-View Schematic of the SMAAS Conceptual Design #4

Advantages of this design concept include; a locking force that accounts for SMA relaxation, a bi-stable operation mode and a relatively low complexity. However, challenges for this design include the vibration of the spring contacts as well as the resultant horizontal force from the SMA actuator.

5. Deformable Contactor Concept

This design concept is a variation of the above concept where the stationary contact is rigid and the metal sphere “bullet” is flexible. It has the similar idea behind it where the restorative energy from the elastic deformation of the sphere would potentially produce a locking force against the fixed contacts. A schematic of this concept is shown in the figure below.

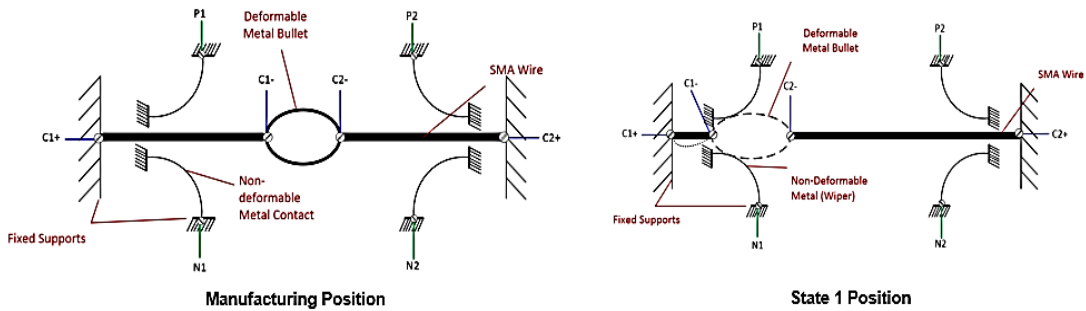


Figure 25: Top-View Schematic of the SMAAS Conceptual Design #5

This design concept have the advantages of resistance to vibration and SMA relaxation as well as a bi-stable operation mode. The only potential challenge with this concept is the design of the sphere material such that it can be deformable but not very elastic such that it would not produce a restorative pressure. Cyclic lifetime of such deformation is also a point of consideration.

6. Normally-Closed Leaf Contacts Concept

This design continues on the same linear plunger concept, however, it operates in a normally-closed mode. It uses an insulating plunger to separate two conducting elastic metal strips to break the electrical connection as shown in the schematic below.

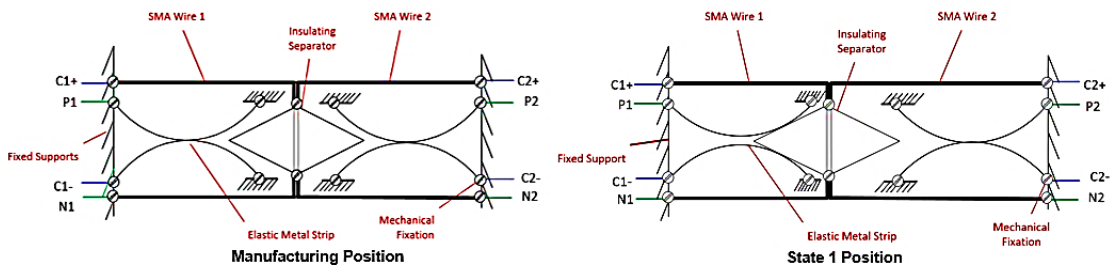


Figure 26: Top-View Schematic of the SMAAS Conceptual Design #6

Similar to the previous metal sphere designs, this concept has the challenge of the horizontal component of the resultant restorative force of the deformable contacts pushing the insulating plunger away from the contacts.

7. Deformable Contactor/Contacts Concept

This concept adds on to the previous concepts of having either deformable/elastic stationary contact or movable contact by having both contacts as elastic or deformable. The idea is that both of the contacts would produce restorative force against each other, thus, lock themselves together and maintain electrical connection along them. A schematic of the design concept is shown below.

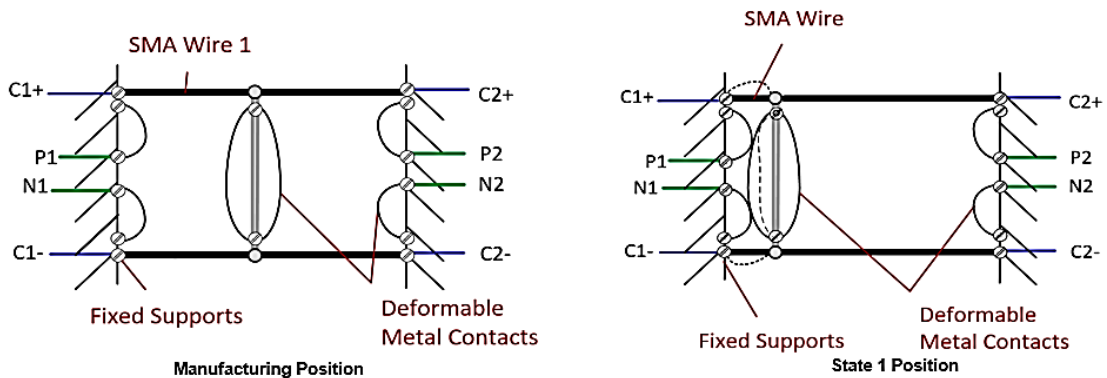


Figure 27: Top-View Schematic of the SMAAS Conceptual Design #7

The advantages of the design concept is the large locking force from both movable and stationary contacts. However, the challenge of designing both contacts and controlling their deformation such that the contacts' restorative forces cancel out each other as well as the susceptibility to vibrations are major points of concern for this design concept.

8. Snap-action Contactor Concept

This concept is inspired from the literature designs where a conductive flexural member supported from both ends is used to close connection between stationary electrical contacts. The concaved flexural member is driven by two antagonistic SMA actuators as shown in the figure below. The idea behind using a concaved elastic member as the main drive unit is that its snap-action restorative force would assist the speed and force of switching states and provide a protection against relaxation of SMA after cooling. The attachment of two competing SMA wire to a thin flexural member however presents a challenge.

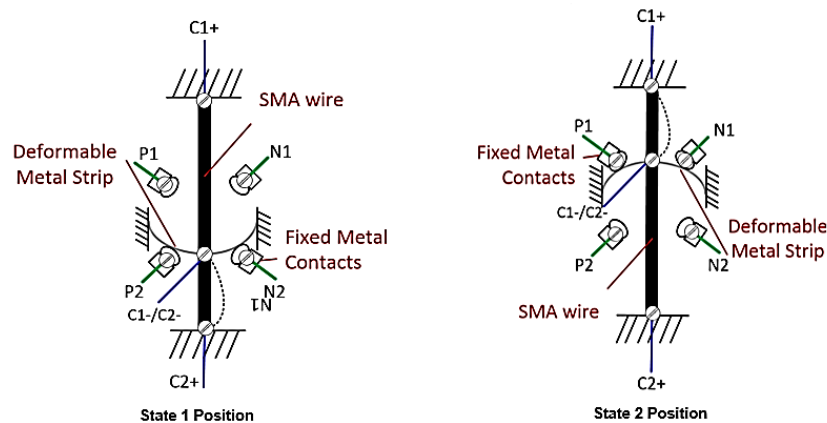


Figure 28: Top-View Schematic of the SMAAS Conceptual Design #8

9. Spring-Loaded Contactor Concept

Adding to the earlier concepts of a linear plunger, this concept uses a compression spring-loaded conductive plunger and a SMA wire routed through it to close a connection between two stationary electric contacts. The idea behind using a

compression spring is that its restorative force when compressed would produce a locking force that is intended to cancel out the relaxation force of the SMA when cooled. Routing the SMA through the plunger would eliminate the need for an electrical connection attached to the moving plunger to heat up the SMA as well as provide a larger available transformation strain at the expense of the energy required to actuate the wire. A schematic of the concept is shown in the figure below.

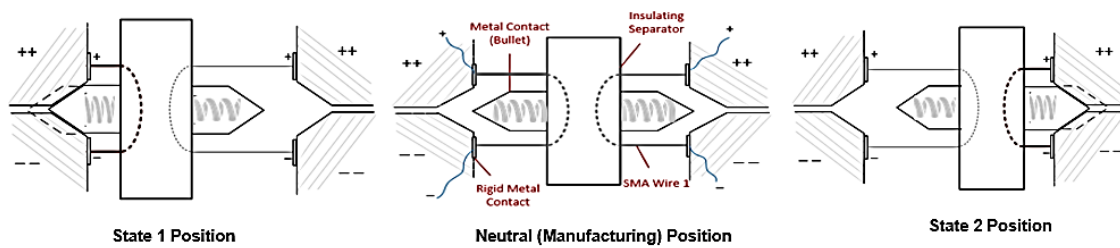


Figure 29: Top-View Schematic of the SMAAS Conceptual Design #9

This concept has the advantages of producing a locking force as well as a bi-stable operation. However, the design of such concept provides a level of complexity to match the relaxation force to that of the compression spring. In addition, this design exhibits susceptibility to vibrations as well as relatively high level of complexity both in design and manufacturability in terms of the moving parts and the micro embedded compression springs.

10. Spring-loaded Profiled Contactor Concept

This design concept adds to the metal sphere concept “bullet” where instead of using elastic leaf spring contacts, this concept uses planar zig-zag compression springs and a profiled plunger to create a latching mechanism. The zig zag springs provides dual

functionality; locking force and conducting current through the plunger for the load circuit. This concept is illustrated in the schematic below.

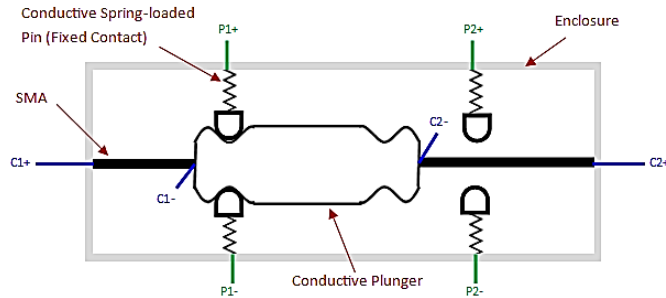


Figure 30: Top-View Schematic of the SMAAS Conceptual Design #10

The advantages of this model versus the “bullet” design is that it has a vertical component only of the restorative “locking” force and provides a mechanical latching function. Therefore, this design is resistant to SMA relaxation and electrical conduction interruption due to vibrations. On the other hand, this design has a high level of manufacturing complexity presented in the manufacturing and assembly of the planar zig zag springs especially in the micro scale.

11. Leaf Spring-loaded Profiled Contactor Concept

To overcome the manufacturability challenge of the previous design, the design was modified through replacing the planar zig zag springs with cantilevered leaf spring contacts while keeping the profiled plunger. This modified design concept is shown in the figure below.

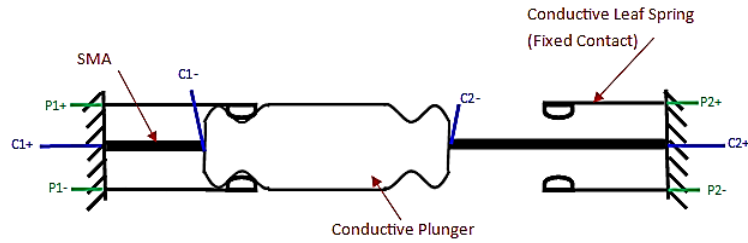


Figure 31: Top-View Schematic of the SMAAS Conceptual Design #11

12. Sliding Contacts Concept

This design concept uses small multiple sliding contacts attached to a conductive plunger such that they provide the dual functionality of providing resistance to the relaxation force of the SMA as well as acting as a grounding terminal for the heating circuits of the SMAs. An illustration of this concept and the working principle is shown in the figure below. The only challenge that arise with such concept is the lack of separation of the control (heating) circuits of the SMAs and the load circuits.

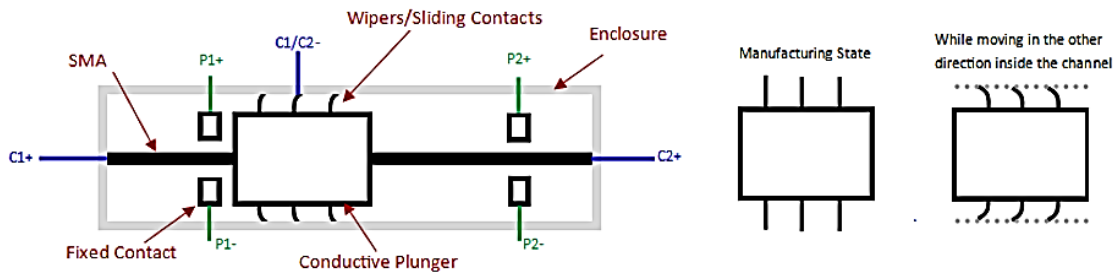


Figure 32: Top-View Schematic of the SMAAS Conceptual Design #12

13. Magnetic-latching Contacts Concept

This concept uses a permanent magnet plunger and a ferromagnetic rod on each side of the plunger, which is actuated by two antagonistic SMA actuators, to create a

magnetic latching mechanism. A schematic of this design concept is shown in the figure below. Advantages of having such system is a light complexity design and manufacturing in addition to strong resistance against electrical conduction interruption due to SMA relaxation or vibrations. The only key challenge for this design is isolating the permanent magnets from load circuit conduction path to avoid damage to them.

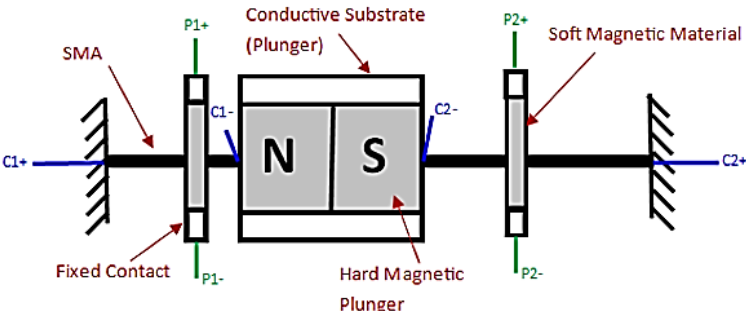


Figure 33: Top-View Schematic of the SMAAS Conceptual Design #13

14. Gripping Contactor Concept

Stemming from a concept in the literature of a micromachined microgripper (shown below – from [26]) and the friction-based locking mechanisms discussed earlier in this chapter, a new concept was generated for a rack-pinion driven plunger concept.

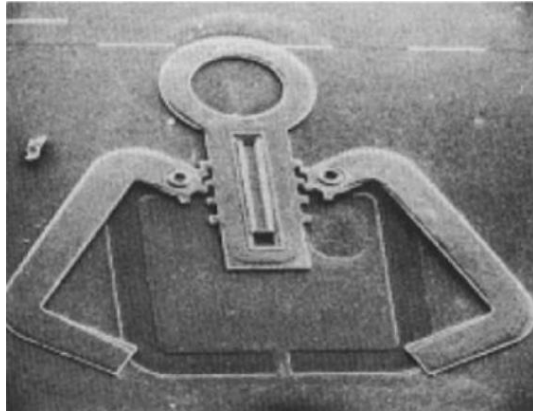


Figure 34: A Micro-Machined Microgripper (Reprinted from [26])

This design concept employs an insulating double-sided rack attached to a conductive plunger from both sides as well as two competing SMA actuators; one on each side as shown in the figure below. When one of the SMAs is activated, the rack moves towards the actuated SMA while simultaneously moving the conductive gripping arms attached to the pinion (which is actuated by the rack tooth) to grip onto the conductive plunger. Therefore, those gripper arms provide a dual functionality as a locking mechanism and as a terminal for the load circuit. The challenge with this design is the level of design and manufacturing complexity and the amount of gripping force left in the arms once the SMA is deactivated and left to cool down.

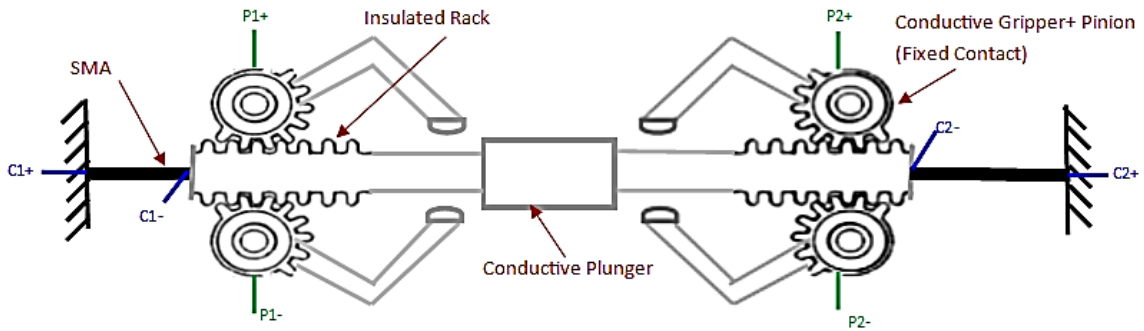


Figure 35: Top-View Schematic of the SMAAS Conceptual Design #14

15. Fixed-path Geared Contactor Concept

Similar to the previous design, this design concept uses a rack and a pinion to create a defined stroke path in addition to a friction-based locking mechanism to account for SMA relaxation as shown in the figure below. This concept has relatively the same advantages and disadvantages attributed to the previous design concept.

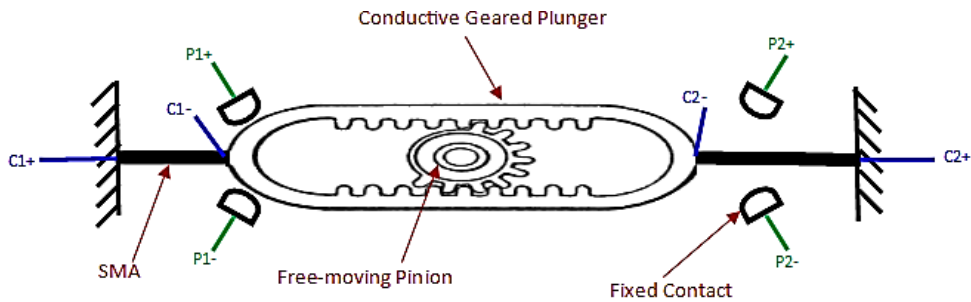


Figure 36: Top-View Schematic of the SMAAS Conceptual Design #15

Qualitative Assessment

Criteria

Based on the list of generated conceptual designs for the SMAAS, a qualitative assessment was conducted to down-select candidate feasible designs that can undergo more detailed analysis. This assessment is done against the following selection criteria:

- Robustness against electrical connection interruption (due to SMA relaxation and vibration)
- Planarity
- Manufacturability
- Complexity
- Ease of miniaturization

The robustness against interruption in electrical connections is assessed based on the existence and efficiency of a locking mechanism incorporated in the design concepts. The planarity is assessed based on the possibility of reducing the design concept to a 2D model (i.e. no multiple overlaying layers or large 3D objects or joints). The manufacturability and complexity are assessed based on the number of moving parts and the presence of joints which is not easy to manufacture/assemble especially in the micro scale. However, for more details on the manufacturability in the micro scale, refer to Chapter IV. Lastly, the ease of miniaturization depends on the number of components (both moving and stationary), complexity of components' geometry and the assembly layout of the design concept.

Assessment

Based on the criteria listed above, a qualitative assessment of the 15 design concepts was conducted in the form of a Pugh Matrix which compares the designs against the pre-set criteria as shown in the table below. The signs used for comparisons; --, -, 0, + and ++ represent a scale from negative to neutral to positive respectively.

Table 8: Pugh Matrix for Qualitative Down Selection of SMAAS Concepts

#	Concept	Robustness	Planarity	Manufacturability	Low Complexity	Ease of Miniaturization
1	Tri-state Spring-Biased Lever	--	-	0	0	0
2	Spring-loaded Lever	++	0	++	+	0
3	Deformable Lever	--	-	+	0	-
4	Leaf-Spring Loaded Contactor "bullet"	+	++	++	+	0
5	Deformable Contactor "bullet"	-	++	+	-	0
6	Normally-Closed Leaf Contacts	--	++	+	-	+
7	Deformable Contactor-Contacts	--	+	+	-	+
8	Snap Action Contactor	+	+	-	0	+
9	Spring-loaded Contactor	--	+	+	-	0
10	Spring-loaded Profiled Contactor	++	0	0	-	-
11	Leaf Spring-loaded Profiled Contactor	++	+	+	++	+
12	Sliding Contacts "wipers"	++	++	0	0	+
13	Magnetic Latching Contacts	++	++	+	+	++
14	Gripping Contactor	+	+	0	-	0
15	Fixed-Path Geared Contactor	+	+	0	-	0

Based on the Pugh matrix analysis of the conceptual designs, 5 designs were down-selected as feasible designs since they possessed a favorable assessment in the overall criteria with no major drawback in any of the areas. Those down-selected

feasible concepts are listed in the table below along with the main qualities of those concepts.

Table 9: Down-Selected Design Concepts After a Qualitative Assessment

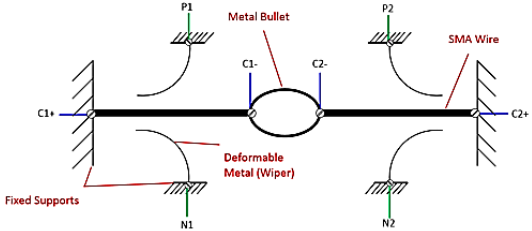
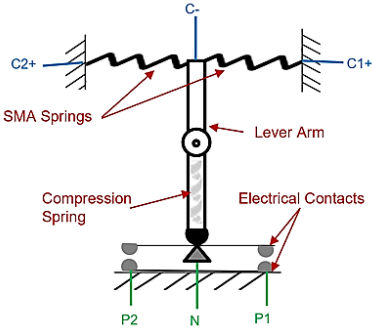
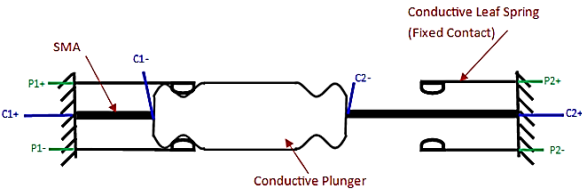
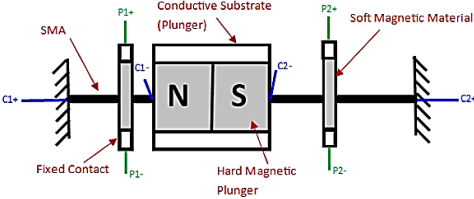
Concept	Illustration	Remarks
<p>Leaf-Spring loaded Contactor Concept</p>	 <p>The diagram shows a horizontal beam with fixed supports at both ends, labeled C1+ on the left and C2+ on the right. A central metal bullet is positioned on the beam. SMA wires are attached to the beam, with one end labeled P1 and the other P2. Deformable metal wipers are shown at the bottom, labeled N1 and N2. Labels C1- and C2- are also present near the bullet.</p>	<ul style="list-style-type: none"> - Easy to manufacture - Scalable - Robust against relaxation
<p>Spring-Loaded Lever Concept</p>	 <p>The diagram shows a vertical lever arm pivoted at the bottom. SMA springs are attached to the top of the lever, with labels C2+ on the left and C1+ on the right. A compression spring is located at the pivot point. Electrical contacts are shown at the bottom, labeled P2, N, and P1. A label C- is at the top of the lever.</p>	<ul style="list-style-type: none"> - Mechanical gain - Manufacturable within the specified footprint but not on the microscale - Enhanced switching speed - Robust against relaxation - Existing large-scale manufacturing systems (toggle switch) - Robustness against lifetime stroke degradation
<p>Leaf Spring-loaded Profiled Contactor Concept</p>	 <p>The diagram shows a horizontal assembly with a central conductive plunger. SMA wires are attached to the plunger, with labels P1+ and P1- on the left, and P2+ and P2- on the right. Labels C1- and C2- are also present. A conductive leaf spring (fixed contact) is shown on the right side.</p>	<ul style="list-style-type: none"> - Micro-manufacturable - Robust against relaxation - Scalable
<p>Magnetic-latching Contacts Concept</p>	 <p>The diagram shows a magnetic latching mechanism. A central conductive substrate (plunger) is shown with North (N) and South (S) poles. SMA wires are attached to the plunger, with labels P1+ and P1- on the left, and P2+ and P2- on the right. Labels C1- and C2- are also present. A fixed contact is on the left, and soft magnetic material is on the right.</p>	<ul style="list-style-type: none"> - High robustness against relaxation - Enhanced switching speed - Scalable - Micro Manufacturable - Robustness against lifetime stroke degradation

Table 9: Continued

Concept	Illustration	Remarks
Sliding Contacts Concept		<ul style="list-style-type: none"> - Micro-manufacturable - Robust against relaxation - Scalable

Prototyping

Following the down-selection of the conceptual designs to feasible designs, proof-of-concept prototypes were required to gain insights on the feasibility of the SMAAS and the potential of the down-selected concepts. Therefore, a macroscale prototyping process using rapid prototyping techniques was performed on two unique design concepts employing both translational and rotational configurations. To test the functionality of the prototypes, a testing apparatus consisting of high-current power supply, oscilloscope, mechanical relay modules, push buttons and a microcontroller board (Arduino Uno) were used. The testing apparatus is shown in the figure below.

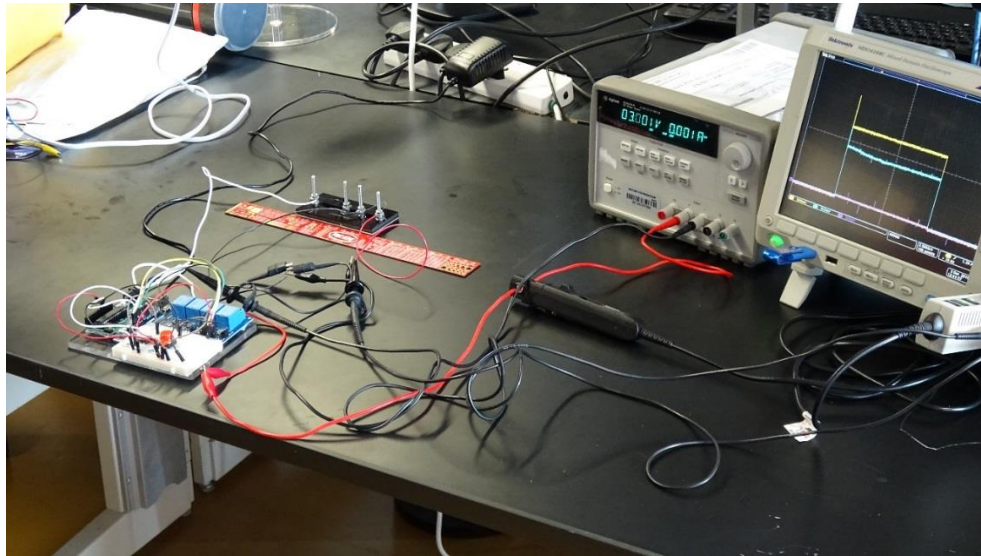


Figure 37: Testing Setup for the Proof-of-Concept Prototypes

The relay modules are used to pass current from the power supply to the SMAs for heating on demand. They were controlled either automatically by the programmed microprocessor board based on pre-set heating time or manually through the push-buttons. The oscilloscope was used to log and visualize voltage, current and time data.

Candidate Design I

The first prototype was made based off the metal plunger “bullet” design concept shown in the top-view schematic below and discussed earlier in the chapter. Employing the concept of sandwiched layers, the prototype consisted of 4 layers namely; a substrate, guide rail + plunger + 2 SMA members, a printed circuit board (PCB) and an enclosure. Those different layers can be shown in the side-view schematic shown below.

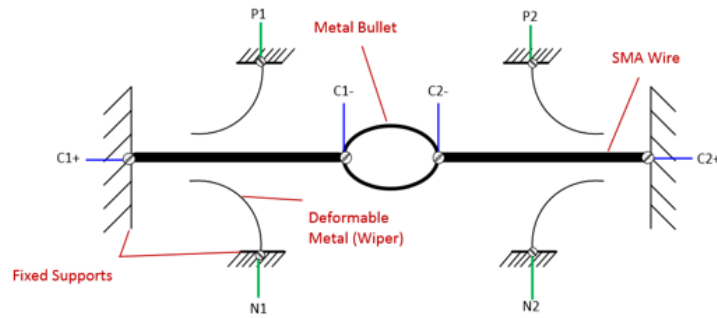


Figure 38: Top-View Schematic of the First Prototype Concept

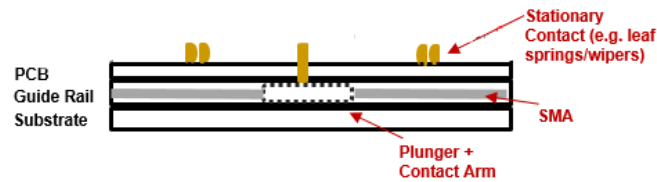
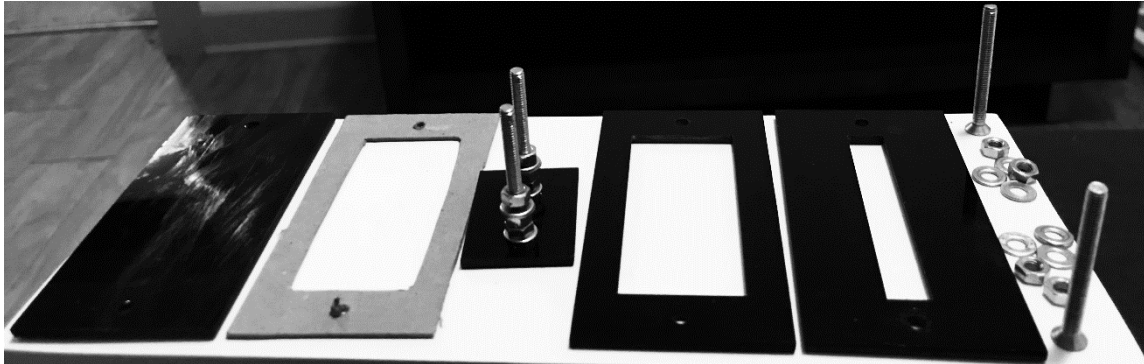


Figure 39: Side-View Schematic of the First Prototype

The substrate provides support for the rest of the structure as well as a surface for the plunger to slide along. The guide rail guides the plunger linearly to move towards its bi-stable positions (at the electrical contacts). The PCB has the leaf spring contacts soldered onto it and routed through copper traces to 2 LEDs (used to demonstrate electrical connection at the stationary contacts). The enclosure is used to provide support for the whole structure if necessary.

The actuation structure consisting of the substrate, guide rail and plunger was fabricated using laser machining of acrylic sheets. The rail layers were separated from the substrate by a thin shim layer to give enough tolerance for the plunger to move freely within the guide rail. The layers were all joined together mechanically using fasteners (screws, nuts and washers) which were also used as crimpers for the SMA actuators

(wires or springs). The figure below show the individual components and the assembled actuation structure.



(a)

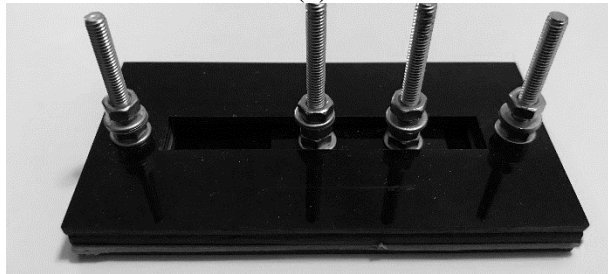


Figure 40: Actuation Structure for Prototype I (a) Individual Components (b) Assembled Structure

SMA wires and springs were then installed onto the actuation structure (using crimping between mechanical fasteners) in a protagonist-antagonist formation. Low-resistance electric wires were also crimped between the mechanical fasteners and along the SMA wires/springs to pass current to them for heating. The SMA members and heating wires are shown in the figure below.

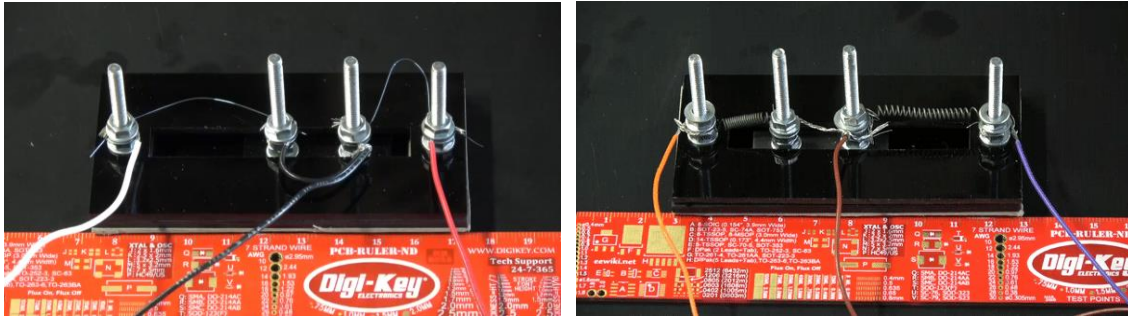


Figure 41: Actuation Mechanism of Prototype I with SMA Actuators Installed

After the actuation mechanism was tested using the testbed discussed earlier for bi-directional actuation, the PCB was milled out of a FR-4 substrate and the stainless-steel leaf spring contacts and LEDs were soldered to it. The PCB was then fastened onto the actuation structure. An exploded view schematic of the full prototype showing both actuation and electrical structures is shown in the figure below.

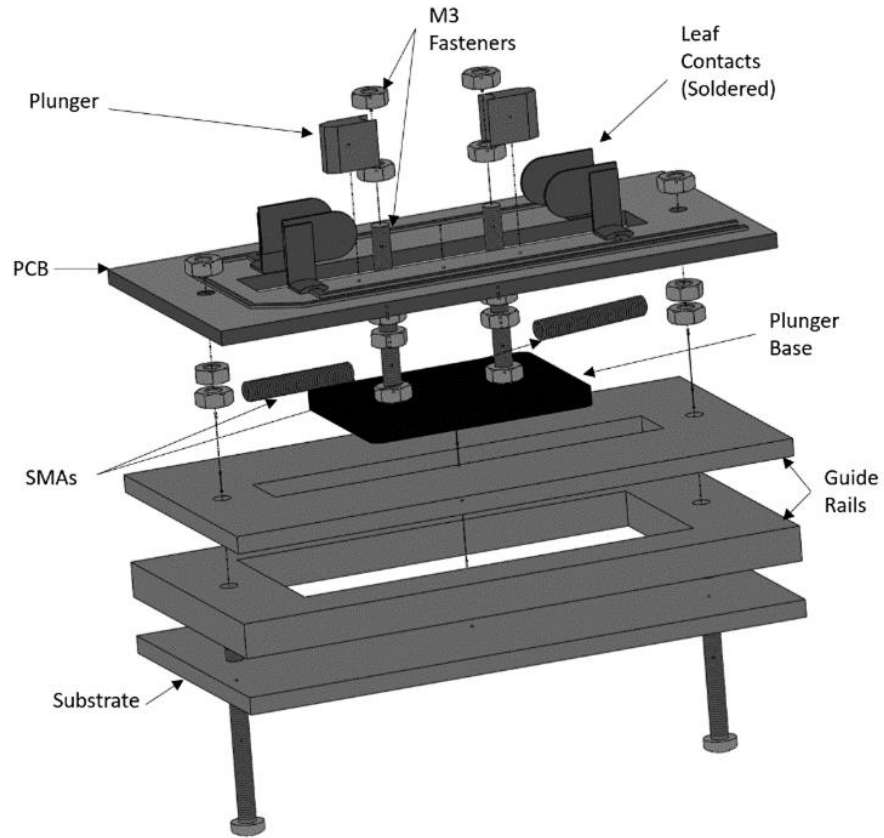


Figure 42: Exploded-View Schematic of the Switch Prototype

The full prototype was tested for bi-stable switching using SMA actuation as shown in the figure below. The prototype proved functionality for stable switching between two states while accounting for relaxation of SMA.

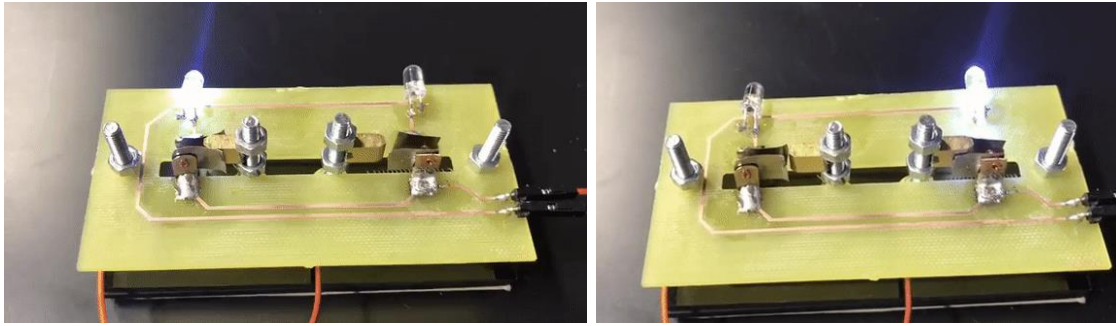


Figure 43: Fully Functional Bistable SMAAS Prototype I

Candidate Design II

The second prototype was developed for the spring-loaded lever concept discussed earlier in this chapter is shown in the figure below. This concept was selected to be prototyped since it involved a different configuration (rotary) and because of its advantages discussed in length in the qualitative assessment section of this chapter.

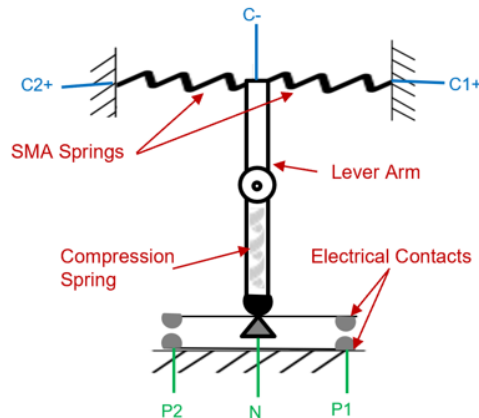


Figure 44: Top-View Schematic of Prototype II Concept

Since this design concept was inspired from the existing mechanism used in toggle switches, a rapid prototype was made that included a commercially available

toggle switch fastened onto a wood substrate and connected electrically to a PCB with LEDs for demonstration of the switching states. In addition, SMA springs and electric heating wires were fastened onto the lever arm of the toggle switch using a threaded brass housing and a screw. The figures below show the components of the prototype and the two switching state functionality. Similarly to the first prototype, this prototype proved functionality for stable bi-state switching using electrically heated SMA actuators.

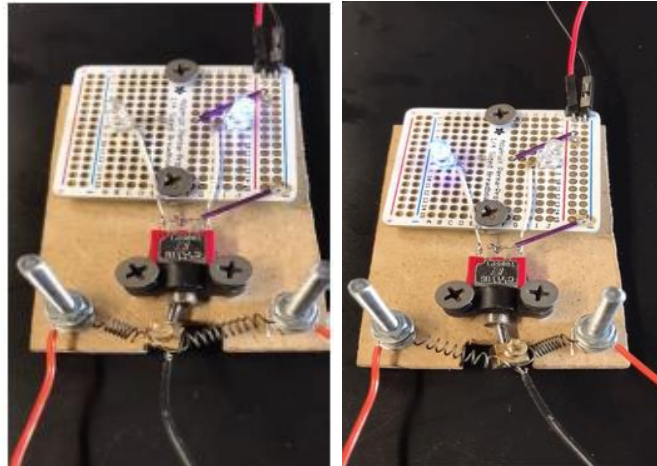


Figure 45: Fully Functional Bi-stable SMAAS Prototype II

Learning from Prototyping

The two prototypes designs proved functional for bi-stable switching using electrically-heated SMAs. They also proven robustness against relaxation of the SMA which was visually noticeable during thermal cyclic testing of SMA actuators without installing the locking mechanisms. However, a degradation in the functional stroke and an increase in the required heating time was noticed during the functional testing of the

switch. This suggests the need to investigate the fatigue of SMA springs and model the heating time of SMA springs as a function of the stress induced which are discussed in the next chapter. Aside from that, another outcome of this prototyping process is that the spring-loaded prototype (II) showed a higher switching speed and higher resistance to relaxation or vibrations. This was expected beforehand as discussed in the qualitative assessment section of the design concepts. However, this observation highlighted the need to employ locking mechanisms that do not produce resultant forces in the direction that follows the relaxation of the SMA.

CHAPTER IV

MODELLING AND ANALYSIS

In this chapter, thermomechanical and heat transfer models for SMA wires and springs are discussed. For design purposes, simplified analytical and empirical models were also discussed in order to be used for first-hand calculations and design choices. In addition, an analysis of the mechanical structure and motion of the SMAAS designs was conducted in order to establish the governing equations that drives the design and optimization of the SMAAS. Those models are used in a case study in Chapter V to numerically optimize a SMAAS design. Lastly, a theoretical analysis of the manufacturability of the SMAAS in the micro scale and that fatiguing of the SMAs as actuators is discussed with reference to the literature. The information gained from this section will be also applied to a case study in Chapter V for the microfabrication of a design concept of the SMAAS.

SMA Models

SMA Wire Models

Constitutive Models

SMAs are typically described with a phenomenological constitutive model that accounts for phase transformations. Among the most common constitutive models is the model developed by Liang & Rogers in 1997 described by the equation below [12] [28].

$$(\sigma - \sigma_0) = E(\xi)(\varepsilon - \varepsilon_0) + \theta_T(T_W - T_0) + \Omega(\xi)(\xi - \xi_0) \quad (1)$$

The σ and ε represents the recovery stresses and strain. ξ represents the martensitic volume fraction during phase transformation. θ_T is the thermoelastic tensor

while E and Ω are the elastic modulus and transformation tensor respectively which are described by the equations below as functions of the martensitic volume fraction and their properties at the two phases.

$$E(\xi) = E_A + \xi(E_M - E_A) \quad (2)$$

$$\Omega(\xi) = -\varepsilon_L E(\xi) = -\varepsilon_L [E_A + \xi(E_M - E_A)] \quad (3)$$

where E_A and E_M are the austenitic and martensitic elastic moduli respectively, and ε_L represents the maximum recoverable strain. Typically, the elastic moduli at the two phases as well as the thermoelastic tensor and maximum recoverable strain are found experimentally through tensile and thermal cyclic testing as shown in the figure below by [12]. The martensitic volume fraction can however be either acquired experimentally or can be predicted through different models. The three main models that are used to predict the martensitic volume fraction are as follows [12]

Liang & Rogers and Brinson Cosine Model (s) [29]:

$$\xi = \underbrace{\frac{\xi_M}{2} \left[\cos \left(\pi \frac{(T_w - A_s - \frac{\sigma}{C_A})}{(A_f - A_s)} \right) + 1 \right]}_{\text{Heating cycle}} = \underbrace{\frac{1 - \xi_A}{2} \left[\cos \left(\pi \frac{(T_w - M_f - \frac{\sigma}{C_M})}{(M_s - M_f)} \right) \right]}_{\text{Cooling cycle}} + \frac{1 + \xi_A}{2} \quad (4)$$

Tanka Exponential Model [28]:

$$\begin{aligned} \xi &= \underbrace{\xi_M \exp \left[\left(\frac{\ln(100 \cdot \xi_M)}{C_A (A_f - A_s)} \right) (C_A (A_s - T_w) + \sigma) \right]}_{\text{Heating cycle}} \\ &= \underbrace{(1 - \xi_A) \exp \left[\left(\frac{\ln(100 \cdot \xi_A)}{C_M (M_f - M_s)} \right) (C_M (M_s - T_w) + \sigma) \right]}_{\text{Cooling cycle}} \end{aligned} \quad (5)$$

Kumar & Lagoudas Linear Model [1]:

$$\xi = \begin{cases} 0, & T \geq M_s^\sigma, \\ \frac{M_s + \frac{\sigma}{C^M} - T}{M_s - M_f}, & M_f^\sigma < T < M_s^\sigma, \\ 1, & T \leq M_f^\sigma, \end{cases} \quad \xi = \begin{cases} 1, & T \leq A_s^\sigma, \\ \frac{A_f + \frac{\sigma}{C^A} - T}{A_f - A_s}, & A_s^\sigma < T < A_f^\sigma, \\ 0, & T \geq A_f^\sigma. \end{cases} \quad (6)$$

Heating cycle
Cooling cycle

Where M_s , M_f , A_s and A_f represent martensitic start, martensitic finish, austenitic start and austenitic finish temperatures respectively. The C^M and C^A represent the stress influence coefficients in the stress-temperature curve shown in the figure below. These are also experimentally obtained and they range between 7 and 10 MPa/C for NiTi [1]. The liang-rogers-brinson model predicts the martensitic volume fraction as a cosine function of the transition temperatures while accounting for stress-induced conditions during phase transformation [12]. On the other hand, the Tanaka model predicts the martensitic fraction as an exponential function. Lastly the simple engineering model proposed by Kumar and Lagoudas provides a linear model for predicting the martensitic fraction as a function of transition temperatures and imposed stress [1].

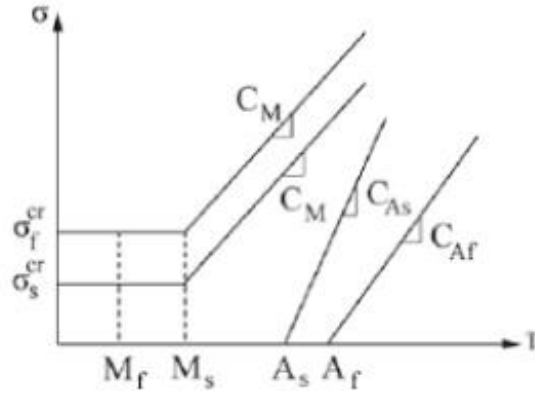


Figure 46: Stress-Temperature Curve of SMAs Showing Linear Stress Coefficients (Reprinted from [1])

Not only does the martensitic volume fraction affects the recovery stress and strain of SMAs, it also affects its electrical properties particularly resistivity [33]. Therefore while predicting the martensitic volume fraction during transformation, the resistivity needs to be corrected as a function of the martensitic fraction as shown in the equations below by [33].

The resistance is presented by the following equation:

$$R = \frac{\rho_e L}{A} \quad (7)$$

Where the equivalent resistivity is represented in terms of the martensitic and austenitic resistivities and the martensitic volume fraction as shown in the following equation.

$$\rho_e = \rho_A + (\rho_M - \rho_A)\xi \quad (8).$$

And the austenite and martensite resistivities are given by their initial experimentally-measured values at their respective states as well while also accounting for thermal expansion as shown in the equations below.

$$\begin{aligned}\rho_A &= \rho_{A0} + \alpha_A(T - T_0) \\ \rho_M &= \rho_{M0} + \alpha_M(T - T_0)\end{aligned}\tag{9}$$

Where α_M and α_A are thermal expansion coefficients at the two phases (measured experimentally too) and T represents the temperature.

Engineering Design Models

For engineering applications that use SMA actuators, the emphasis is put on the end conditions of transformation rather than the conditions during transformation. Therefore, for a first-order simple design analysis and for the selection of SMA actuators, a design model based on interpolating manufacturer's data is recommended [12] as opposed to a constitutive model. This model interpolates the SMA forces at the room temperature (restorative force) and transformation temperature (heating force) of SMA wires based on recommended 4% transformation strain as function of the diameter of the wire. In addition, this model interpolates the resistance and max current of the SMA wires as a function of their diameter. Graphs showing the interpolation of manufacturer's datasheet (Dynalloy [8]) is shown in the figure below.

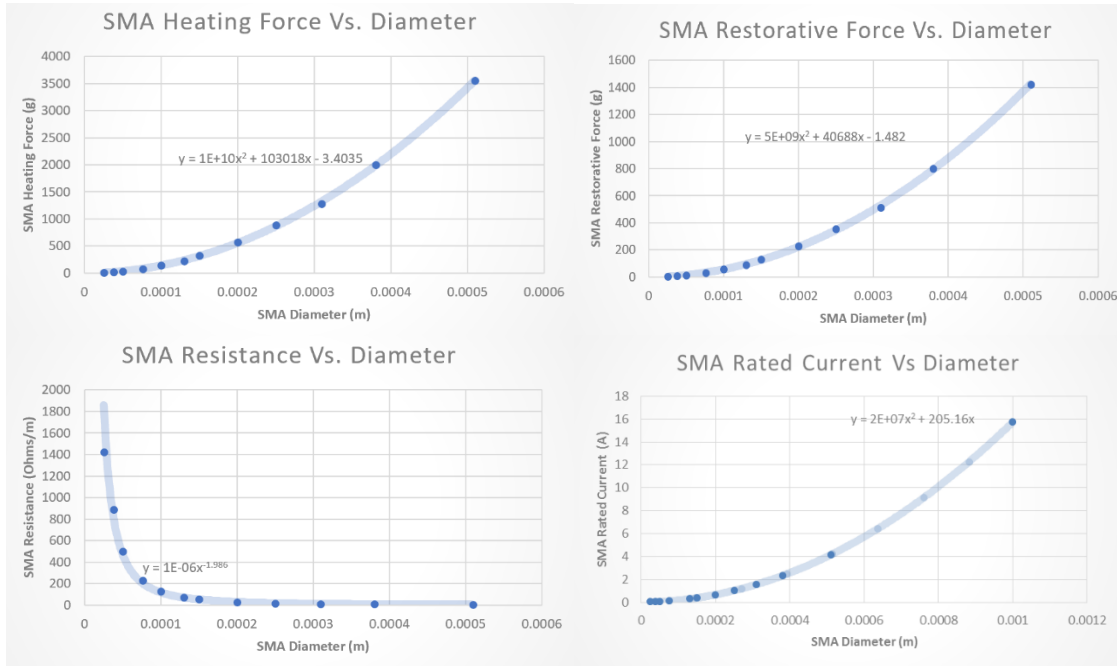


Figure 47: Curve-Fitted SMA Wire Properties Produced from Manufacturer Datasheet ([8])

Curve-fitting those data from the manufacturer yields the following equations for the forces, resistance and max current of SMA wires as a function of their diameter:

$$F_{heating} = 10^{10}d_{sma}^2 + 1.03 * 10^5d_{sma} - 3.4 \quad (10)$$

$$F_{restorative} = 5 * 10^9d_{sma}^2 + 4.07 * 10^4d_{sma} - 1.48 \quad (11)$$

$$R = L_{sma} \times 10^{-6}d_{sma}^{-1.986} \Omega \quad (12)$$

$$I_{max} = 2 \times 10^7d_{sma}^2 + 205.16d_{sma} \quad (13)$$

These design equations can be used for a preliminary analysis of SMA wire actuators as well as for the selection of the diameter of SMA wires for the intended application.

SMA Spring Models

The SMA springs as actuators can be also modelled using the constitutive models discussed earlier. However, springs are 3 dimensional objects and axially stretching it involves more than one type of force and in 3 different directions. Therefore, a 3D constitutive model is required to accurately model the SMA springs transformation. Therefore, for practical applications of SMA spring actuators, spin-off models from Hook's law are being used [30]. Two types of models were discussed in the literature; Two-state models that apply hook's law at the two material states (austenite and martensite) without accounting for what's happening in the process and temperature-dependent models which captures the transformation. These two different models are discussed in this section.

Two-State Model

Traditional Two-State Model

The traditional two-state model directly applies Hook's law to the two different material states at low and high temperatures through the use of the state-dependent elastic shear modulus as given by the following equations [30]:

$$F = \frac{G_A d^4}{8D^3 n} \delta \quad (14)$$

$$F = \frac{G_M d^4}{8D^3 n} \delta \quad (15)$$

Where G_A and G_M are the austenitic and martensitic shear moduli (experimentally-measured or provided by manufacturer), d and D are the diameters for the spring wire and outer coil, n is the number of active coils and δ is the axial deflection of the spring.

Improved Two-State Model

Another accredited model by [30] proposes a new two-state hook's law adaptation for SMA coil spring actuators using the traditional spring coil model but applying it for a large deformation. This is useful since SMA springs are typically used for larger deformations (multiple times of its original un-deformed length). This model accounts for larger deformations through incorporating initial and final coil pitch angles as shown in the austenitic and martensitic formulations below.

For the A100% state at high temperature,

$$F_A = \frac{G_A d^4}{8D^3 n} \left(\frac{\cos^3 \alpha_i}{\cos^2 \alpha_{Af} (\cos^2 \alpha_{Af} + \sin^2 \alpha_{Af} / (1 + \nu))} \right) \delta_A \quad (16)$$

For the M100% state at a low temperature,

$$F_M = \frac{G_M d^4}{8D^3 n} \left(\frac{\cos^3 \alpha_i}{\cos^2 \alpha_{Mf} (\cos^2 \alpha_{Mf} + \sin^2 \alpha_{Mf} / (1 + \nu))} \right) \delta_M - \frac{\pi d^3}{8D} G_M \gamma_L \xi_{S\tau} \quad (17)$$

Where α_f is the final coil spring pitch angle, δ is the deflection, G_M & G_A are the elastic shear modulus of the martensitic and austenitic phases, $\xi_{S\tau}$ is the martensitic volume fraction and γ_L is the maximum residual strain. G_M , G_A , γ_L and maximum critical shear stresses (τ^{cr}) are found experimentally from tensile testing and the martensitic volume fraction is found using this equation.

$$\xi_{S\tau} = \frac{1}{2} \cos \left[\frac{\pi}{\tau_s^{cr} - \tau_f^{cr}} (\tau - \tau_f^{cr}) \right] + \frac{1}{2} \quad (18)$$

If the diameter reduction and bending moments are ignored, the values in the parenthesis becomes equal to 1, thus, for the A100% state at high temperature the simplified equation becomes,

$$F = \frac{G_A d^4}{8D^3 n} \delta \quad (19)$$

For the M100% state at a low temperature,

$$F = \frac{G_M d^4}{8D^3 n} \times \delta - \frac{\pi d^3}{8D} G_M \gamma_L \xi_{S\tau} \quad (20)$$

And the maximum force of the SMA spring as a function of the critical shear stress is given by the following equation. The maximum shear stress is either specified by the designer or provided by the manufacturer.

$$F_{max} = \frac{\pi d^3}{8D} \tau^{cr} \quad (21)$$

After verifying this model experimentally by [30], this improved model predicted the stroke within 98% accuracy as opposed to 21.3% accuracy from the traditional model.

Temperature-dependent Model

A model developed by [47] provides a formulation for the spring force as a function of the temperature as it is being heated. At low temperatures (martensitic state), the model suggests the use of the traditional hook's law formulation given by this equation where the subscripts stand for low temperature.

$$F_{low\ temperature} = \frac{d^4 G_M}{8D^3 n} \delta \quad (22)$$

However, as the spring is being heated, the shear modulus changes as a function of the temperature, thus, the force changes in response too as shown in the equation below.

$$F_{heating}(T) = \frac{G(T) d^4}{8D^3 n} \delta \quad (23)$$

The shear modulus changes as a function of temperature as follows.

$$G(T) = G_M + \frac{G_A - G_M}{2} [1 + \sin \phi(T - T_m)] \quad (24)$$

Where

$$T_m = \begin{cases} \frac{A_s + A_f}{2} \\ \frac{M_s + M_f}{2} \end{cases} \quad \phi = \begin{cases} \frac{\pi}{A_f - A_s} & \text{while heating} \\ \frac{\pi}{M_s - M_f} & \text{while cooling} \end{cases} \quad (25)$$

The M and A represent the martensitic and austenite temperatures and the subscripts represent the start and finish temperatures.

In an antagonistic actuation experiment of a SMA spring actuator against a steel spring, the model described above was verified in comparison with experimental results as shown in the figure below from [47].

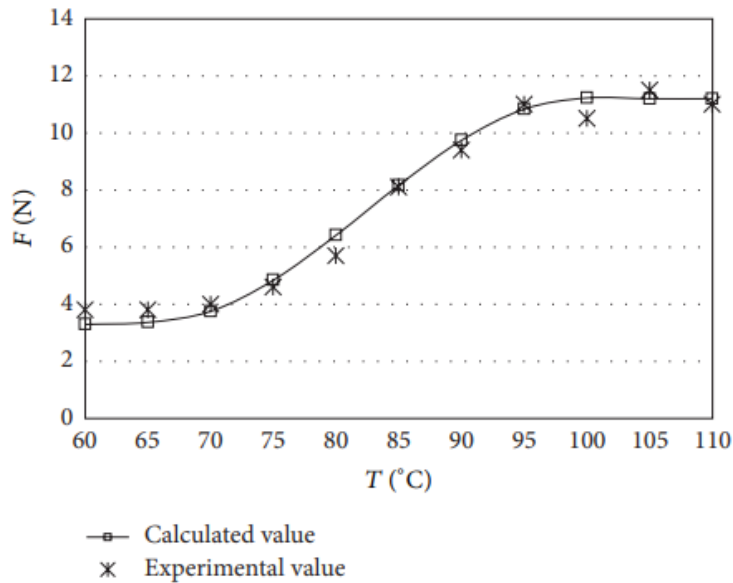


Figure 48: Calculated and Measured SMA Spring Force vs. Temperature (Reprinted from [47])

Mechanical Structure & Motion

In order to design a SMAAS and besides modelling the SMA actuator, an analysis of the motion and structure of the switch is required. This analysis would provide the governing equations for the switch design which can then be used either for optimization or for numerical modeling or for components selection. In this section, free-body analysis of the two prototyped design concepts is performed and a design approach for each of the designs is recommended. Following that, an analysis of the locking mechanisms forces and the SMA relaxation forces is presented based on recommendations from literature.

Free-Body Diagrams

Design Concept #1

This design concept is selected to be analyzed since it was down-selected and successfully prototyped in Chapter III. A schematic of the design concept is shown in the figure below and the free-body diagrams and equations of motion of this concept under different cases are presented after. The free-body analysis is performed at 4 different points or “snapshots” of the motion of the plunger between states as listed below. The motion is assumed to be completely horizontally (x-direction), therefore, the net vertical forces are assumed to be equal to zero

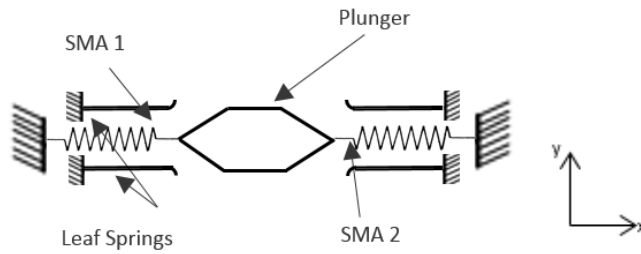
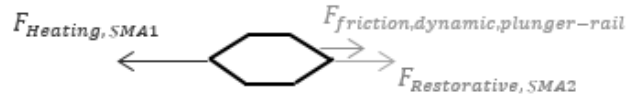


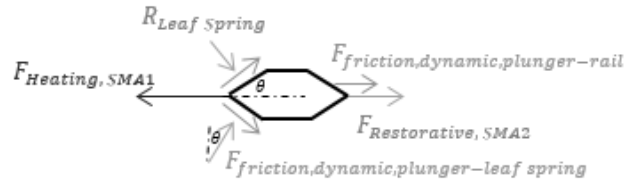
Figure 49: Schematic of the First Design Concept to be Analyzed

Case 1: when heating SMA 1 and the plunger is moving along the rail:



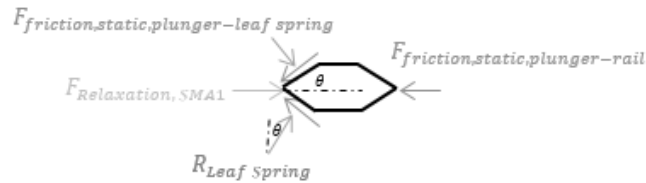
$$\sum F_x = F_{Heating, SMA1} - F_{friction,dynamic,plunger-rail} - F_{Restorative,SMA} = ma_x \quad (26)$$

Case 2: when the plunger is moving between the leaf springs:



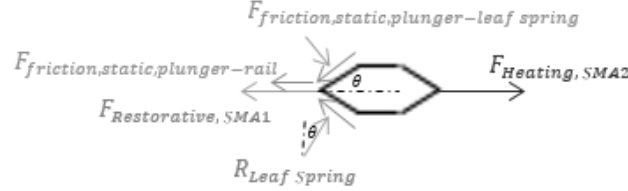
$$\sum F_x = F_{Heating, SMA1} - F_{friction,dynamic,plunger-rail} - F_{Restorative.SMA2} - 2R_{Leaf Spring} \sin \theta - 2F_{friction,dynamic,plunger-leaf spring} \cos \theta = ma_x \quad (27)$$

Case 3: when the plunger is locked between the leaf springs and SMA 1 is cold:



$$\begin{aligned} \sum F_x &= 2 F_{friction,static,plunger-leafspring} \cos \theta - \\ 2R_{Leaf Spring} \sin \theta - F_{relaxation,SMA1} + F_{friction,static,plunger-rail} &= 0 \end{aligned} \quad (28)$$

Case 4: When SMA 2 is heated and the plunger is about to leave the leaf springs



$$\begin{aligned} \sum F_x &= F_{Heating,SMA2} - F_{friction,static,plunger-rail} - F_{Restorative,SMA1} + \\ 2R_{Leaf Spring} \sin \theta - 2F_{friction,static,plunger-leafspring} \sin \theta &= ma_x \end{aligned} \quad (29)$$

The restorative force of the SMA $F_{Restorative,SMA}$ represents the force required to strain the opposing cold SMA while the relaxation force $F_{relaxation,SMA}$ corresponds to the relaxation stress found in the SMA after cooling down. The relaxation force is useful for the design of the locking mechanism (leaf contacts) such that it produces a locking force that overcomes the relaxation force. The reaction force from the leaf springs $R_{Leaf Spring}$ represent the equivalent of the force produced by the plunger on the leaf springs to bend them in order to fit the plunger in between. Formulations for the SMA forces were discussed earlier in the next section except for relaxation forces which discussed later in this chapter. The friction forces are described as follows:

$$F_{friction,static,plunger-leafspring} = \mu_s R_{Leaf Spring} \quad (30)$$

$$F_{friction,static,plunger-rail} = \mu_s m_{plunger} g \quad (31)$$

$$F_{friction,dynamic,plunger-rail} = \mu_d m_{plunger} g \quad (32)$$

Where μ represent the coefficient of friction (subscripts s and d represent static and dynamic coefficients) and it depends on the materials of the friction surfaces while m represents the plunger mass and g represents the gravitational force. The friction forces along the rail represent the friction between the plunger and the substrate and ignores the friction with any side walls.

Designing this switch concept requires using Eq. 28 to design the leaf springs such that it produces enough force to overcome the opposing forces (mainly SMA relaxation force and frictional forces). This is done in parallel with using Eq. 26, 27 and 29 to design/select SMA components such that the heating forces overcomes all other opposing forces.

Design Concept #2

Similarly to first design concept, this concept is selected to be analyzed since it was down-selected and successfully prototyped in Chapter III. A schematic of the design concept is shown in the figure below and the free-body diagrams and equations of motion of this concept under different cases are presented after.

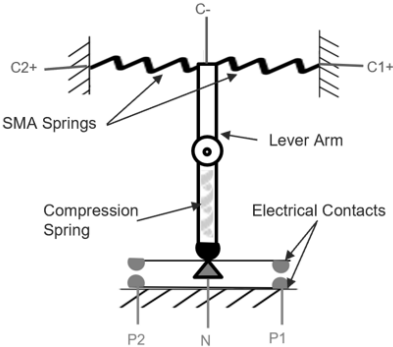
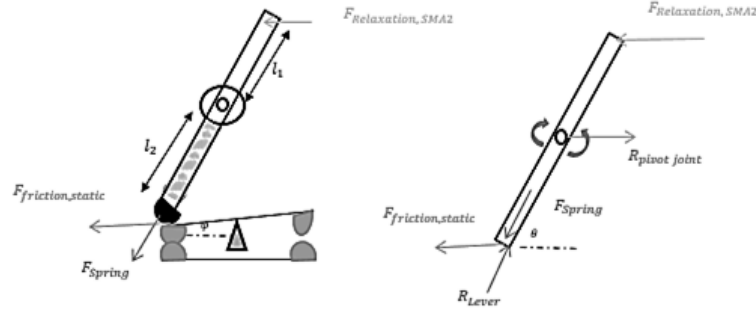


Figure 50: Schematic of the Second Design Concept to be Analyzed

Case 1: when lever is stable at state 1 and both SMAs are cold



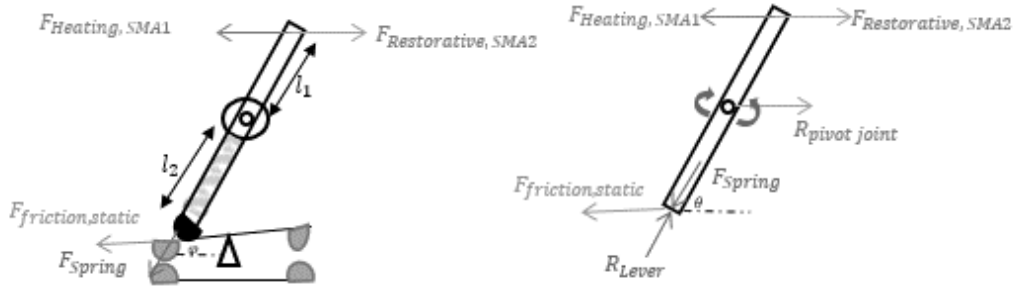
$$\sum F_x = F_{Relaxation, SMA2} - F_{friction, static} + R_{Pivot joint} + F_{Spring} \cos \theta - R_{lever} \cos \theta = 0$$

$$\sum F_y = F_{Spring} \sin \theta - R_{lever} \sin \theta = 0$$

$$\sum M_{pivot} = F_{Relaxation, SMA2} l_1 - F_{friction, static} l_2 = 0$$

$$(F_{friction, static} = \mu_s F_{spring} \cos(\theta); \cos(\theta)=1) \quad (33)$$

Case 2: when SMA1 is heated and the lever starts rotating counter-clock-wise:



$$\sum F_x = F_{Heating, SMA1} + F_{Restorative, SMA2} - F_{friction, static} + R_{Pivot joint} + F_{Spring} \cos \theta - R_{lever} \cos \theta = 0$$

$$\sum F_y = F_{Spring} \sin \theta - R_{lever} \sin \theta = 0$$

$$\sum M_{pivot} = F_{Heating, SMA1} l_1 - F_{friction, dynamic} l_2 = I \alpha$$

$$(F_{friction, dynamic} = \mu_d F_{spring} \cos(\theta); \cos(\theta)=1) \quad (34)$$

Formulations for the SMA forces were discussed earlier in the next section except for relaxation forces which discussed later in this chapter. The friction forces are described earlier in equation 30, 31 and 32. The force of the compression spring is given by the equation below.

$$F_{Spring} = K\delta = k \frac{l_{lever}}{2} \sin \varphi = R_{lever} \quad \text{where } K = \frac{Gd^4}{8D^2n} \quad (35)$$

Therefore, using this analysis to fully design this concept, the moment equation in **Eq. 33** can be used to design the pivot arm such that the force resulting from the friction with it is enough to overcome the other forces (mainly restorative force of competing SMA). This should be done in parallel with evaluating **Eq. 34** to make sure that the SMA chosen has enough heated pulling force to overcome the other opposing forces. This analysis was used to numerically optimize this design concept as discussed in the case study in Chapter V.

Locking Mechanisms

The actuation locking mechanisms incorporated in the down-selected design concepts in Chapter III employed either compression springs, flat springs or cantilevered leaf springs. Therefore, in this section, the equations governing the forces exerted by those locking mechanisms are provided as reported by literature [31] [32]. Those equations can be used along with the free-body diagram equations obtained earlier to fully design the SMAAS down-selected concepts.

Table 10: Force-Deflection Equations of Locking Components (Adapted from [31] [32])

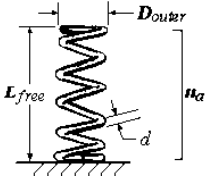
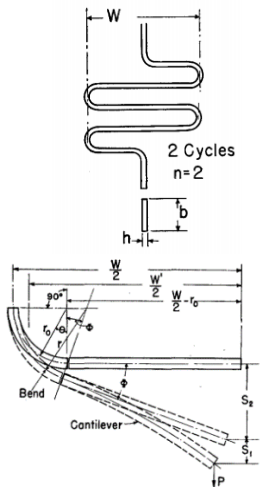
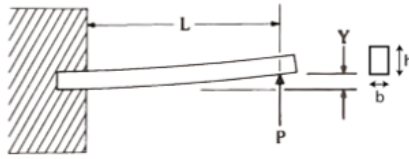
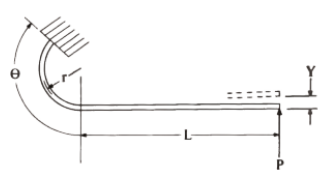
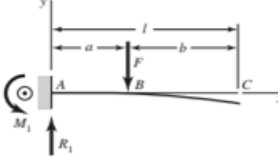
Type	Schematic	Equations
Compression Spring		$F = \frac{Gd^4}{8D^2n} \delta$
Flat Zigzag Spring		$S = \frac{2PW^3}{Ebh^3} \left\{ \left[1 + \frac{3r_0}{W} (\pi - 2) \left(1 - \frac{4r_0}{W} \right) \right] n - \left[\frac{3}{8} + \frac{3r_0}{W} (\pi - 2) \right] \right\}$
Leaf Springs		$P = \frac{Eh^3b}{0.00881L^3} Y$
Leaf Springs		$Y = \frac{0.0264Pr^3}{Eh^3b} \left[\frac{1}{3} \left(\frac{L}{r} \right)^3 + \left(\frac{L}{r} \right)^2 \frac{\theta}{57.3} + 2 \frac{L}{r} (1 - \cos\theta) + \frac{\theta}{114.6} - \frac{\sin 2\theta}{4} \right]$

Table 10: Continued

Type	Schematic	Equations
Leaf Springs		$y_{AB} = \frac{Fx^2}{6EI}(x - 3a)$ $y_{AB} = \frac{Fa^2}{6EI}(a - 3x)$ $y_{AB} = \frac{Fa^2}{6EI}(a - 3l)$

Relaxation Model

As discussed in Chapter II, SMAs arranged in a protagonist-antagonist formation experience a relaxation once they contract (when heated) and while cooling down. This relaxation was attributed by literature to the competing restorative force of the antagonistic SMA actuator which cause detwinning of the fully twinned martensite in the protagonist SMA actuator [15]. It is important to quantify this relaxation phenomena since the SMAAS is required to have a locking mechanism at the two switch states that overcomes this relaxation in order to have a stable electrical connection at the states. This relaxation is usually quantified experimentally. For instance, an experiment conducted by [15] for two competing protagonist-antagonist NiTi ribbons showed the following results in Figure 50. The details of the experiments are discussed in Chapter II Figure 9.

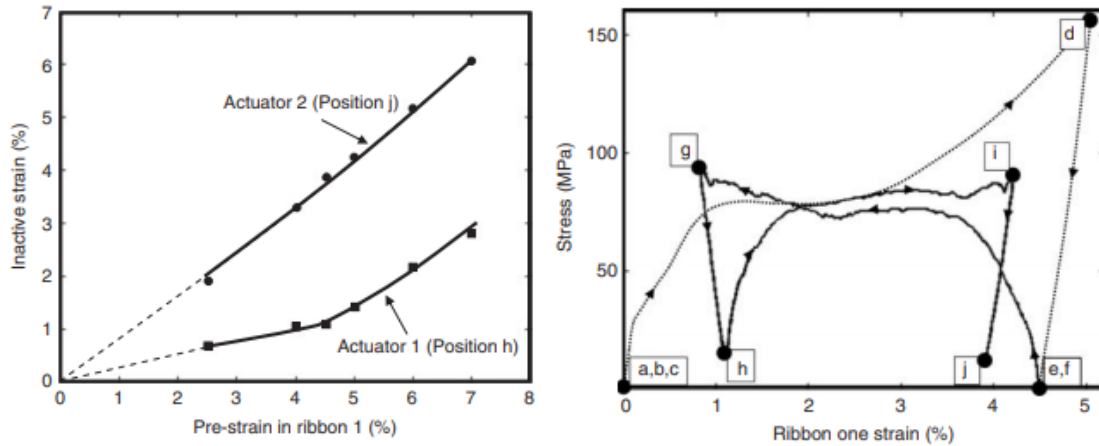


Figure 51: Inactive Strain Vs. Pre-Strain Curve (Left) and Stress-Strain Curve (Right) of a SMA Ribbon (Reprinted from [15])

The a,b,c,d,e and f steps in the above figure (right) present the process of pre-straining the first SMA actuator before attaching it to the second. f->g and h->I represent heating of SMA actuator 1 and 2 respectively (i.e. transformation/recovery process) while g->h and i->j represents cooling of the two SMA actuators respectively (i.e. the relaxation process). Since the strain in this experiment was measured from one position through a laser extensometer, the inactive strain values in the figure above (left) presents the relaxation strain + permanent unrecoverable strain (for actuator 1) and the actuation stroke - the relaxation strain (for actuator 2).

The takeaway from this experiment is that the relaxation strain changes with the pre-strain values (observed in the left curve). It also showed that the inactive equilibrium stresses are found experimentally to be **15 MPa** and **13 MPa** (at points h and j in the figure above) as opposed to heating stresses of **94** and **92 MPa** [15]. It also showed a

relaxation strain of $\sim 0.3-0.5\%$ for a typical 4%-5% pre-strained SMA actuator (shown in points g to h and I to j in the figure above).

In a separate experiment conducted by a colleague [49], the relaxation phenomena manifested itself when a SMA wire was segmented at the center by attaching an electric wire to it and each segment was selectively heated to have back and forth motion. A sample thermal cyclic testing experimental data obtained by him shown in the figure below (the red color represents heating/hot state while the blue color represents cooling/cold state).

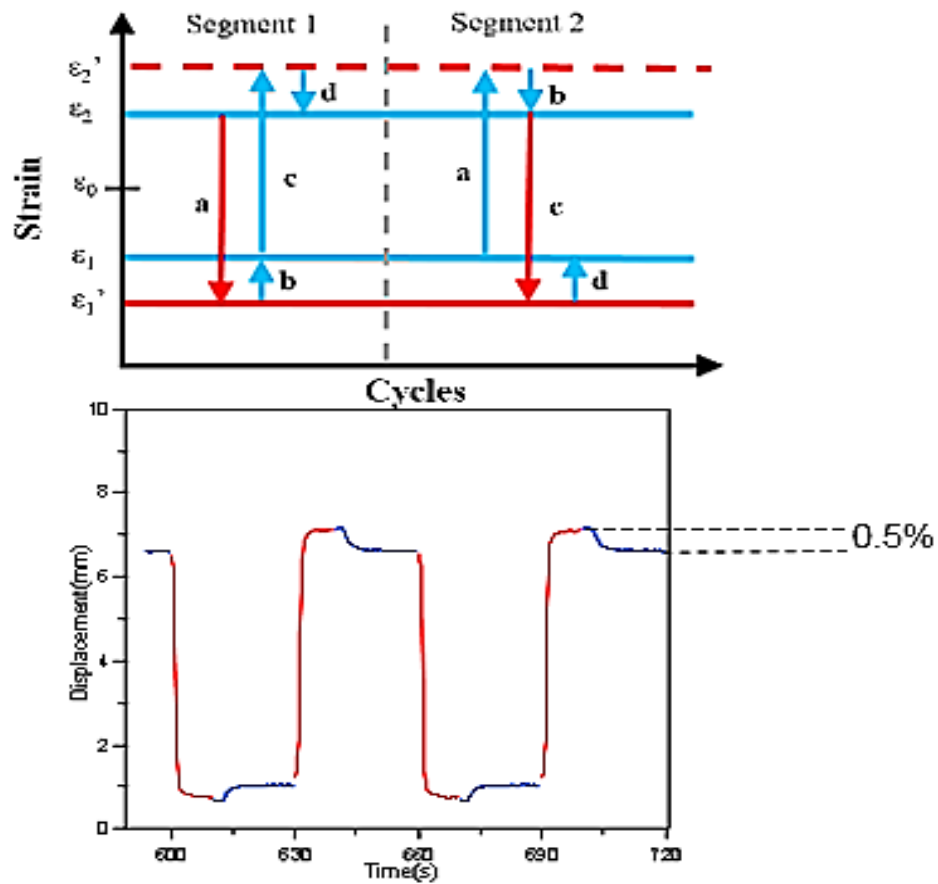


Figure 52: Sample Thermal Cycling Test for SMA Wire Segments (Reprinted from [48])

According to him, the maximum relaxation strain observed amounted to 0.5% for experiments with a maximum pre-strain of 5% [49].

Therefore, based on these experiments, the SMA relaxation force can be quantified using one of the following methods:

- 1- Measure experimentally using load cells in a thermal cycle test of antagonistic SMA actuators and find the inactive stress as done by [15] and discussed earlier.

Then the relaxation force can be calculated using $F_{relaxation} =$

$\sigma_{inactive (relaxation)} \times A$. This is the most reliable method to quantify the relaxation force.

- 2- The reported result from [15] for a relaxation strain is 13-15 MPa for a heating stress of 93-94 MPa for NiTi ribbons (~16%). Typically, SMAs are described as having a cold force roughly 1/3 of its hot force [8]. Therefore, the same expression can be generalized for the relaxation stress and estimating it to be ~1/5th of the heating stress/force (from the 16% experimental data). This generalization needs to be experimentally verified, however, it can give a crude estimation in the absence of any other methods. For example, load cells cannot be used for very small SMA wires/springs which are needed for a SMAAS.

3- In cases where experimental data for the relaxation stress cannot be obtained (e.g. short micro wires), the observed relaxation strain can be used to estimate the corresponding stress using the equation below by [1] for stress in a fully martensitic state at room temperature.

$$\sigma = E^M(\varepsilon - H^{cur}(\sigma)) \quad (36)$$

Where E^M is the martensitic elastic modulus, ε is the total strain and H is the recoverable strain. For instance, the experimental data observed by [49] that was discussed earlier shown a 0.5% maximum relaxation strain. The corresponding stress in the martensitic state can be estimated then using the equation below.

$$\sigma_{relaxation} = 0.5\% \times E_M \quad (37)$$

This amounted to be 17.5 MPa for a 35 GPA E^M nitinol. It is worth noting that this formation assumes elastic deformation which is not true for the case of the relaxation strain, however, this is useful only for crude approximation for first-order design choices.

Energy Model

Among the variables of the SMAAS that need to be characterized in order to have a detailed design are the heating/cooling times and energy consumption for switching. Those values represent the switching time/frequency and energy which are major characteristics for the selection of electric switches. Therefore, in this section, energy models for the ohmic heating and natural free convection cooling of SMA wires and springs are discussed. Simplified and empirical models were also discussed for crude estimation for engineering design purposes.

Transient-State Model

Starting from the one dimensional heat equation for a cylinder with electric power supply, the transient-state model for heating an SMA wire can be written as:

$$\rho \left(c_p \frac{\partial T}{\partial t} + \Delta H \frac{\partial \xi}{\partial t} \right) - k \frac{\partial^2 T}{\partial x^2} = \frac{I^2 R(\xi)}{\pi d L} - \left(\frac{4hL}{\pi d^2} \right) (T - T_\infty) \quad (38)$$

Where c_p , ρ , k , h , L , d , ξ and ΔH the specific heat capacity, density, thermal conductivity, heat convection coefficient, length, diameter, martensitic fraction and latent heat of transformation respectively. This equation is applicable to all wires of constant diameter but typically used for shorter wires since it accounts for conduction along the wire and the development of the thermal boundary layer [33]. A simplified model is suggested that ignores heat conduction along the wire and it is described by the following equation.

$$\rho L \left(\frac{\pi d^2}{4} \right) \left(c_p \frac{dT}{dt} + \Delta H \xi \right) = I^2 R(\xi) - h \pi d L (T - T_\infty). \quad (39)$$

Simplified Design Model

Further simplification for the abovementioned equation is usually done for first-order design calculations by ignoring the latent heat of transformation and solving for the following temperature profile [33]

$$T(t) = T_{\infty} + \frac{I^2 R}{h\pi dL} + \left(T_0 - T_{\infty} - \frac{I^2 R}{h\pi dL} \right) e^{-\left(\frac{4h}{\rho d c_p}\right)t} \quad (40)$$

This equation gives the time response for the heating of SMA wires. The heat convection coefficient is the only missing parameter and it can be found from reproducing the Churchill–Bernstein relationship for a horizontal cylinder under natural convection from low-velocity to still air. The equation for estimating the heat convection of SMA wires is given by the following equation where the diameter is in millimeters and the temperatures are in degrees Celsius [33].

$$h = 65.5 e^{\frac{-d}{4}} (T - T_{\infty})^{1/6} \quad (40)$$

Those equations can be rewritten to yield first-order equations for the cooling and heating times as well as the cyclic frequency and energy consumption of NiTi wires that are useful to make design choices [37].

$$t_{cool} = D^2/0.0172 \quad (42)$$

$$t_{heat} = 19000 * A/I \quad (43)$$

$$t_{cycle} = t_{heating} + t_{cooling} \quad (44)$$

$$f = \frac{1}{t_{cycle}} \quad (45)$$

$$E_{switching\ event} = I^2 R t_{heating} \quad (46)$$

Where $E_{switching\ event}$ represents the energy per switch/actuation event and it is calculated from the product of input electrical power and the heating time assuming constant input power.

SMA Springs Energy Model

For SMA springs, a model developed by [13] for estimating heating and cooling times of SMA springs under a stress is given by the following equations:

$$\Delta t_{MA,\sigma} = \frac{-\rho c_{MA} d}{4h} \ln \left[\frac{A_f + \frac{\sigma}{C^A} - \left(\frac{I^2 R_e'}{\pi d h} + T_\infty \right)}{A_s + \frac{\sigma}{C^A} - \left(\frac{I^2 R_e'}{\pi d h} + T_\infty \right)} \right] \quad \Delta t_{AM,\sigma} = \Delta t_{AM,\sigma} = \frac{-\rho c_{AM} d}{4h} \ln \left[\frac{M_f + \frac{\sigma}{C^M} - T_\infty}{M_s + \frac{\sigma}{C^M} - T_\infty} \right] \quad (47)$$

Where ρ , c and d represent the density, specific heat capacity and diameter of the SMA actuator while h and T_∞ represent the convection coefficient and ambient temperature. C^M and C^A represent the stress-influence coefficients for the martensitic and austenitic states as discussed earlier in this chapter. A_s , A_f , M_s , M_f represent the start and finish temperatures of the austenitic and martensitic phases respectively while I and R represent the current passed through and resistance of the SMA actuator.

This model predicted response times for SMA actuators that fell within 10% of experimental values [13]. Estimating the heat convection coefficient of a spring is rather challenging and it requires experimental measurement of the exact setup. However, an experiment conducted on different SMA springs under various conditions showed a heat convection value ranging from 100-148 W/m².K [35]. This value was also used by [36] to model SMA springs behavior and yielded favorable results.

Manufacturing Analysis

Another important aspect for SMA-actuated devices and SMAAS particularly is the fabrication/assembly of the actuation mechanism. Since SMAs are available commercially in different sizes and shapes in the macroscale, the first part of this section will focus on the joining techniques of pre-fabricated commercial SMAs rather than the fabrication of the SMAs. However, since the SMAAS requires miniaturization, the second part of this section will focus on micro fabrication and micro joining techniques for micro SMA actuators.

Joining Techniques

Joining options for SMA actuators include:

- 1- Mechanical Assembly (e.g. crimping): This is one of the most widely used methods especially for resistive heating due to the ease of use and the absence of heat which could affect the SMA microstructure. The figure below shows the smallest SMA crimp available in the market [dim are in mm] which accommodates SMA wires with diameters 0.025 – 0.38 mm [8].

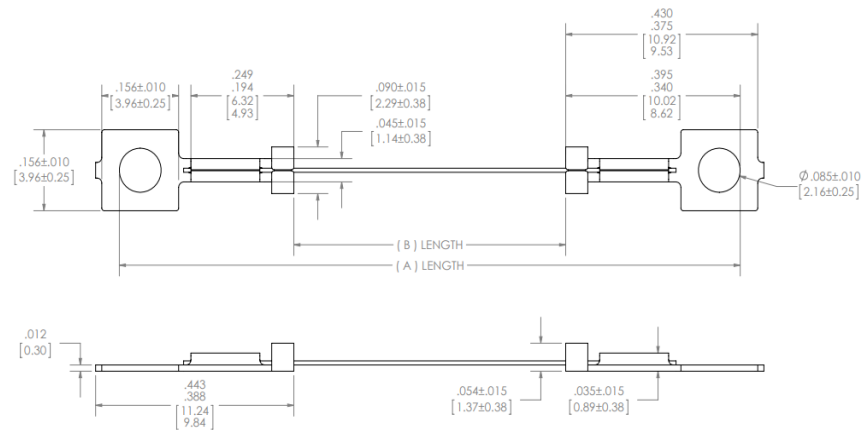


Figure 53: Smallest Ring Terminal for Crimping Resistively-heated SMAs (Reprinted from [8])

However, mechanical crimping can be done through other methods aside from using ring terminals (e.g. using flaps machined out of a substrate).

- 2- Bonding with structural adhesives: Epoxies, acrylics, silicones and hot melts are typically used [16].
- 3- Soldering: SMAs generally cannot be soldered directly. However, soldering it can be done through the abrasion of the titanium oxide layer on the surface before using 6.5%Sn 3.5%Ag or 80%Au 20%Sn solder wires. Abrasion is done mechanically (if possible for larger diameters) or using a flux (for small wires) [38]. Another way of soldering is to electroplate it with a layer of copper then directly soldering it [17].
- 4- Welding: Laser welding is the most widely used in the industry by SMA manufacturers and users. It targets precise spots and has the least heat-affected zone (HAZ). A laser welded SMA ensures up to 88% of its shape memory property [16].

Other options for joining SMAs include friction welding and arc welding but are not very common. In terms of joining SMAs in Micro devices, spot micro welding and bonding in the wafer level are the most common techniques [39] [8][40].

Micro-Fabrication & Assembly Techniques

In micro applications of SMAs, helical springs are not viable options. Therefore, the only available options for micro actuators are wires, slabs/ribbons and flat springs. Slabs/ribbons do not add any additional advantage to wires unlike flat springs which offer higher stroke lengths. Therefore, the focus of this section will be on micromachining of flat SMA springs and micro-joining of both wires and flat SMA springs.

Micromachining

One of the main techniques used for fabricating micro SMA actuator planar springs is micromachining. In this technique, a pulsed femtosecond laser is used to cut through a micro-thickness sheet of SMA. This technique was used to fabricate multiple shapes of planar SMA springs as shown in the examples below from the literature.



Figure 54: Micro-Snake NiTi Actuator Machined Using Laser from a 120µm NiTi Sheet (Reprinted from [41])

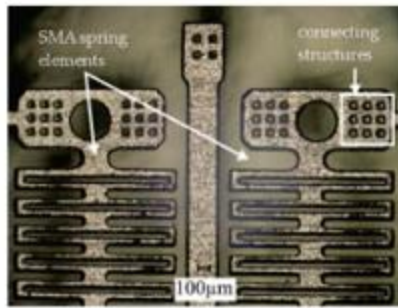


Figure 55: Micro “Box”-Type SMA Spring Actuator Laser-Machined (Reprinted from [44])



Figure 56: A Micro-Gripper Laser Machined out of SMA Sheet (Reprinted from [46])

Micro-Integration

As for the micro-integration of SMA wires and flat (planar) springs, four sample techniques were found in the literature that would support the microfabrication of the SMAAS. Those techniques are:

1. Micro Integration using wire bonding

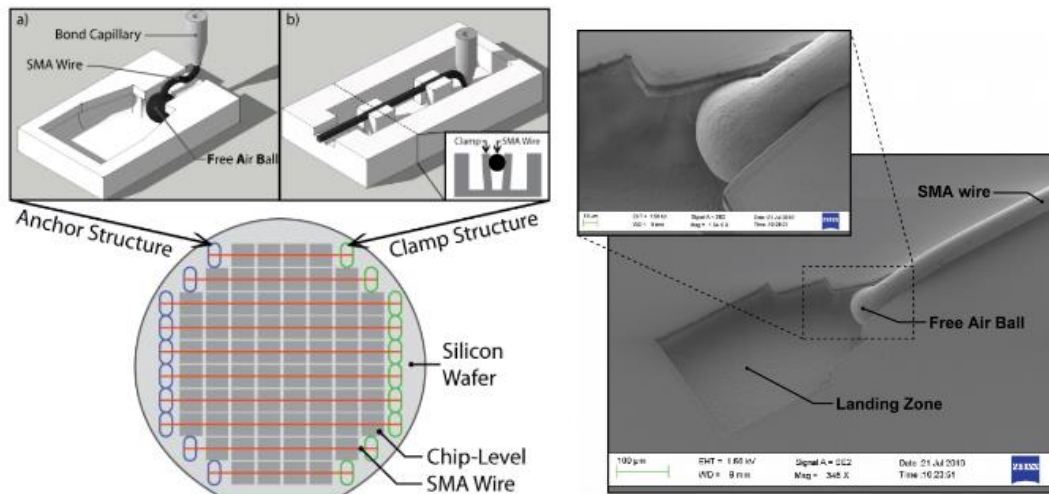


Figure 57: Wire Bonding of Micro SMA Wire (Reprinted from [45])

This process uses the traditional wire bonding technology currently used in the microfabrication of ICs and applies it to SMA wires. An electric current is used to melt the tip of the SMA wires forming a ball that is then placed in a groove “landing zone” or in between two clamps at one end of the wafer and the wire is the routed to the other end before breaking off the wire and forming another ball. To summarize, this method uses mechanical crimping as the main attachment technique of SMA wires through using bonding techniques to melt the two ends of the SMA wire forming balls that are being either held behind two clamps while the wire goes through them or in a being placed in a groove. This process is illustrated in the figure above.

2. Galvanic riveting



Figure 58: Galvanic Riveting of Micro SMA Springs (Reprinted from [44])

This process uses electroplating to form rivets out of a seed layer (made out of any conductive material – typically Cu or Ni) that was deposited on the substrate beforehand. The SMA spring would have holes in it that the rivet structure will go through and form a cap at the end of it when a current with high energy density is passed through the seed layer [44]. Using micro-rivets offer a dual functionality; mechanical fixation and electric current conduction (required for heating the SMAs). This method was tested by the researchers in [44] and yielded resistance against a stress of 7-11 MPa. The SMA element need to be coated with a metallization layer prior to riveting.

3. Submerging + UV curing

This process uses micro SMA wires and submerges them in an untreated SU-8 layer before curing it with a UV radiation. The cured SU-8 layer then solidifies around the SMA wires holding them in place. The SMA wires need to be pre-strained before submergence. The only challenge with this method is handling the wires during pre-straining and submergence, therefore, this is usually done on the wafer/batch level rather than individual device level [39].

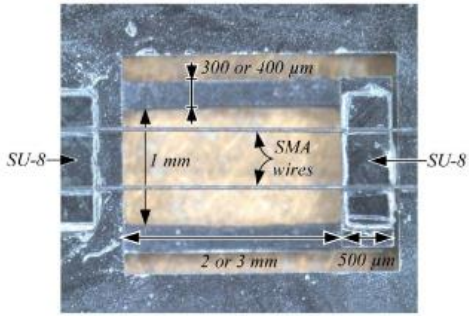


Figure 59: SMA Wires Submergence Example (Reprinted from [39])

Micro attachment of SMA wires through submergence and UV curing by [39]
Lastly, another joining technique reported by manufacturers for micro wires is micro spot laser welding [8] [17].

Fatigue

Fatigue in SMAs can be structural or functional. Typically SMAs do not fracture under normal conditions since they are operated significantly under their strain and stress limit to prevent any plastic unrecoverable strain. Therefore, emphasis on the fatigue life of SMAs is placed on their functionality degradation over life. This functionality deterioration manifests itself in the loss of shape recoverability by SMAs which are controlled by two quantities; recovery stress and recovery strain [7]. As shown in the figure below, as the number of cycles increase, the recovery stress and recovery strain generally decreases.

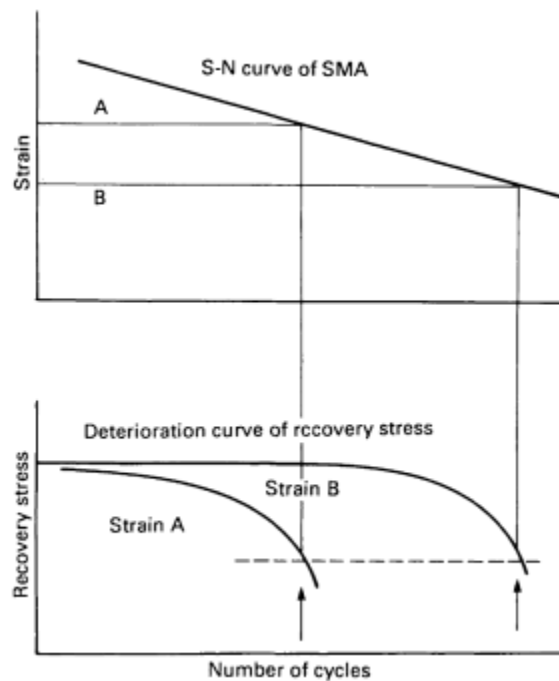


Figure 60: Schematic S-N Fatigue and Deterioration Curves for SMAs (Reprinted from [7])

However, these S-N and strain-N curves are very product-specific. Unlike other metals (e.g. Stainless Steel), there is no specific S-N curve for Nitinol or other SMAs. Wires of different diameters or different manufacturers were found to have different fatigue life [43]. In addition, developing a model for predicting the thermal cycle lifetime of SMAs is currently an active area of research. Therefore, experimental cyclic testing is required for each application using the exact same SMA actuators for the intended application to mimic their fatigue life cycle [7]. However, some conservative recommendations for lifecycles of NiTi wires can be found in the table below by [42].

Table 11: Recommended Maximum Strain and Stress for SMA Cycle Life (Reprinted from [42])

Cycles	Max. Strain	Max. Stress
1	8%	500 MPa
100	4 %	275 MPa
10000	2 %	140 MPa
100000+	1 %	70 MPa

Another advantage of performing experimental cyclic testing on the designed actuator is realizing the active stroke length and stabilizing the actuation stroke. Typically SMAs need to be pre-strained by a larger amount than the required strain since SMAs don't recover the full pre-strain as mentioned in Chapter II. In addition SMAs also require "training" or cyclic testing for 100-150 cycles to remember the same actuation stroke and stabilize. This is better illustrated in the graph below of the cyclic testing results obtained by [1].

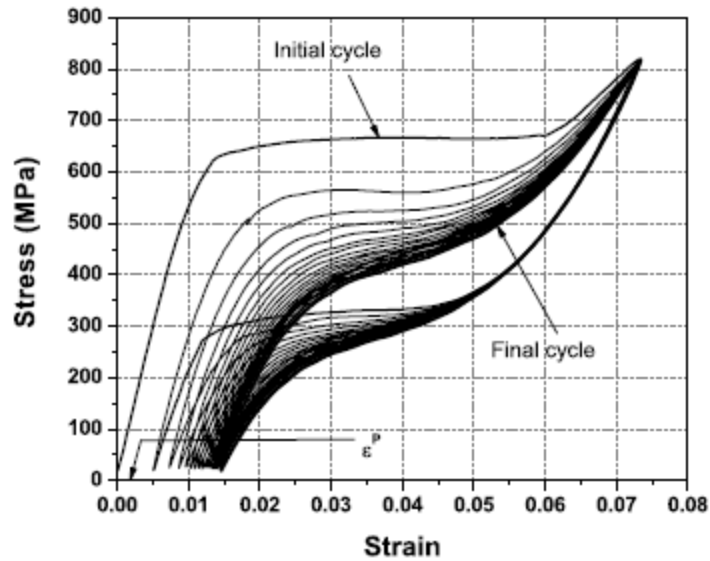


Figure 61: Cyclic Training of SMAs (Reprinted from [1])

To recap, there is no current model in the literature that predicts functional fatigue life of SMAs as it is an active area of research. S-N curves and deterioration profiles provide insights to the functional lifetime of SMA actuators but they are very product specific. Therefore, engineers and designer can either use the generalized empirical values estimated in the literature or obtain it experimentally through cyclic testing or use recommendations from manufacturer's data sheets. For instance, Dynalloy recommends 2%-5% max strain under a maximum stress of 70 MPa and 172 MPa for cold and hot condition respectively for a lifecycle of more than a million cycle [8]. Lastly, SMAs active stroke lengths vary from the pre-strain value (always less) so designers and engineers should account for that in the design. The SMA actuators need to be cycles 100-150 times in order to stabilize and have a uniform actuation stroke.

CHAPTER V

CASE STUDIES

In this chapter, two case studies are presented for the microfabrication of a SMAAS design and numerical optimization of another design concept using MATLAB. Those case studies are based on the analysis and models discussed in Chapter IV and are based on the down-selected design concepts presented in Chapter III.

Case Study I: Micro Fabrication of SMAAS Design

One of the down-selected design concepts in Chapter III was the leaf-spring loaded plunger concept shown in the figure below. This concept utilizes a profiled conductive plunger that is actuated by SMA actuators from both sides and are contacted by two leaf spring electric contacts from each side. Those leaf spring contacts are connected to external load circuits and have the dual functionality of conducting current through the plunger as well as lock the plunger in place during conduction.

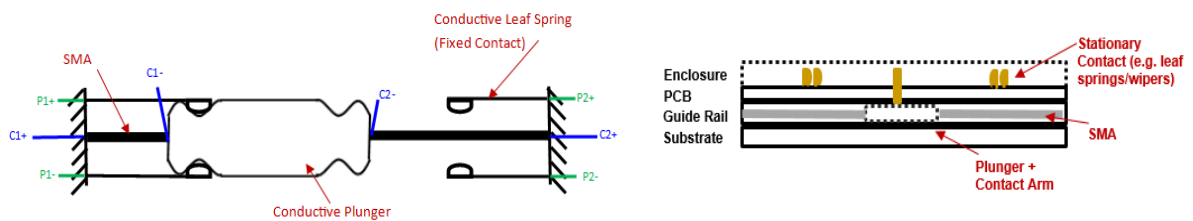


Figure 62: SMAAS Design Schematic: Top View (Left) and Side View (Right)

This design was selected for this case study since it has one of the highest micro manufacturability and functionality potential. This is because of its low complexity, few moving parts and planar configuration. This concept consists of 5 unique parts namely;

substrate, SMA actuator(s), plunger, leaf spring contacts and enclosure/casing. The table below shows the desired properties (mostly mechanical) and candidate materials for each of the components. It also provides the selected material for each component.

Table 12: Component-Specific Requirements and Material Selection for Fabricating the SMAAS Concept

Component	Requirement (s)	Options	Selection
Substrate	<ul style="list-style-type: none"> - High mechanical strength - Electrically and thermally insulating - Low friction 	Si Glass	Si
SMA Actuator	<ul style="list-style-type: none"> - Exhibits one-way shape memory effect - Transformation temperature above 80C 	Cu- Al-Ni NiTi	Nickel Titanium (Nitinol)
Plunger	<ul style="list-style-type: none"> - High mechanical strength - Electrically conductive - Low friction 	Al, Cu, Au	Al
Contacts/Leaf Springs	<ul style="list-style-type: none"> - Moderately elastic with high fracture strength - Electrically conductive - High friction 	Al, Au	Al
Casing	<ul style="list-style-type: none"> - Thermally & mechanically stable - Electrically insulating - High impact strength 	Thermally moldable plastics	Epoxy

For the substrate SI was selected because of its stable mechanical properties as well as its thermal insulation and relatively low friction. In addition, existing MEMS fabrication landscape excessively use Si substrates, thus, the technology and existing manufacturing systems are configured to produce it easily. The SMA actuator material is set for NiTi since it is the most available and most studied SMA material as discussed earlier in Chapter II. For the plunger, Aluminum was selected for its low cost and ease of manufacturing, however, the other alternatives are viable options. Aluminum could also be gold coated for better conductivity. Same reasoning applies to the leaf springs. As for the casing, since the end goal for the micro SMAAS to have the same outer structure as an IC, the case's material is then chosen to be thermally-molded epoxy. The manufacturing of each of the SMAAS components is described in the following sections as well as the assembly and packaging of the complete SMAAS design concept.

Substrate

The substrate structure shown in the figure below consists of a Si wafer and a guide channel etched into it horizontally using chemical etching (e.g. KOH etching – which is a common well-documented etching method for Silicon). This guide channel will define the path along which the metal plunger would move. The two edges on the sides will have holes drilled or etched into it for integration purposes (discussed later in the assembly section. In addition, those two edges will be sputter-coated with a metal layer for conduction and integration purposes (e.g. Ni or Cu) in addition to the areas surrounding the holes. The guide channel could potentially be coated with PTFE to have

a smooth low-friction surface for the plunger to slide along as well as complete electrical isolation from the plunger.

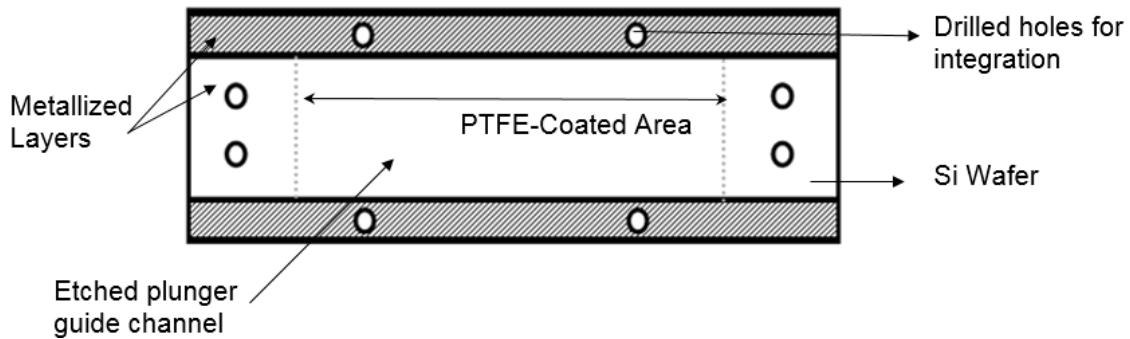


Figure 63: Schematic of the Micro SMAAS Substrate

Conductive Plunger

The conductive plunger is to be cut out of aluminum sheets using micro wire EDM (electric discharge machining) in order to have smooth round edges as shown in the schematic in the figure below. Having smooth curved edges is important for the lead spring contacts to slide along. A possible alternative to wire EDM is micro laser machining. The holes in the center are required for integration and are to be drilled using ultrasonic micromachining (A common method uses alumina abrasive slurry). This is assuming micro wire EDM was used, however, if laser machining was used for the aluminum sheets cutting then it can also be used for cutting out the holes. Lastly, the bottom of the plunger is to be coated by an insulating adhesive layer (e.g. epoxy or polyurethane or PTFE).

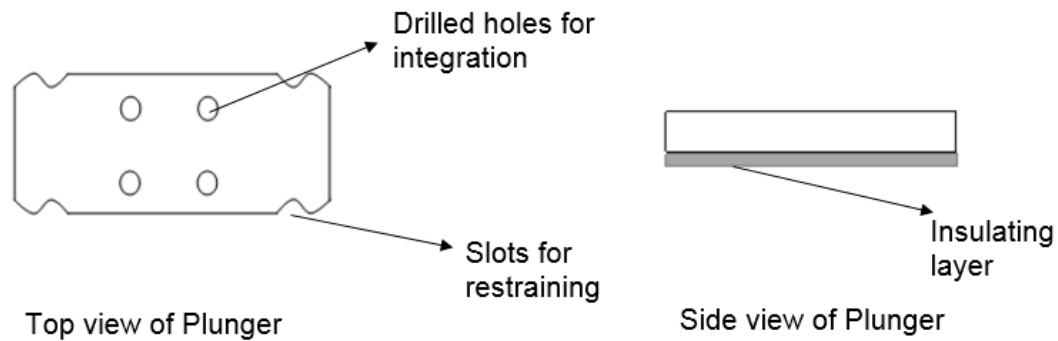


Figure 64: Schematic of the Micro SMAAS Plunger

SMA Members

Inspired from the microgripper design in the literature [44] discussed in Chapter IV, the SMA members are to be cut out of NiTi micro-thickness sheets using femtosecond laser ablation and will have a flat “box” spring shape as shown in the figure below. An advantage of laser-machining a NiTi sheets is that a spring structure is obtained which has higher allowable strain when compared to the 3-5% strain allowed in wire. In addition, the antagonistic actuation mechanism will be inherently integrated in one-piece, thus, no need for subsequent integration process. Not to mention that this method eliminates the need for a movable electrical connection at the end of the SMA at the plunger since the SMA is connected so only positive/negative connections are required at the two terminals located at each end of the SMA. The design in the literature recommended the use of a Yb-KGW SSD laser with 515nm wavelength [44]. Pre-straining this SMA member should be done at this stage before assembly through the use of a pre-straining using micrometer screw process recommended by [39] for wafer-level pre-straining as shown in the figure below (right).

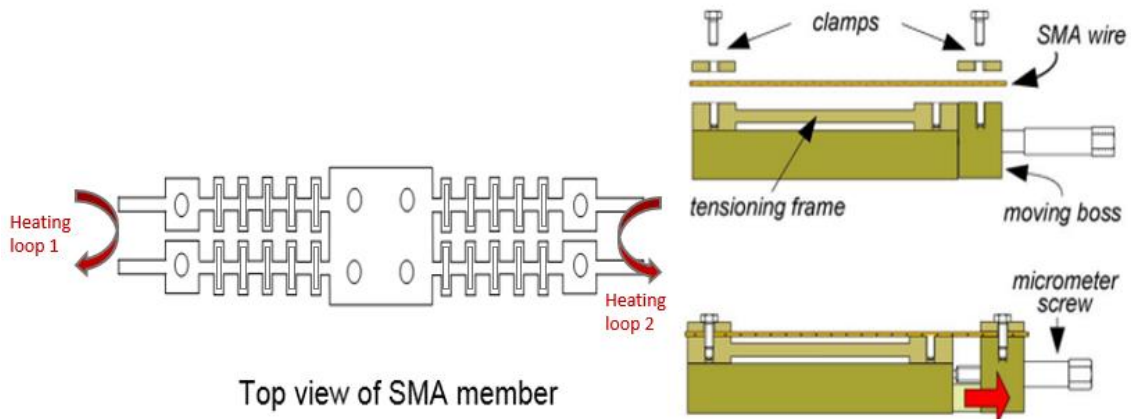


Figure 65: Schematic of the Micro SMAAS Plunger and Micrometer Pre-Straining Process (Reprinted from [39])

Leaf Springs

The leaf springs will be cut out of an Aluminum micro-thickness sheet using EDM (wire) in order to achieve smooth round corners. However, as discussed earlier for the plunger laser micro machining would also be a viable option for such object. The holes will be either drilled using ultrasonic machining or laser micromachining.

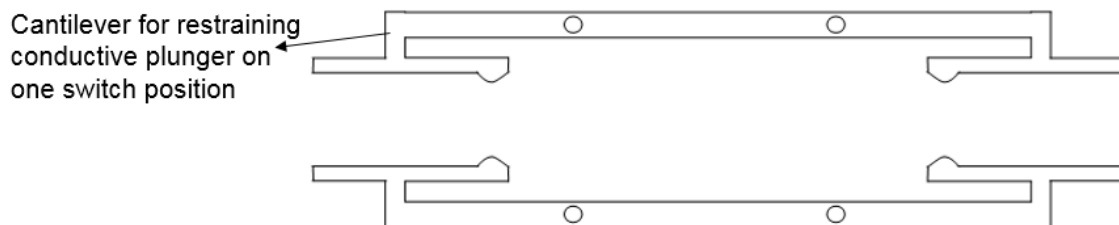


Figure 66: Schematic of the Micro SMAAS Electrical Contacts Structure

Assembly

The assembly and packaging of the 4 components of the SMAAS is done over 4 steps:

1. The plunger is to be joined to the SMA actuator after it was pre-strained using adhesive bonding.
2. The SMA-Plunger subassembly is then joined to the substrate using electroplated micro-rivets at the holes as discussed in Chapter IV.
3. The leaf springs are finally joined to the substrate using micro-rivets at the holes.

The areas surrounding the holes were coated by metal seed layer (Ni or Cu) for the reason of using it in an electroplating process to form micro-rivets. The rectangular end terminals of the SMA member and leaf springs are protruding out of the assembly for external electric connections to load and heating circuits.

4. After the 4 components of the SMAAS are assembled, the entire assembly will be packaged using epoxy molding to have the same IC external structure.

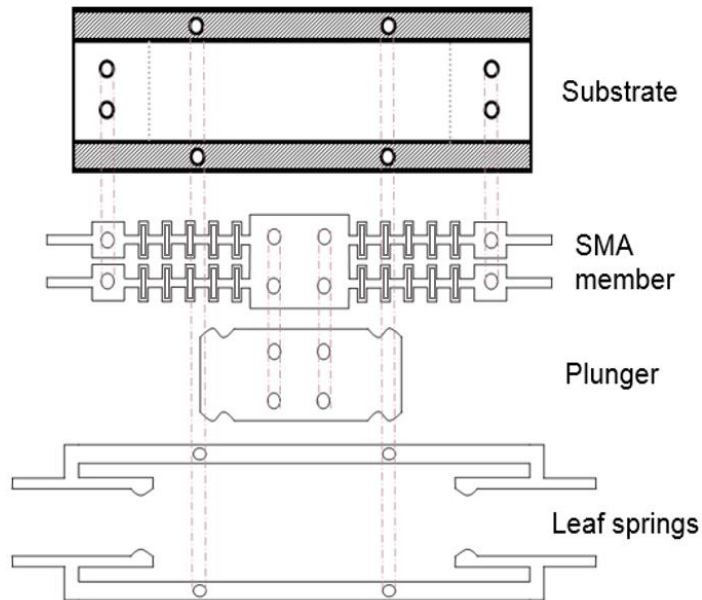


Figure 67: Schematic of the Assembly Process of the Micro SMAAS

Case Study II: Numerical Optimization of SMAAS Design

In this case study, a numerical optimization model is investigated for one of the down-selected SMAAS design concepts. The model developed in this design concept can be applied to the other design concepts with minor changes in the constraints and variables.

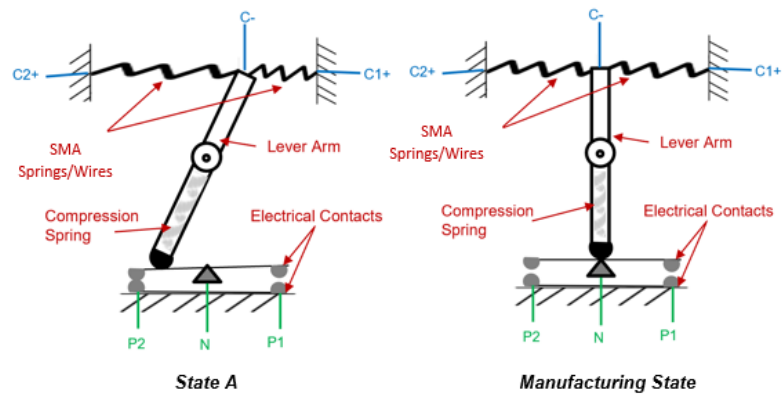


Figure 68: A Schematic of the Conceptual Design of the SMAAS to be Optimized

Problem Formulation

First step for optimizing the design is to formulate the optimization problem.

This is done through identifying the design vector in terms of the design variables then identifying the design parameters, variable bounds, objectives and design constraints. In the following section, the above mentioned aspects of the optimization problem are formulated.

Design Vector

The design vector for this concept consists of 10 dimensional variables and 1 functional variable namely I_{supply} which is the current supplied to the SMA to heat it. The 11 design variables are listed and illustrated geometrically as shown below.

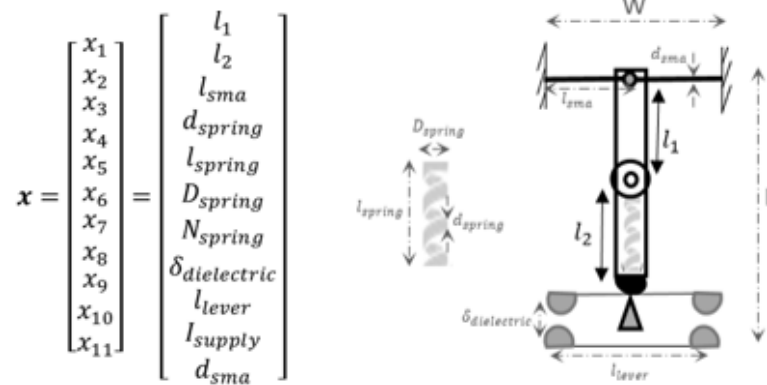


Figure 69: Design Variables Illustration for the Optimal SMAAS Concept

Parameters

Some parameters were fixed in this problem to avoid discretized variables and due to the availability of resources. The SMA material was chosen to be Nitinol since it is the most SMA material available commercially as well as well-researched in the literature as discussed earlier in Chapter II. Accordingly, the following material properties in Table 1 were obtained from the manufacturer data sheet and used as parameters in the optimization algorithm [8].

Other parameters include user-dictated parameters like the ambient temperature, blocking voltage, maximum dimension, maximum strain, modulus of rigidity of the spring (steel material was selected and fixed for this problem) and coefficient of friction for the moving parts (brass was selected and fixed for this problem for its' high electrical conductivity). Other fixed parameter that is a property of the environment is dielectric strength of air. Those fixed parameters and their corresponding values are also shown in the table below. The blocking voltage and maximum dimension are discussed in the design framework section of Chapter III.

Table 13: Material Properties and User-specified Parameters [8]

Parameter	Value
ρ	6.45E3 kg/m ³
c_p	0.8368E3 J/kg °C
E_A	70E9 Pa
E_M	30E9 Pa
T_f	70°C
V_{block}	500 V
l_{max}	0.01 m
T_∞	25°C
ϵ_{max}	0.05
$\epsilon_{dielectric,air}$	2E6 V/m
G	79.3E9 Pa
$\mu_s \& \mu_d$	0.51, 0.44

Bounds

The bounds for the 11 design variables identified earlier in this section and their respective units are listed below.

$$\begin{bmatrix}
 0.5 \text{ mm} \\
 0.5 \text{ mm} \\
 2 \text{ mm} \\
 0 \text{ mm} \\
 0 \text{ mm} \\
 0.05 \text{ mm} \\
 4 \text{ coils} \\
 V_{block} \\
 \hline
 \epsilon_{dielectric, air} \\
 0 \text{ mm} \\
 5 \text{ mA} \\
 0.025 \text{ mm}
 \end{bmatrix}
 \leq x \leq
 \begin{bmatrix}
 l_{max}/2 \text{ mm} \\
 l_{max}/2 \text{ mm} \\
 l_{max}/2 \text{ mm} \\
 l_{max}/2 \text{ mm} \\
 l_{max}/2 \text{ mm} \\
 l_{max}/2 \text{ mm} \\
 l_{max}/2 \text{ mm} \\
 10 \text{ coils} \\
 l_{max}/4 \text{ mm} \\
 l_{max}/2 \text{ mm} \\
 3000 \text{ mA} \\
 2 \text{ mm}
 \end{bmatrix}$$

The dimensional variables were set in respect to the maximum specified dimension (L_{\max}) which comes from the design footprint constraint. The number of coils were arbitrarily set to 10 coils. It was noticed later that increasing it will not affect the optimization problem. The SMA diameter and supply current bounds were set to the maximum provided by the manufacturer's datasheet shown in Appendix B.

Objectives

Two objectives were identified for the switch as per the intended application as discussed in the design framework in Chapter III. Those objectives are:

$$J = \begin{bmatrix} E \\ Z \end{bmatrix} = \begin{bmatrix} \text{Energy per switch event} \\ \text{out - of - plane height} \end{bmatrix}$$

Where energy per switch event E is calculated from electric power input over the heating time and the out-of-plane height Z is dictated by the maximum dimension of the switch components as shown below:

$$E(x) = I_s^2 R t \quad (48)$$

$$Z(x) = \max \{D_{spring}, dsma\} \quad (49)$$

Constraints

A list of 8 non-linear and 3 linear inequality constraints were devised for this problem and listed below:

$$\mathbf{g}(\mathbf{x}) = \begin{bmatrix} Y(\mathbf{x}) \\ C(\mathbf{x}) \\ dL_{pivot}(\mathbf{x}) \\ dL_{solid}(\mathbf{x}) \\ dL_{footprint}(\mathbf{x}) \\ dL_{actuator}(\mathbf{x}) \\ dL_{contacts}(\mathbf{x}) \\ dL_{spring\ def}(\mathbf{x}) \\ dI(\mathbf{x}) \\ dF_{rest}(\mathbf{x}) \\ dF_{motion}(\mathbf{x}) \end{bmatrix} \leq 0$$

Where the first 8 constraints are geometric in nature and represented in terms of the design geometric variables:

$$\gamma(\mathbf{x}) = 1 - \frac{l_2}{l_1} \leq 0 \quad (50)$$

This constraint is related to the mechanical stroke advantage. In other words, a small movement in the SMA shall produce large motion at the contacts.

$$C(\mathbf{x}) = 6 - \frac{D_{spring}}{d_{spring}} \leq 0 \quad (51)$$

This constraint is related to the spring index of the compression spring. Generally speaking, a spring index less than 4 is very hard to manufacture, while from 4 to 6 are hard and expensive but possible so a spring index of 6 or more is constrained for this problem.

$$dL_{pivot}(\mathbf{x}) = l_{spring} - l_2 \leq 0 \quad (52)$$

This constraint limits the length of the compression spring to be less than or equal to the lever arm length from the pivot point.

$$dL_{solid}(\mathbf{x}) = l_{spring} - (N_{spring} \times d_{spring}) - \delta_{dielectric} \leq 0 \quad (53)$$

This constraint imposes the deflection of the spring to be less than the pitch gap.

$$dL_{contacts}(x) = 2 \epsilon_{max} l_{SMA} \frac{l_2}{l_1} - l_{lever} \leq 0 \quad (54)$$

This constraint forces the length of the lever contact to be long enough to at least cover the total actuation length.

$$dL_{spring\ def}(x) = \sqrt{l_{spring}^2 - (l_{spring} - \delta_{dielectric})^2} - \epsilon_{max} l_{SMA} \frac{l_2}{l_1} \leq 0 \quad (55)$$

This constraint forces the horizontal distance between the fully-compressed and fully-retracted spring position to not exceed the actuation stroke length.

$$dL_{footprint}(x) = l_1 + l_2 + \delta_{dielectric} - l_{max} \leq 0 \quad (56)$$

This intuitive constraint is put in place to limit the total dimension of the switch (sum of its collinear dimensions) not to exceed the maximum dimension set as a parameter.

$$dL_{actuator}(x) = (2 + \epsilon_{max})l_{SMA} - l_{max} \leq 0 \quad (57)$$

Similarly, this constraint limits the dimension in the y-direction to be less than or equal to the maximum dimension allowed. The last three constraints are functional in nature and are related to the rated current of the nitinol wire as well as its' forces:

$$dI(x) = 2 \times 10^7 d_{sma}^2 + 205.16 d_{sma} - I_{supply} \leq 0 \quad (58)$$

This constraint limits the supply current not to exceed the rated current as set by the manufacturer and discussed in Chapter IV.

$$dF_{rest}(x) = F_{relaxation,SMA}l_1 - F_{Spring}l_2 \leq 0 \quad (59)$$

This constraint is used to design the spring such that it can produce enough force to overcome the relaxation force of the SMA i.e. maintain the electrical connection at the switch state.

$$dF_{motion}(x) = F_{restorative, SMA}l_1 + \mu_d F_{Spring}l_2 - F_{heating, SMA}l_1 \leq 0 \quad (60)$$

On the other hand, this constraint is set to choose the SMA wire such that its pulling force exceeds the restorative force of the other competing SMA as well as the friction in order to successfully switch states. Those constraints were formulated from a free body diagram analysis in Chapter IV.

Governing Equations

The governing equations for the forces and energy of the SMAs are given by the simplified design equations discussed in greater details in Chapter IV. Those equations are tabulated below.

Table 14: Governing Equations for the Optimization of the SMAAS

Property	Equation
Heating time of SMA wires	$T_f = T_\infty + \frac{I^2 R}{h\pi d_{sma} l_{sma}} + \left(T_0 - T_\infty - \frac{I^2 R}{h\pi d_{sma} l_{sma}} \right) e^{-\frac{4h}{\rho d_{sma} c_p} t}$
Heat convection coefficient of SMA	$h(T, T_\infty, d_{sma}) = 65.5 e^{-\frac{d_{sma}}{4}} (T - T_\infty)^{\frac{1}{6}} \quad [W m^{-2} K^{-1}]$
Resistance of SMA wires	$R = L_{sma} \times 10^{-6} d_{sma}^{-1.986} \Omega$
Heating force of SMA wires	$F_{heating} = 10^{10} d_{sma}^2 + 1.03 \times 10^5 d_{sma} - 3.4$
Restorative force of antagonistic SMA wire	$F_{restorative} = 5 \times 10^9 d_{sma}^2 + 4.07 \times 10^4 d_{sma} - 1.48$
Relaxation force of SMA wires post-cooling	$F_{relaxation} = 0.5\% \times E_M \times \frac{\pi d_{sma}^2}{4}$

As for the retaining force of the compressive spring located in the lever arm, this force is described by Hook's law and elastic shear modulus as follows [31].

$$F_{Spring} = \frac{d^4 G}{8D^3 N} \delta_{dielectric} \quad (61)$$

Block Diagram

The diagram below shows the interaction between different multi-discipline modules involved in this optimization problem as well as the input parameters and design variables. The output of those modules are the objective values as well as the constraint values. This model was coupled with the optimization algorithm and iterated as discussed in the following section to find the optimal design vector that meets the constraints and the minimum objective(s) value(s).

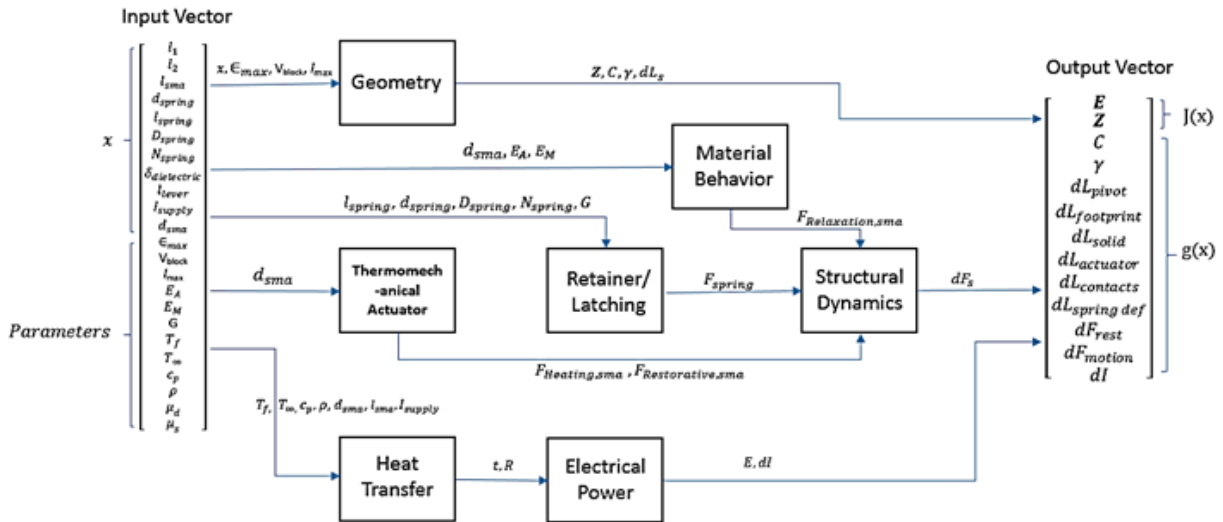


Figure 70: Block Diagram of Multi-Disciplinary Modules Interactions.

Optimization

The SMAAs design problem consists of 11 continuous design variables. For that reason, a gradient-based method is a better fit compared to heuristic methods for multiple reasons. The first reason is that all the design variables are continuous. The second reason is that it converges much faster thus reducing the computational cost. The gradient-based method of choice is Sequential Quadratic Programming (SQP). SQP was selected due to its effectiveness in dealing with non-linearly constrained optimization problems. The main downside for SQP, which is the downside of many gradient-based algorithms, is that it is highly dependent on the starting point. Every time the SQP is ran, a different solution is found. This can be attributed to the large design space (11 dimensions), therefore, it is expected to have multiple local optima. To circumvent this problem, to increase the chance of finding a global optimum, a multi-start SQP algorithm was used.

Single Objective Optimization

The first experiment ran was to optimize for a single objective. The main objective for this design problem is to minimize energy per switch event (EPSE) since this is the main selling point of this novel switch design. Multi-start FMINCON from MATLAB was then used. 200 starting points were used; 199 randomly generated points and 1 point obtained from the GA after performing DOE. Out of the 200 local solvers, only 4 converged to a feasible local optima. The best out solution out of the 4:

$$x_0 = [0.0005, 0.00353, 0.003335, 8.3e - 5, 0.001245, 0.001, 5.141, 0.000292, 0.004995, 0.042899, 2.5e - 5]$$

For that local optimum, EPSE was found to be 0.436 mJ, while the maximum thickness of the switch design was found to be 1 mm. The constraints check shows that the design is feasible with a tolerance of 10^{-8} as shown in the constraints vector result below.

$$C = [-6.0596, -5.25e - 4, -3.76e - 4, -3.49e - 4, 1.24e - 9, -2.439e - 5, -0.0026, -5.984]$$

Sensitivity Analysis

Sensitivity analysis was performed to study the effects of each design variable on the objective function. Only 3 out of the 11 design variables affect the EPSE objective function (d_{sma} , L_{sma} , and I_{sup}). The Jacobian was calculated using MATLAB:

$$\nabla J = \frac{\partial J}{\partial x} |_{x^*} = [0 \ 0 \ 0.1308 \ 0 \ 0 \ 0 \ 0 \ 0 \ 0 \ -0.0018 \ 36.1137]$$

The normalized jacobian is found to be:

$$\underline{\nabla J} = \frac{x^*}{J(x^*)} \nabla J = [0 \ 0 \ 0.9 \ 0 \ 0 \ 0 \ 0 \ 0 \ 0 \ -0.177 \ 2.07]$$

A tornado chart was created to visualize the effects of the design variables on the objective function EPSE.

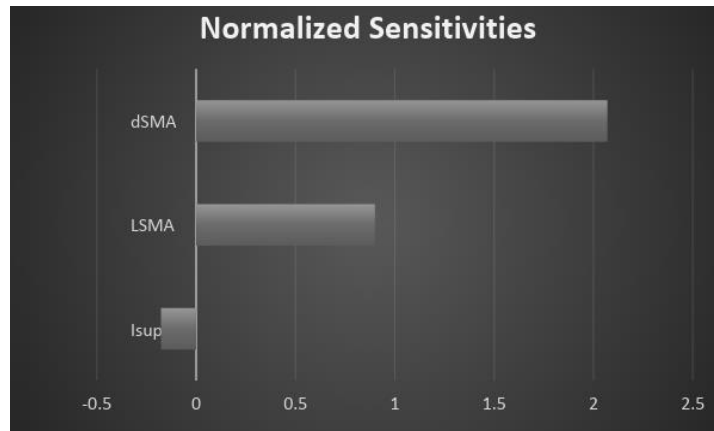


Figure 71: Normalized Sensitivities of the Design Variables.

As expected, the diameter of the SMA wire is the most influential design variable on the objective function. This is because the SMA diameter dictates the actuation force and subsequently the energy needed to actuate it. The length of the SMA is only dictated by the recoverable strain while supply current is dictated by the diameter itself.

Multi-Objective Optimization

For the second experiment, a second objective was added to the formulation. The second objective is to minimize the out-of-plane Z height of the switch since it needs to be embedded into a photovoltaic skin. Therefore,

$$J = [EPSE, Z]$$

PARETOSEARCH from MATLAB was used to find non-dominated points to create the pareto front. The way PARETOSEARCH works is it uses Pattern Search to find the optimal points.

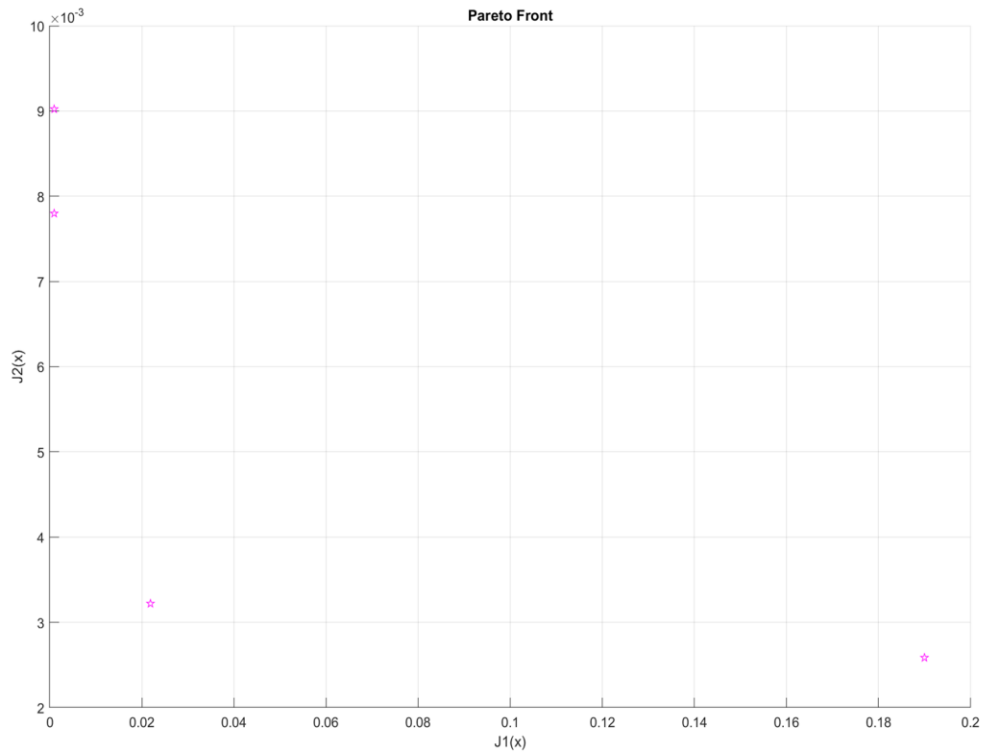


Figure 72: Pareto Front for the Design Objective Functions.

PARETOSEARCH initially did not find any pareto optimal solution, therefore, the constraints were relaxed even further and it eventually found 4 points. The constraints were violated by 0.041837 (which is considerably high considering the 10E-08 maximum violation limit obtained with single objective optimization).

Trade-Off Analysis

An alternative method was needed to optimize for both objectives. Therefore, another approach was to optimize each objective function separately and then perform a trade-off analysis to select the best design. While optimizing for EPSE, the solver found

4 local minima, and while optimizing for Z, the solver found 11 local minima. A visualization of those single-objective optimal solutions is shown in the figures below.

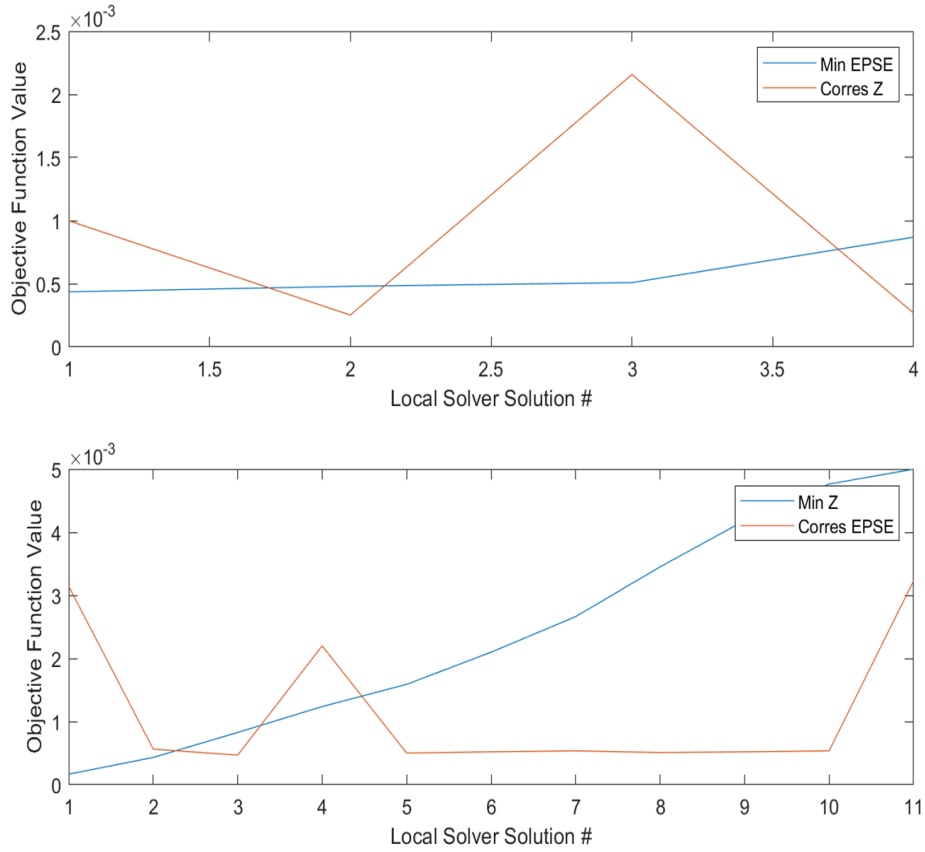


Figure 73: Trade-off Analysis from Optimizing Design Objectives Separately.

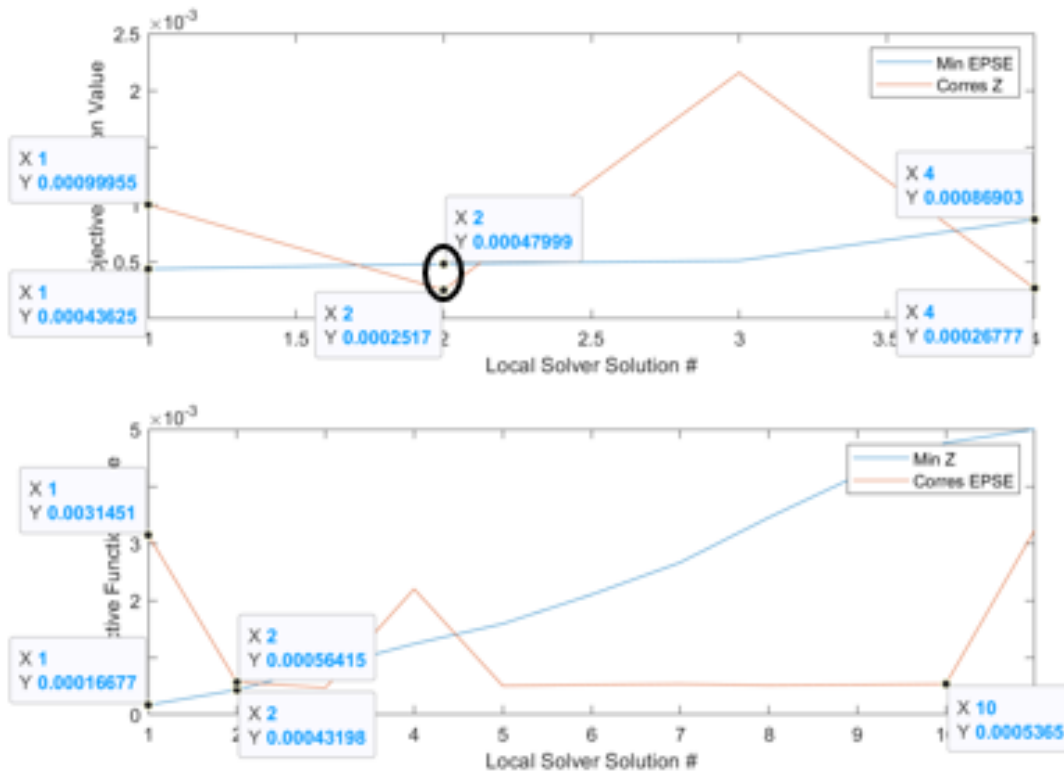


Figure 74: Selected Trade-off Point from Optimizing Design Objectives Separately.

After picking out the key local minima points for the two single-objective optimization runs, the highlighted trade-off point shown in the figure above was selected since it has the lowest combination of the two objectives. The corresponding solution for this trade-off point and the objective functions values are as follows:

$$\mathbf{x}^* = \begin{bmatrix} l_1 \\ l_2 \\ l_{sma} \\ d_{spring} \\ l_{spring} \\ D_{spring} \\ N_{spring} \\ \delta^{dielectric} \\ l_{lever} \\ I_{supply} \\ d_{sma} \end{bmatrix} = \begin{bmatrix} 0.5 \text{ mm} \\ 2.8 \text{ mm} \\ 3.5 \text{ mm} \\ 0.0322 \text{ mm} \\ 0.796 \text{ mm} \\ 0.2517 \text{ mm} \\ 6.5 \\ 0.3256 \text{ mm} \\ 4.9 \text{ mm} \\ 35 \text{ mA} \\ 0.025 \text{ mm} \end{bmatrix} \quad \begin{aligned} EPSE(\mathbf{x}^*) &= 0.5 \text{ mJ} \\ Z(\mathbf{x}^*) &= 0.252 \text{ mm} \end{aligned}$$

This vector gives the values for the 11 design variables for the spring-loaded lever design concept of the SMAAS. Those design variable values yield a maximum thickness of the switch of 0.252mm and a switching energy of 0.5mj per event. The complete MATLAB code for this optimization is found in Appendix C. As discussed over the course of this case study, this is an 11-dimensional problem. There is no single optimal design for it. In fact, the solution found at the end is a trade-off solution obtained from optimizing each objective separately. Nevertheless, the model developed through this case study can give insights during a detailed design process for a SMAAS. It is recommended to apply the same optimization process to the other down-selected concepts while including more rigorous models for the SMAs and the mechanical structure to realize an actual optimal fully-detailed SMAAS design.

CHAPTER VI

CONCLUSIONS

Thesis Conclusion

This thesis involved the investigation of the feasibility of a shape memory alloy actuated switch (SMAAS) for the potential application of smart photovoltaic cells. This was achieved through conducting an extensive literature review of state of the art SMA-actuated switches as well as the models used to describe them. This was followed by a conceptual design process where 15 novel design concepts were generated for the SMAAS; six of which were down-selected after a qualitative assessment. The assessment judged the conceptual designs against manufacturability, robustness, complexity and other criteria relevant to the intended application. Two of these down-selected concepts were prototyped in the macroscale as a proof of concept and their functionality was successfully tested for stable bi-state electrical switching.

A technical review of the models used to analyze thermomechanical behavior of SMAs as actuators as well as their ohmic heating models, fatigue behavior and micro fabrication was also conducted in this thesis. In addition to the models in the literature, empirical models for the design of SMA actuators were developed through the interpolation of manufacturer's data sheet. These models are useful for preliminary first-order design equations to select SMA components and evaluate the feasibility of some design concepts. Lastly, case studies for the numerical optimization and micro-

fabrication processes of two of the down-selected design concepts were conducted as part of this work. Therefore, the main outcomes of this thesis work can be listed as:

- Novel design concepts for a SMAAS. A patent was filed for the concepts developed as part of this work.
- Two fully functional SMAAS prototypes in the macro scale.
- An extensive review and analysis of analytical and experimental models for SMA actuators (both wires and springs).
- A numerical optimization models for the SMAAS concept.
- A micro-fabrication and assembly proposal for a SMAAS concept supported by similar applications in the literature.
- Design recommendations for SMA-actuated devices that covers material and geometry selection, fatigue characterization, locking mechanisms and joining techniques.

This thesis provides a framework for the design of a shape memory alloy actuated switch (SMAAS). It is intended to provide an overview of all the aspects and challenges of designing such a device and surveys all potential concepts rather than focusing on designing a single concept. As such, someone with an interest in developing this switch concept as a product would be able to take this work including the selected designs, their analyses and the design recommendations and successfully develop this SMAAS product.

Future Work

In order to take the work of this thesis to the next step of developing a SMAAS, the following areas are recommended to be explored:

- Microscale prototyping of one of the down-selected design concepts. A good starting point is the design concept analyzed in the micro manufacturing case study in Chapter V.
- Modeling (either analytically, experimentally or using finite element analysis) of SMA planar spring elements manufactured out of thin sheets. This concept of micro planar SMA springs has a significant potential for the development of SMA MEMS actuators and switches.
- Developing a fatigue and functional deterioration model as well as a relaxation model for SMAs from cyclic experimental data. This cyclic experiments need to employ down-selected SMA shapes and geometry recommended from the work in the previous point.

REFERENCES

- [1] P. K. Kumar and D. C. Lagoudas (2008). “*Introduction to shape memory alloys*” In: *Shape Memory Alloys*. Springer, Boston, MA (2008). https://doi.org/10.1007/978-0-387-47685-8_1
- [2] Soderholm, L. H. and Bern, Carl J. (1976). “*Solid-State Relays for Control*”. Agricultural and Biosystems Engineering Publications. 455. https://lib.dr.iastate.edu/abe_eng_pubs/455
- [3] L. Alpuerto and R. S. Balog (2019). “*Energy Harvest Potential of Flexible Photovoltaics on Curved Surfaces*” in IEEE Texas Power and Energy Conference (TPEC). College Station, Texas USA.
- [4] Yee, Teh (2017). “*Fast, Accurate Force and Position Control of Shape Memory Alloy Actuators*” (Master Thesis). The Australian National University.
- [5] M. Kohl (2004). “*Shape Memory Microactuators*”. Springer. pp 5-24. <https://doi.org/10.1007/978-3-662-09875-2>
- [6] Liang, C. (1990). “*The Constitutive Modelling of Shape Memory Alloys*”. PhD Dissertation. Department of Mechanical Engineering. Virginia Polytechnic Institute and State University
- [7] Duerig, T. W. (1990). “*Engineering aspects of shape memory alloys*”. London: Butterworth-Heinemann. pp 256-266.
- [8] Dynalloy, Inc.(2011). “*Technical Characteristics of Flexinol Actuator Wires.*” Dynalloy Inc. Tustin. Retrieved from <https://www.dynalloy.com/pdfs/TCF1140.pdf>.
- [9] Wayman, C. & Duerig, T. (1990). “*An Introduction to martensite and shape memory*” In: *Engineering Aspects of Shape Memory Alloys*. Duerig, T. (Ed.). Butterworth – Heinemann Ltd.. London. pp 3-20.
- [10] Krishnan, Vinu Bala (2004). “*Design, Fabrication And Testing Of A Shape Memory Alloy Based Cryogenic Thermal Conduction Switch*”. Master Thesis. University of Central Florida. Electronic Theses and Dissertation.100. <http://stars.library.ucf.edu/etd/100>
- [11] Motzki, Paul (2018). “*Advanced design and control concepts for actuators based on shape memory alloy wires*”. Doctor of Philosophy (PhD), Faculty of Natural Science & Technology, University of Saarlandes. 10.22028/D291-27354.

- [12] Mohd Jani, J (2016). “*Design optimisation of shape memory alloy linear actuator applications*”. Doctor of Philosophy (PhD). Aerospace, Mechanical and Manufacturing Engineering. RMIT University.
- [13] De la Flor, Silvia & Urbina, C. & Ferrando, F. (2006). “*Constitutive model of shape memory alloys: Theoretical formulation and experimental validation*”. Materials Science and Engineering: A. 427. 112-122. 10.1016/j.msea.2006.04.008.
- [14] Van Humbeeck, J. (2001). “*Shape Memory Alloys: A Material and a Technology*”. Adv. Eng. Mater., 3: pp. 837-850. doi:[10.1002/1527-2648\(200111\)3:11<837::AID-ADEM837>3.0.CO;2-0](https://doi.org/10.1002/1527-2648(200111)3:11<837::AID-ADEM837>3.0.CO;2-0)
- [15] Sofla, A. Y. N., Elzey, D. M., & Wadley, H. N. G. (2008). “*Two-way Antagonistic Shape Actuation Based on the One-way Shape Memory Effect*”. Journal of Intelligent Material Systems and Structures, 19(9), pp. 1017–1027. <https://doi.org/10.1177/1045389X07083026>
- [16] Benafan, Othmane & Brown, Jeff & Calkins, Tad & Kumar, Parikshith & Stebner, Aaron & Turner, Travis & Vaidyanathan, Raj & Webster, John & Young, Marcus. (2014). “*Shape memory alloy actuator design: CASMART collaborative best practices and case studies*”. International Journal of Mechanics and Materials in Design. 10. 10.1007/s10999-013-9227-9.
- [17] “*Nitinol Supplier: Retail and Wholesale.*” Kellogg's Research Labs, www.kelloggsresearchlabs.com/nitinol-shop/.
- [18] Motzki, Paul & Seelecke, S. (2016). *Bi-stable SMA Actuator*. Actuator 16 - 15th International Conference on New Actuators. 10.13140/RG.2.2.12065.20325.
- [19] Clover Aguayo, Brent Utter, Jonathan Luntz, Richard Gonzalez, Diann Brei, Nancy L. Johnson, Paul W. Alexander (2014). “*Damper-controlled switch for SMA motion smoothing*” Proc. SPIE 9059. Industrial and Commercial Applications of Smart Structures Technologies 2014. 90590H.
- [20] Morgan, R. and Yee, H. (1999). “*Electro-thermal bi-stable actuator*”. United States patent US5977858A.
- [21] Menard, S., Villeneuve, J., Lassonde, N. and Decarie, M. (2005). “*Bistable switch with shape memory metal*”. United States patent US6917276B1.
- [22] Woychik, G., Olson, S., Legge, R. and McCoy, B. (2011). “*Electrical switching devices using a shape memory alloy (SMA) actuation mechanism*”. United States patent US7928826B1.

- [23] Alacqua, S. and Butera, F. (2015). “*Bistable electric switch with shape memory actuator*”. United States patent US20150048921A1.
- [24] Minners, R. (2001). “*Bistable micro-switch and method of manufacturing the same*”. United States patent US6236300B1.
- [25] Barnes, G., Skekloff, J., Martin, D. and Ray, D. (2000). “*Switch and relay using shape memory alloy*”. United States patent US6133816A.
- [26] haillet N, Régnier S. (2010). “*Microrobotics for Micromanipulation*. Edited by Nicolas Chaillet, Stéphane Règnier. ISTE.
- [27] M. Plooij, G. Mathijssen, P. Cherelle, D. Lefeber and B. Vanderborght (2015). “*Lock Your Robot: A Review of Locking Devices in Robotics*”. IEEE Robotics & Automation Magazine. vol. 22. no. 1. pp. 106-117. doi: 10.1109/MRA.2014.2381368
- [28] Tanaka, K. (1986). “*A thermomechanical sketch of shape memory effect: one-dimensional tensile behavior*”. Res Mechanica. Vol. 18. pp 251-263.
- [29] Liang, C., & Rogers, C. A. (1990). “*One-Dimensional Thermomechanical Constitutive Relations for Shape Memory Materials*”. Journal of Intelligent Material Systems and Structures. Vol. 1(2). pp 207–234.
<https://doi.org/10.1177/1045389X9000100205>
- [30] An, Sung-Min & Ryu, Junghyun & Cho, Maenghyo & Cho, Kyu-Jin (2012). “*Engineering design framework for a shape memory alloy coil spring actuator using a static two-state model*”. Smart Materials & Structures. Vol. 21. 10.1088/0964-1726/21/5/055009.
- [31] Budynas, R., Nisbett, J. and Shigley, J. (2008). “*Shigley's mechanical engineering design*”. Boston [Mass.]: McGraw-Hill Higher Education.
- [32] G. L. Tawney (1939). “*Zigzag and Helical Springs; Elastic Properties of Molybdenum*”. Review of Scientific Instruments 10:5. pp 152-159.
<https://doi.org/10.1063/1.1751509>
- [33] Lambert, T., Gurley, A. and Beale, D. (2017). “*SMA actuator material model with self-sensing and sliding-mode control; experiment and multibody dynamics model*”. Smart Materials and Structures. Vol. 26(3). p.035004
- [34] Yates, Shane & Kalamkarov, Alexander (2013). “*Experimental Study of Helical Shape Memory Alloy Actuators: Effects of Design and Operating Parameters on Thermal Transients and Stroke*”. Metals. Vol. 3. Pp. 123-149. 10.3390/met3010123.

- [35] Follador, Maurizio & Cianchetti, Matteo & Arienti, Andrea & Laschi, Cecilia. (2012). "A general method for the design and fabrication of shape memory alloy active spring actuators". *Smart Materials and Structures*. 21. 115029. 10.1088/0964-1726/21/11/115029.
- [36] Hadi, Alireza & Yousefi-Koma, Aghil & M. Moghaddam, Majid & Elahinia, Mohammad & Ghazavi, A. (2010). "Developing a novel SMA-actuated robotic module. *Sensors and Actuators*". A: Physical. Vol. 162. Pp. 72-81. 10.1016/j.sna.2010.06.014
- [37] Gurley, Austin (2017). "Enabling Shape Memory Alloys as Actuators for Robotics." (Phd Dissertation). Auburn University.
- [38] Indium Corporation, "Nitinol Soldering Kit". 98790. Retrieved from <https://www.indium.com/medical/soldering-to-nitinol/>
- [39] D. Clausi et al. (2010). "Design and Wafer-Level Fabrication of SMA Wire Microactuators on Silicon," in *Journal of Microelectromechanical Systems*. Vol. 19. No. 4. Pp. 982-991. doi: 10.1109/JMEMS.2010.2049474
- [40] J. Barth, C. Megnin and M. Kohl (2012). "A Bistable Shape Memory Alloy Microvalve With Magnetostatic Latches," in *Journal of Microelectromechanical Systems*. vol. 21. no. 1. pp. 76-84. doi: 10.1109/JMEMS.2011.2174428
- [41] Adelaide Nespoli, Carlo Alberto Biffi, Riccardo Casati, Francesca Passaretti, Ausonio Tuissi and Elena Villa (2012). "New Developments on Mini/Micro Shape Memory Actuators, Smart Actuation and Sensing Systems - Recent Advances and Future Challenges" Giovanni Berselli, Rocco Vertechy and Gabriele Vassura, IntechOpen, DOI: 10.5772/50473. Available from: <https://www.intechopen.com/books/smart-actuation-and-sensing-systems-recent-advances-and-future-challenges/new-developments-on-mini-micro-shape-memory-actuators>).
- [42] Stöckel D. (1992). "Status and Trends in Shape Memory Technology". Actuator'92. 3rd International Conference on New Actuators. Bremen, Germany. Pp.79-84.
- [43] Norwich, Dennis & Fasching, Audrey (2009). "A Study of the Effect of Diameter on the Fatigue Properties of NiTi Wire". *Journal of Materials Engineering and Performance - J MATER ENG PERFORM*. Vol. 18. Pp. 558-562. 10.1007/s11665-009-9415-9.
- [44] Garcés-Schröder, M.; Hecht, L.; Vierheller, A.; Leester-Schädel, M.; Böhl, M.; Dietzel, A (2017). "Micro-Grippers with Femtosecond-Laser Machined In-Plane Agonist-Antagonist SMA Actuators Integrated on Wafer-Level by Galvanic Riveting". *Proceedings 2017*. 1. 385.

- [45] Fischer, Andreas & Gradin, H. & Braun, Stefan & Schroder, S. & Stemme, Göran & Niklaus, Frank (2011). “*Wafer-level integration of NiTi shape memory alloy wires for the fabrication of microactuators using standard wire bonding technology*”. Proceedings of the IEEE International Conference on Micro Electro Mechanical Systems (MEMS). Pp. 348 - 351. 10.1109/MEMSYS.2011.5734433.
- [46] Kohl, Manfred & Krevet, Berthold & Just, Elmar. (2002). “*SMA microgripper system. Sensors and Actuators*”. A: Physical. Pp. 97-98. 646-652. 10.1016/S0924-4247(01)00803-2.
- [47] Jianzuo Ma, Haolei Huang, and Jin Huang (2013). “*Characteristics Analysis and Testing of SMA Spring Actuator*,” Advances in Materials Science and Engineering. Vol. 2013. Article ID 823594. 7 pages. <https://doi.org/10.1155/2013/823594>
- [48] Lei Xue (2017). [Antagonistic SMAs Cyclic Testing]. Unpublished raw data.

APPENDIX A

FIRST-ORDER DESIGN EQUATIONS FOR SMA WIRES*

Area	$A = \frac{\pi}{4} D^2$	mm ²	(1)
Max force (for 100k cycles)	$F_{max} = 170 * A$	N	(2)
Min. required preload (to ensure extension)	$F_{preload} = 100 * A$	N	(3)
Min. expected stroke	$\delta_{max} = 0.04 * L$	mm	(4)
Safe bending radius	$r_{min} = 50 * D$	mm	(5)
Cooling time (in still, room temp air 25 °C)	$t_{cool} = D^2/0.0172$	seconds	(6)
Electrical resistance	$R = 0.001 * L/A$ $= 0.0012 * L/D^2$	Ohm	(7)
Safe continuous current to prevent damage	$I_{max} = 20000 * A + 40$	mA	(8)
Safe continuous voltage to prevent damage	$V_{max} = I_{max}R$	Volts	(9)
Heating current	$I = V/R$	Amp	(10)
Heating time	$t_{heat} = 19000 * A/I$	Seconds	(11)
Cycle time	$t_{cycle} = t_{heat} + t_{cool}$	Seconds	(12)
Cost (MuscleWire from Dynalloy)	$L * 0.0045$	USD	(13)
SMA Energy (force*stroke)	$E_{sma} = \delta_{max}(F_{max} - F_{preload})$ $= 2.2 * L * D^2$	Nm	(14)
SMA steady-state power consumption	$P = 405 * D * L * (A_f - 20)$	W	(15)
Heat transfer coefficient	$65.5e^{-\frac{d}{4}(T - T_{\infty})^{\frac{1}{6}}}$	W/m ² /C	(16)
Actuator Efficiency	$\eta = \frac{0.025309}{\frac{0.000026}{d} \left(\frac{L}{V}\right)^2 + 1}$		(17)

* Reprinted from [37]

* These rules are considered conservative (life cycle of 100k to 1 million)

APPENDIX B

MATLAB OPTIMIZATION CODE

```
global G;global Tf; global Tinf; global rouD; global lmax;global cp; global dH; global
TAs;global TAf; global TMs; global TMf; global Ea; global Em; global Vblock;global
dielecAir; global strainMax;global mius;global miud;
rouD=6.45*10^3; cp= 0.8368*10^3; dH=24.2; alphaA=11*10^-6; alphaB=6.6*10^-6;
TAs=52.54; TAf=60.9; TMs=44.78; TMf=32.84;Tinf=25;
Ea=70*10^9;Em=30*10^9; G=79.3*10^9; lmax=0.01;
Tf=70;Vblock=500;dielecAir=2*10^6;strainMax=0.05;mius=0.51;miud=0.44;
lb=[0.0005 0.0005 2*10^-3 0.025*10^-3 0 0.05*10^-3 4 Vblock/dielecAir 0 0.005
0.025*10^-3];
ub=[lmax/2 lmax/2 lmax/2 2*10^-3 lmax/2 lmax/2 10 lmax/4 lmax/2 3 0.51*10^-3];
A=[1 1 0 0 0 0 1 0 0 0;0 0 2+strainMax 0 0 0 0 0 0 0;0 0 0 4 0 -1 0 0 0 0 0;0 0 0 0 -1
0 0 1 0 0 0;0 -1 0 0 1 0 0 0 0 0 0];
b=[lmax;lmax;0;0;0];global obj;
global g;g=9.81;
options=optimoptions(@fmincon,'Algorithm','sqp','TolCon',1e-06,'MaxIter',300,'TolX',1e-
06)%,'PlotFcn',@gsplotbestf);
for i=1:1
    x0=[0.00495220772711355 0.00271340109243592 0.00236419842822604
0.00102917074530039 0.000864391610254733 0.000489705057642176 10
0.000855870357442526 0.00140332583830589 1.59696410845467
6.42707663703075e-05];
    global obj;
    obj=true;
    problem=createOptimProblem('fmincon','x0',x0,'objective',@myfun,'Aineq',A,'binedq'
,b,'lb',lb,'ub',ub,'nonlcon',@nonlcon,'options',options);
    ms=MultiStart('StartPointsToRun','bounds');
    [x,fval,exitflag,output,solutions]=run(ms,problem,200);
    disp ("Optimal design vector:");
    disp(mat2str(round(x,6)));
    disp ("Min EPSE value & corresponding Z value:");
    disp(strcat(num2str(round(fval,8))," & ",num2str(round(x(6),6))));
    w=length(solutions);
    obj1=zeros(w,11);
    val1=zeros(w,1);
    Zs=zeros(w,1);
    for p=1:length(solutions)
        obj1(p,:)=solutions(1,p).X;
        val1(p,1)=solutions(1,p).Fval;
        Zs(p,1)=obj1(p,6);
    end
    subplot(2,1,1);
    plot([1:1:w],val1);
    hold on;
```

```

plot([1:1:w],Zs);
hold off;
legend("Min EPSE", "Corres Z");
obj=false;
problem=createOptimProblem('fmincon','x0',x0,'objective',@myfun,'Aineq',A,'bineq'
,b,'lb',lb,'ub',ub,'nonlcon',@nonlcon,'options',options);
ms=MultiStart('StartPointsToRun','bounds');
[x,fval,exitflag,output,solutions]=run(ms,problem,200);
k=length(solutions);disp ("Optimal design vector:");
disp(mat2str(round(x,6)));disp ("Min Z value & corresponding EPSE value:");
dd=x(11);
resista= 10^-6*(dd^-1.986);
hh=65.5*exp(-dd*0.25)*((Tf-Tinf)^(1/6));
valu=1-((45*pi*dd*hh*x(3))/(x(10)*x(10)*resista*x(3)));
timet= -1*rouD*dd*cp*(0.25/hh)*log(valu);
fff=x(10)^2 * resista * x(3) * timet;
disp(strcat(num2str(round(fval,8)), " & ",num2str(fff,6)));
obj2=zeros(k,11);
val2=zeros(k,1);
fun2=zeros(k,1);
for j=1:length(solutions)
    obj2(j,:)=solutions(1,j).X;
    val2(j,1)=solutions(1,j).Fval;
    d=obj2(j,11);
    resist= 10^-6*(d^-1.986);
    h=65.5*exp(-d*0.25)*((Tf-Tinf)^(1/6));
    val=1-((45*pi*d*h*obj2(j,3))/(obj2(j,10)*obj2(j,10)*resist*obj2(j,3)));
    time= -1*rouD*d*cp*(0.25/h)*log(val);
    ff=obj2(j,10)^2 * resist * obj2(j,3) * time;
    if ff<0
        ff=-1.*ff;
    end
    ff=5.*ff;
    fun2(j,1)=ff;
end
subplot(2,1,2);
plot([1:1:k],val2);
hold on;
plot([1:1:k],fun2);
hold off;
legend("Min Z", "Corres EPSE");
end
function f=myfun(x)
    global Tf; global Tinf; global rouD; global cp; global obj;
    d=x(11);
    resis= 10^-6*(d^-1.986);
    h=65.5*exp(-d*0.25)*((Tf-Tinf)^(1/6));
    val=1-((45*pi*d*h*x(3))/(x(10)*x(10)*resis*x(3)));

```

```

t= -1*rouD*d*cp*(0.25/h)*log(val);

Z=max(x(6),d);
f2=Z;
f1=x(10)^2 * resis * x(3) * t;
if obj==true
    f =f1;
else
    f=f2;
end
end
function [c]=nonlcon(x)
    global Ea;global Em; global G;global mius;global strainMax;global miud;global g;
    d=x(11);
    Fh= (1*10^10*d.^2 + 103018*d - 3.4035)*g*10^-3;
    Fr= (5*10^9*d.^2 + 40688*d - 1.482)*g*10^-3;
    Frelax=0.25*pi* d.^2 * (Em)* 0.005;
    Fspring=x(4)^4 * G * x(8) * (1/(8* x(6).^3 * x(7)));
    Ffrictions=Fspring*mius;
    Ffrictiond=Fspring*miud;
    c(1)= 1 - (x(2)/x(1));
    c(2)= (x(8)) + ( x(7)*x(4) ) - x(5);
    c(3)= sqrt( (x(5)^2 - ((x(5)-x(8)).^2)) - (strainMax*x(3)*(x(2)/x(1)));
    c(4)= x(10) - ( (1e07*d.^2) + (246.48*d) +0.034);
    c(5)= (Frelax*x(1))-(Ffrictions*x(2));
    c(6)= (Fr*x(1)) + (Ffrictiond*x(2))-(Fh*x(1));
    c(7)= (2*strainMax*x(3)*(x(2)/x(1)))-x(9);
    c(8)= 6 - (x(6)/x(4));
end

```